

PDF hosted at the Radboud Repository of the Radboud University Nijmegen

The following full text is a publisher's version.

For additional information about this publication click this link.

<http://hdl.handle.net/2066/113737>

Please be advised that this information was generated on 2018-07-08 and may be subject to change.

The
Nucleus Basalis of Meynert complex
and adjacent structures in

normal aging and



Alzheimer's disease



The Nucleus Basalis of Meynert complex and adjacent structures in normal aging and Alzheimer's disease

A neuroanatomical, neuropathological and stereological study

The Nucleus Basalis of Meynert complex and adjacent structures in normal aging and Alzheimer's disease

A neuroanatomical, neuropathological and stereological study

een wetenschappelijke proeve op het gebied van
GENEESKUNDE en TANDHEELKUNDE

PROEFSCHRIFT

ter verkrijging van de graad van doctor
aan de Katholieke Universiteit te Nijmegen,
volgens besluit van het College van Decanen
in het openbaar te verdedigen
op vrijdag 23 februari 1990
des namiddags te 2.15 uur precies

door

OSCAR JOSEPH MARIA VOGELS

geboren op 28 september 1957 te Oss

1990

Druk: SSN-Nijmegen

Promotores: Prof. Dr. R. Nieuwenhuys
Prof. Dr. B.P.M. Schulte

Co-referent: Dr. H.J. ter Laak

The investigations described in this thesis were carried out at the Research Laboratory for Morphological Neurology, Institute of Neurology, Catholic University of Nijmegen, Nijmegen, the Netherlands.

The studies presented in this thesis were supported by the JANIVO foundation.

Financial support by Sanofi BV, Sandoz BV, Schering Nederland BV, Nutricia Nederland BV en UCB Farma Nederland BV for the publication of this thesis is gratefully acknowledged.

Ter nagedachtenis

aan Moeder,

voor Vader

en Dorine

"CIP-gegevens Koninklijke Bibliotheek Den Haag"

The nucleus basalis of Meynert complex and adjacent structures in normal aging and Alzheimer's disease.

A neuroanatomical, neuropathological and stereological study.

Oscar Joseph Maria Vogels

(S.l: s.n.). - Ill.

Thesis Nijmegen. - With ref. - With summary in Dutch.

ISBN 90-9003279-7

Subject heading: Alzheimer's disease

CONTENTS

Chapter	page
1. Introduction	11
2. Neuroanatomy of the human nucleus basalis Meynert complex, the human supraoptic and paraventricular nuclei, and the human organum vasculosum of the lamina terminalis	21
3. Material and methods	57
4. The nucleolus in quantitative morphology (submitted for publication)	73
5. Cell loss and shrinkage in the nucleus basalis Meynert complex in Alzheimer's disease (Neurobiology of Aging 1990;11: in press)	85
6. Neuronal hypertrophy in the human supraoptic and paraventricular nucleus in aging and Alzheimer's disease (Neuroscience Letters 1990: in press)	115
7. Neuropathology of the nucleus basalis of Meynert complex, the supraoptic and paraventricular nuclei, and the organum vasculosum of the lamina terminalis in aging and Alzheimer's disease	125
8. Galanin-like immunoreactivity within Ch2 neurons in the vertical limb of the diagonal band of Broca in aging and Alzheimer's disease (Acta Neuropathologica 1989;78:90-5)	153
9. Correlations of neuron counts in the nucleus basalis of Meynert complex and hypothalamus with neuropathological determinants in cortical and subcortical structures in Alzheimer's disease	167
Summary and conclusions	175
Samenvatting and conclusies	179
Dankwoord	183
Curriculum vitae	184

ABBREVIATIONS

AChE	acetylcholine esterase
AD	Alzheimer's disease
AON	anterior olfactory nucleus
BPP	β -protein precursor
CA	conophilic angiopathy
CE	coefficient of error
ChAT	choline acetyltransferase
CV	coefficient of variation
d_{max}	maximum diameter
FAD	familial Alzheimer's disease
GABA	gamma-aminobutyric acid
GVD	granulovacuolar degeneration
IGF	insulin-like growth factor
LC	locus coeruleus
MAP	microtubule-associated protein
NFT	neurofibrillary tangle
NBMC	nucleus basalis Meynert complex
NGF	nerve growth factor
NGF-r	nerve growth factor receptor
OVL	organum vasculosum of the lamina terminalis
PD	Parkinson's disease
PHF	paired helical filaments
PVN	paraventricular nucleus
SD	standard deviation
SDAT	senile dementia of the Alzheimer type
SEM	standard error of the mean
SON	supraoptic nucleus
SP	senile plaque

INTRODUCTION

1.1 The cholinergic hypothesis

Alzheimer's disease (AD) was first described by Alois Alzheimer, who identified the cortical senile plaques and neurofibrillary tangles which are its classical neuropathological hallmarks [2]. The functional importance of these cortical abnormalities was indicated by a report that showed a correlation between cortical plaque counts and scores upon both a functional rating scale of dementia and a short information-memory-concentration test [8]. Further progress was made when three independent research groups showed that AD brains had consistently low levels of cholinergic markers, especially the synthesising enzyme choline acetyltransferase (ChAT) [10, 17, 40]. The reduced cortical ChAT activity in AD was inversely related to cortical plaque densities and paralleled the degree of cognitive impairment [41]. Other indices of cholinergic function such as measurements of acetylcholinesterase (AChE) levels which are relatively specific to cholinergic cells [42], the very specific high-affinity choline uptake system [43], and the capability of cerebral biopsy samples to synthesise acetylcholine [11] have all confirmed a true loss of cholinergic function in AD.

The fact that the decreased ChAT activity in AD brains was greater than the degree of cortical cell loss [50] suggested that the cholinergic cell bodies might reside in a subcortical location, as was already indicated by earlier work, that showed a pronounced decrease in cortical AChE and ChAT levels by undercutting the overlying cortex [28]. With the use of antibodies to the specific cholinergic marker ChAT, it has been firmly established that most large neurons in the subcortical nucleus basalis of Meynert, the diagonal band of Broca and the medial

septal nucleus are cholinergic [29, 39, 47, 48]. These cholinergic neurons send projections directly to the cerebral cortex and hippocampus [33, 34, 39] and are selectively lost in AD, whereas no consistent reduction in neurons was observed in adjacent structures [3, 52, 53]. This loss of cholinergic neurons in AD is correlated with the number of cortical senile plaques [4] and is inversely related with cortical ChAT levels [23]. Furthermore, the distended neurites of primitive and mature senile plaques in the cerebral cortex show immunoreactivity against (axons and axonal endings of) cholinergic neurons [5]. These observations strengthened the association between cholinergic dysfunction, neuropathological findings, and the intellectual impairments in patients with AD. These biochemical, neuropathological and behavioural studies have been repeated extensively confirming the cholinergic dysfunction in AD. Moreover, early psychopharmacological studies showed that suppression of cholinergic function in normal subjects can produce learning and memory disturbances [21, 24]. In humans, the centrally acting anticholinergic drug, scopolamine, produced disturbances in the memory for recent events. These effects could be reversed by enhancing the cholinergic activity with the anticholinesterase agent physostigmine, but not by enhancing the noradrenergic activity with D-amphetamine [25]. In the early stages of Alzheimer's disease small improvements in cognitive functioning have been reported by administering anticholinesterase agents as physostigmine [51] and tetrahydroaminoacridine [49].

In its commonest form the cholinergic hypothesis states that loss of cholinergic function causes or contributes to some of the intellectual impairments particularly the memory deficits of AD [6, 14, 13, 43]. More than a decade after its formulation the cholinergic hypothesis is still subject to critical evaluation. Until now, it is largely based on evidence of neurochemical and neuropathological disturbances in affected brain tissue, but still awaits an effective therapy for its ultimate validation. The pattern of memory failure induced in normal people by scopolamine (which blocks muscarinic receptor sites) is said to be distinct from that seen in AD [7]. The effect of THA is not

only due to acetylcholinesterase-blocking, but probably also to activation of cortical monoaminergic systems [1]. Moreover, certain neuroactive peptides are hydrolysed or actually produced as a result of acetylcholinesterase action [32], and its inhibition by THA may thus be associated with functional alterations of cerebral neuropeptides rather than enhancing the availability of acetylcholine [45].

The cholinergic deficit is unlikely to be specific to AD in view of the many diverse disorders associated with cortical cholinergic degeneration and/or reductions in neuron numbers in the nucleus basalis of Meynert: Parkinson's disease, Parkinson's disease with dementia, Parkinsonism-dementia of Guam, Down's syndrome, Gerstmann-Straussler syndrome, hereditary olivopontine cerebellar degeneration, progressive supranuclear palsy, dementia pugilistica, and Korsakoff's psychosis [43]. In the Parkinsonian group over 70% of cortical ChAT loss has been measured, and yet only a mild form of dementia which is not typical of AD is present. This suggests that the cholinergic system is unlikely to be involved in all aspects of cognitive function affected in AD, and that other neuronal systems may also be involved. This difference in cognitive profiles between Parkinson's disease and AD has been ascribed to a compensating denervation-induced muscarinic-receptor supersensitivity evident in important projection areas as the hippocampus in Parkinson's disease but not in AD [44].

As in most neurodegenerative diseases numerous different neurotransmitter systems are affected to a greater or lesser extent. The noradrenergic deficit in AD (reduced locus coeruleus neuron numbers [9] and/or cortical dopamine- β -hydroxylase deficiency [15]) does not relate closely to cognitive impairment, but to a diminishing general arousal and emotional response, as recently has been demonstrated by a remarkable case of congenital dopamine- β -hydroxylase deficiency with apparently normal intellectual function, but a tendency to "be apathetic and avoid physical exercise" [37]. The clinical significance of serotonergic deficit has not been demonstrated yet [11]. Several lines of evidence implicate reductions of excitatory amino-acid abnormali-

ties e.g. glutamate in AD [38], but not in Parkinson's disease [16]. The clinical significance of the cortical glutamate reduction in AD remains to be established. Cortical reductions of the neuropeptides somatostatin [18, 46] and substance-P [19] have been reported. It is unlikely that all of these neurochemical disturbances are of equal importance in relation to the core symptoms of AD, and most of them are probably not clinically relevant due to the compensatory mechanisms of the human brain.

The role of acetylcholine in memory processing is still obscure. At the molecular level stimulation of the nicotinic cholinergic receptor by nicotine or acetylcholine induces transcription of the actin gene and a proto-oncogene [27]. Nicotinic-receptor binding is substantially reduced in AD, Parkinson's disease and Down's syndrome [44, 54], but it is not established yet whether this is reflected by altered protein transcriptions. At the cellular level, cholinergic neurons of the nucleus basalis of Meynert (nbM) could be involved in memory processing because animal lesion studies of this nucleus generally result in learning deficits [for review: 6, 13, 20]. The trophic state of cholinergic neurons depends on the cortical production of nerve growth factor (NGF) that promotes the survival and recovery of these neurons in the mammalian brain. Immunocytochemical studies have shown extensive loss of nbM neurons in AD positive for nerve growth factor-receptors (NGF-r) [30, 35]. It was recently demonstrated that NGF-r gene expression is extensively decreased in the nbM [31]. Other studies suggest that NGF itself regulates the expression of its own NGF-receptor in the central nervous system [26, 36]. Therefore, the decrease in NGF-r gene expression in nbM neurons in AD may result from a lack of NGF support due to general cortical atrophy in AD. The latter suggests a secondary rather than a primary degeneration of the cholinergic system in AD. It is at the systematic or multicellular level, however, that learning and other cognitive functions must eventually be understood. Hippocampus and temporal neocortex are considered as areas associated with learning and memory. These areas receive major cholinergic inputs from the nucleus basalis of Meynert, the diagonal band of

Broca and the medial septal nucleus [39]. In AD, the hippocampus and temporal neocortex show severe atrophy and cell loss [12, 22]. However, whether this degeneration of hippocampus and temporal neocortex is the primary event in AD with subsequent retrograde degeneration of the cholinergic system, or whether it is secondary to a primary degenerating cholinergic system, remains to be established.

Undoubtedly, the cholinergic hypothesis of dementia in Alzheimer's disease has been the single greatest impetus to research into AD. However, whether the cholinergic deficiency can provide any clues regarding the pathogenesis depends on the extent to which it is a major and early involvement, and the extent to which it is specific to the Alzheimer's disease process. Rather, it would seem that cell loss of cholinergic neurons is a common feature of a variety of distinct disease processes. This vulnerability may well be related to the dependency on nerve growth factor, indicated by the selective NGF-receptor localisation on the cholinergic neurons, as opposed to most other neurons in the brain.

1.2 Aim of the study

With regard to the cholinergic hypothesis the loss of large cholinergic neurons in the nucleus basalis Meynert complex (NBMC, i.e., the nucleus basalis Meynert, the diagonal band of Broca, and the medial septal nucleus) is a central issue. This cell loss correlates with the degree of dementia, the number of senile plaques and neurofibrillary tangles in the neocortex and hippocampus, and the amounts of choline acetyltransferase in these structures (see 1.1). However, a closer look at these neuropathological and morphometric studies reveals several methodological errors especially in the counting procedures applied. Moreover, most studies considered only magnocellular neurons and excluded shrunken neurons from being counted. The neuropathological parameters investigated in this thesis include total neuron number, neuron size, the number of senile plaques

and neurofibrillary tangles, and the distribution of congophilic angiopathy and lipofuscinosis. The following questions will be considered in this thesis:

1. What are the neuroanatomical boundaries of the NBMC and its subdivisions (Chapter 2)?
2. What are the most appropriate morphometric counting and sampling methods (Chapters 3 and 4)?
3. Do the neuropathological parameters of (the subdivisions of) the NBMC change in normal aging (Chapters 5 and 7)?
4. Do the neuropathological parameters of (the subdivisions of) the NBMC in Alzheimer's disease differ from normal aging (Chapters 5 and 7)?
5. With regard to the specificity of the changes of the NBMC in normal aging and AD, do the supraoptic and paraventricular nuclei show similar changes in normal aging and AD (Chapters 6 and 7)?
6. Are there left-right differences in the neuropathological parameters; are there differences between the subdivisions of the NBMC (Chapters 5, 6 and 7)?
7. With regard to the role of interneurons in the NBMC, does the Galanin-like immunoreactivity change in AD (Chapter 8)?
8. Does the degeneration of the NBMC reflects a primary or a secondary process in the pathogenesis of AD; consequently, does the degeneration of the NBMC in AD correlate with changes found in its projection areas, the neocortex and hippocampus, and with changes in the brainstem (Chapter 9)?

1.3 References

1. Albin RL, Young AB and Penney JB. THA increases action potential duration of central histamine neurons in vitro. *Eur J Pharmacol* 1988; 155:265-70.
2. Alzheimer A. Über ein eigenartige Erkrankung der Hirnrinde. *Allg Z Psychiat* 1907;64:146-8.
3. Arendt T, Bigl V, Arendt A and Tennstedt A. Loss of neurons in the nucleus basalis of Meynert in Alzheimer's disease, paralysis agitans and Korsakoff's disease. *Acta Neuropathol* 1983;61:101-8.
4. Arendt T, Bigl V, Tennstedt A and Arendt A. Neuronal loss in different parts of the nucleus basalis is related to neuritic plaque formation in

- cortical target areas in Alzheimer's disease. *Neurosci* 1985;14:1-14.
5. Armstrong DM, Bruce G, Hersh LB, Terry RD. Choline acetyltransferase immunoreactivity in neuritic plaques of Alzheimer brain. *Neurosci Lett* 1986;71:229-34.
 6. Bartus RT, Dean RL, Beer B and Lippa AS. The cholinergic hypothesis of geriatric memory dysfunction. *Science* 1982;217:408-17.
 7. Beatty WW, Butters N and Janowsky DS. Patterns of memory failure after scopolamine treatment: implications for the cholinergic hypothesis of dementia. *Behav Neural Biol* 1986;45:196-211.
 8. Blessed G, Tomlinson BE and Roth M. The association between quantitative measures of dementia and of senile changes in the cerebral gray matter of elderly subjects. *Br J Psychiat* 1968;114:797-811.
 9. Bondareff W, Mountjoy CQ and Roth M. Selective loss of neurons of origin of noradrenergic projection to cerebral cortex (nucleus locus coeruleus) in senile dementia. *Lancet* 1981;i:783-4.
 10. Bowen DM, Smith CB, White P and Davison AN. Neurotransmitter related enzymes and indices of hypoxia in senile dementia and other abiotrophies. *Brain* 1976;99:459-96.
 11. Bowen DM and Davison AN. Biochemical studies of nerve cells and energy metabolism in Alzheimer's disease. *Br Med Bull* 1986;42:75-80.
 12. Broere CAJ. The neocortex in Alzheimer's disease. Thesis Nijmegen 1990
 13. Collerton D. Cholinergic function and intellectual decline in Alzheimer's disease. *Neurosci* 1986;19:1-28.
 14. Coyle JT, Price DL and DeLong MR. Alzheimer's disease: a disorder of cortical cholinergic innervation. *Science* 1983;219:1184-90.
 15. Cross AJ, Crow TJ, Perry EK, Perry RH, Blessed G and Tomlinson BE. Reduced dopamine- β -hydroxylase in Alzheimer's disease. *Br Med J* 1981;282:93-4.
 16. Cross AJ, Slater P, Simpson M, Deakin JFW, Perry RH and Perry EK. (^3H)-Aspartate binding in cerebral cortex in patients with Alzheimer's and Parkinson's disease. *Neurosci Lett* 1987;79:213-7.
 17. Davies P and Maloney AJ. Selective loss of central cholinergic neurons in Alzheimer's disease. *Lancet* 1976;ii:1403.
 18. Davies P, Katzmann R and Terry RD. Reduced somatostatin-like immunoreactivity in cerebral cortex from cases of Alzheimer disease and senile dementia of the Alzheimer type. *Nature* 1980;288:279-80.
 19. Davies P, Katz DA and Crystal HA. Choline acetyltransferase, somatostatin, and substance P in selected cases of Alzheimer's disease. *Aging NY* 1982;19:9-14.
 20. DeFeudis FV. Cholinergic systems and Alzheimer's disease. *Drug Dev Res* 1988;14:95-109.
 21. Deutsch JA. The cholinergic synapse and the site of memory. *Science* 1971;174:788-94.
 22. De Vries H. The hippocampus in Alzheimer's disease. Thesis Nijmegen 1990
 23. Doucette R, Fisman M, Hachinsky VC and Mersky M. Cell loss from the nucleus basalis of Meynert in Alzheimer's Disease. *Can J Neurol Sci* 1986;13:435-40.
 24. Drachmann DA and Leavitt J. Human memory and the cholinergic system, a relationship to ageing? *Arch Neurol* 1974;30:113-21.
 25. Drachmann DA. Memory and cognitive function in man: does the cholinergic system have a specific role? *Neurology* 1977;27:783-90.
 26. Gage FH, Batchelor P, Chen KS, Chin D, Deputy S, Rosenberg MB, Higgins GA, Koh S, Fischer W and Bjorklund A. NGF-receptor re-expression and NGF-mediated cholinergic neuronal hypertrophy in the damaged adult

- neostriatum. *Neuron* 1989;2:1177-84.
27. Greenberg ME, Ziff EB and Greene LD. Stimulation of neuronal acetylcholine receptors induces rapid gene transcription. *Science* 1986;234:80-2.
 28. Hebb CO, Krnjevic K and Silver A. Effect of undercutting on the acetylcholinesterase and choline acetyltransferase activity in cat's cerebral cortex. *Nature* 1963;198:692.
 29. Hedreen JC, Bacon SJ, Cork LC, Kitt CA, Crawford GD, Salvaterra PM and Price DL. Immunocytochemical identification of cholinergic neurons in the monkey central nervous system using monoclonal antibodies to choline acetyltransferase. *Neurosci Lett* 1983;43:173-7.
 30. Hefti F and Mash DC. Localization of nerve growth factor receptors in the normal human brain and in Alzheimer's disease. *Neurobiol Aging* 1989;10:75-87.
 31. Higgins GA and Mufson EJ. NGF receptor gene expression is decreased in the nucleus basalis in Alzheimer's disease. *Exp Neurol*, in press, 1989.
 32. Ismail Z, Millar TJ, Smith DB and Chubb IW. Acetylcholinesterase generates enkephalin-like immunoreactivity when it degrades soluble proteins (Chromogranins) from adrenal chromaffin granules. *Brain Res* 1986;376:230-8.
 33. Jones EG, Burton H, Saper CB and Swanson LW. Midbrain diencephalic and cortical relationships of the basal nucleus of Meynert and associated structures in primates. *J Comp Neurol* 1976;167:385-420.
 34. Kievit J and Kuypers HGJM. Basal forebrain and hypothalamic connections to the frontal and parietal cortex of the monkey. *Science* 1975;187:660-2.
 35. Kordower JH, Gash DM, Bothwell M, Hersh L and Mufson EJ. Nerve growth factor receptor and choline acetyltransferase remain colocalized in the nucleus basalis (Ch4) of Alzheimer's patients. *Neurobiol Aging* 1989;10:67-74.
 36. Larkfors L, Ebendahl T, Whittemore SR, Persson H, Hoffer B and Olson L. Decreased levels of nerve growth factor (NGF) and its messenger RNA in the aged rat brain. *Mol Brain Res* 1987;3:55-60.
 37. Man in 't Veld AJ, Boomsma F, Moleman P and Schalekamp MADH. Congenital dopamine-beta-hydroxylase deficiency. *Lancet* 1987;1:183-7.
 38. Maragos WF, Greenamyre JT, Penney JB and Young AB. Glutamate dysfunction in Alzheimer's disease: a hypothesis. *TINS* 1987;10:65-8.
 39. Mesulam M-M, Mufson EJ, Levey AI and Wainer BH. Cholinergic innervation of cortex by the basal forebrain: cytochemistry and cortical connections of the septal area, diagonal band nuclei, nucleus basalis (substantia innominata) and hypothalamus in the rhesus monkey. *J Comp Neurol* 1983;214:170-97.
 40. Perry EK, Perry RH, Blessed G and Tomlinson BE. Necropsy evidence of central cholinergic deficits in senile dementia. *Lancet* 1977;1:189.
 41. Perry EK, Tomlinson BE, Blessed G, Bergmann K, Gibson PH and Perry RH. Correlations of cholinergic abnormalities with senile plaques and mental test scores in senile dementia. *Br Med J* 1978;2:1457-9.
 42. Perry EK, Curtis M, Dick DJ, Candy JM, Atack JR, Bloxham CA, Blessed G, Fairbairn A, Tomlinson BE and Perry RH. Cholinergic correlates of cognitive impairment in Parkinson's disease: comparisons with Alzheimer's disease. *J Neurol Neurosurg Psychiatr* 1985;48:413-21.
 43. Perry EK. The cholinergic hypothesis - 10 years on. *Br Med Bull* 1986;42:63-9.
 44. Perry EK, Perry RH, Smith CJ, Purohit D, Bonham J, Dick DJ, Candy JM, Edwardson JA and Fairburn A. Cholinergic receptors in cognitive disorders. *Can J Neurol Sci* 1986;13:521-7.

45. Perry EK. Acetylcholine and Alzheimer's disease. *Br J Psychiat* 1988;152:737-40.
46. Rossor MN, Emson PC, Mountjoy CQ, Roth M and Iversen LL. Reduced amounts of immunoreactive somatostatin in the temporal cortex in senile dementia of Alzheimer type. *Neurosci Lett* 1980;20:373-7.
47. Satoh K and Fibiger HC. Distribution of central cholinergic neurons in the baboon (*Papio papio*): I. General morphology. *J Comp Neurol* 1985;236:197-214.
48. Satoh K and Fibiger HC. Distribution of central cholinergic neurons in the baboon (*Papio papio*): II. A topographic atlas correlated with catecholamine neurons. *J Comp Neurol* 1985;236:215-33.
49. Summers WK, Majovski LV, Marsh GM, Tachilzi K and Kling A. Oral tetrahydroaminoacridine in long-term treatment of senile dementia, Alzheimer type. *N Engl J Med* 1986;315:1241-5.
50. Terry RD and Davies P. Dementia of the Alzheimer type. *Ann Rev Neurosci* 1980;3:77-95.
51. Thal LJ, Masur DM, Blau AD, Fuld PA and Klauber MR. Chronic oral physostigmine without lecithin improves memory in Alzheimer's disease. *J Am Geriatr Soc* 1989;37:42-8.
52. Whitehouse PJ, Price DL, Clark AW, Coyle JT and DeLong MR. Alzheimer disease: evidence for selective loss of cholinergic neurons in the nucleus basalis. *Ann Neurol* 1981;10:122-6.
53. Whitehouse PJ, Price DL, Struble RG, Clark AW, Coyle JT and DeLong MR. Alzheimer's Disease and Senile Dementia: loss of neurons in the basal forebrain. *Science* 1982;215:1237-9.
54. Whitehouse PJ, Martino AM, Antuono PG, Lowenstein PR, Coyle JT, Price DL and Kellar NJ. Nicotinic acetylcholine binding sites in Alzheimer's disease. *Brain Res* 1986;371:146-51.

NEUROANATOMY OF THE HUMAN NUCLEUS BASALIS MEYNERT COMPLEX,
THE SUPRAOPTIC AND PARAVENTRICULAR NUCLEI,
AND THE ORGANUM VASCULOSUM OF THE LAMINA TERMINALIS

2.1 Neuroanatomy of the human nucleus basalis of Meynert

2.1.1 Topography of the human nucleus basalis Meynert complex

The nucleus basalis of Meynert was first identified in passing in 1872 by Meynert [84], who described the nucleus as a population of large, hyperchromatic neurons in the basal forebrain (Kern der Linsenkernschlinge). His description was confined to the sublenticular part of the nucleus basalis. Later on the nucleus basalis was described in toto and in more detail by Kölliker [60]. He located the main body of this nucleus between the optic tract and the anterior commissure. Foix and Nicolesco [33] identified loosely scattered neurons outside the main body which were cytologically identical to those in the nucleus basalis. These neurons were present in the internal capsule, and the medial and lateral medullary laminae of the globus pallidus. Brockhaus [16] termed the main body "the pars compacta" and the regions with scattered neurons "the pars diffusa". Moreover, he considered the nucleus basalis of Meynert, together with the nuclei of the diagonal band of Broca, the medial septal nucleus, and with loosely arranged similarly appearing neurons in the olfactory tubercle, as one morphologic and functional entity, "the Basalkern-komplex". This entity-concept was elaborated by Divac [28], who postulated that the magnocellular neurons in the medial septal nucleus, the nuclei of the diagonal band of Broca and the nucleus basalis of Meynert all form part of a single system of neurons with projections to all parts of the pallium.

Abbreviations for all figures

acc	nucleus accumbens
al	ansa lenticularis
amy	amygdala
ap	ansa peduncularis
bnst	bed nucleus of the stria terminalis
ca	commissura anterior
cdt	caudate nucleus
ce	capsula externa
cg1	corpus geniculatum laterale
Ch1	medial septal nucleus
Ch2	vertical limb nucleus of the diagonal band of Broca
Ch3	horizontal limb nucleus of the diagonal band of Broca
Ch4am	anteromedial part of the nucleus basalis of Meynert
Ch4al	anterolateral part of the nucleus basalis of Meynert
Ch4i	intermediate part of the nucleus basalis of Meynert
Ch4p	posterior part of the nucleus basalis of Meynert
ci	capsula interna
cl	claustrum
cm	corpus mamillare
co	chiasma opticum
fx	fornix
gpe	globus pallidus, external segment
gpi	globus pallidus, internal segment
hip	hippocampus
hy	hypothalamus
ins	insular cortex
isC	islands of Calleja
lme	lamina medullaris externa (nuclei lentiformis)
lmi	lamina medullaris interna (nuclei lentiformis)
npv	nucleus paraventricularis
ns	nucleus subthalamicus
nsm	nucleus septi medialis
nso	nucleus supraopticus
ovlt	organum vasculosum of the lamina terminalis
pc	pedunculus cerebri
put	putamen
ro	recessus opticus
rub	nucleus ruber
sa	subcallosal area
sn	substantia nigra
sol	stria olfactoria lateralis
som	stria olfactoria medialis
spe	septum pellucidum
tha	thalamus
tol	tuberculum olfactorium
topt	tractus opticus
vl	ventriculus lateralis
vp	ventral pallidum
vt	ventriculus tertius

Confirmation came from several studies [53, 56, 76]. The latter study combined retrograde horseradish peroxidase techniques with histochemistry (acetylcholinesterase) and immunochemistry (choline acetyltransferase) in the rhesus monkey, demonstrating widespread projections to the entire cortical surface, hippocampus, olfactory bulb and amygdala. The continuum of the cholinergic perikarya in the basal forebrain extended from the medial septal nucleus rostrally to the lateral geniculate body caudally, and its neurons were in close contact with fiber bundles of the diagonal band of Broca, the anterior commissure, the medial forebrain bundle, the ansa lenticularis, the ansa peduncularis, the internal and external capsules, the medullary laminae, the fornix, the stria terminalis and the inferior thalamic peduncle. Four subdivisions could be distinguished on behalf of their topology and projection patterns. These subdivisions were designated as Ch1-Ch4, and were also readily identifiable in a series of Nissl-stained sections through a single human basal forebrain [76]. The Ch1 group in the rhesus monkey corresponded to the medial septal nucleus (10% of its neurons are cholinergic); the Ch2 group corresponded to the vertical limb nucleus of the diagonal band of Broca (about 70% of its neurons are cholinergic); the Ch3 group most closely corresponded to the horizontal limb nucleus of the diagonal band of Broca (only 1% is cholinergic); the Ch4 group corresponded to the nucleus basalis of Meynert (at least 90% of the neurons are cholinergic), that could be further subdivided into an anteromedial (Ch4am), an anterolateral (Ch4al), an intermediate (Ch4i) and a posterior part (Ch4p).

The same topography of the Ch1-Ch4 groups was demonstrated in the human brain and maps of these cell masses were provided using Nissl-staining [45], using combined acetylcholinesterase histochemistry with thionin-staining [113] or with Nissl-staining [97], or using lipofuscin-pigment-staining [135]. Although these maps of the nucleus basalis Meynert complex (NBMC) provide already sufficient insight into its topography, a new series of sections will be presented here in order to get a distinct definition of the different subdivisions of the NBMC (Ch1-Ch4) in

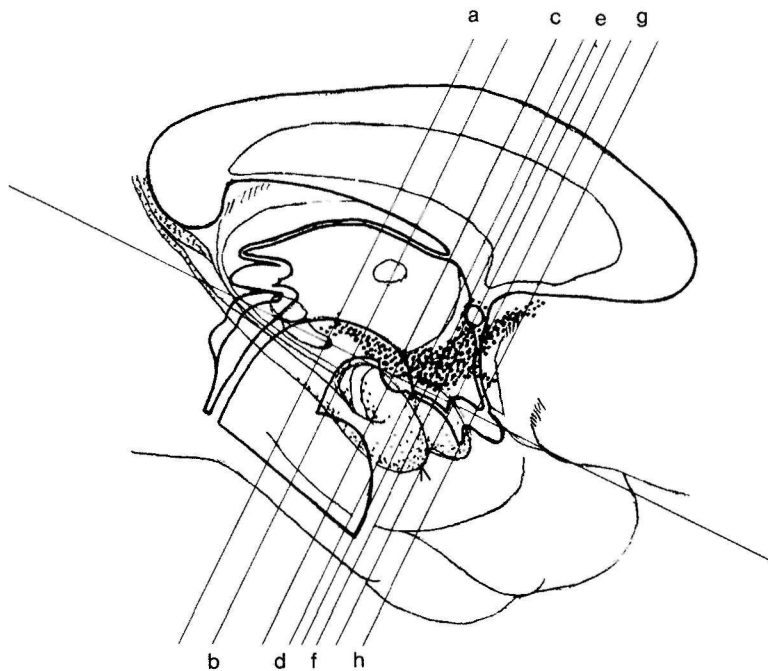


Fig. 2.1 Diagram showing level and plane of sections in Fig. 2.2

rostrocaudal direction in relation to its surrounding structures.

The most rostrally located part of the NBMC is localized in the medial part of the septum verum. Its boundaries are as follows (Fig. 2.2a):

- medial: the median plane of both hemispheres;
- dorsal: nuclei with small-sized neurons in the septum verum;
- lateral: nuclei with small-sized neurons in the septum verum;
- ventral: the diagonal band of Broca.

The septum verum is well developed in the human brain contrary to the dorsally located septum pellucidum [4], and contains several small, rather poorly individualized cell groups. Due to the presence of these ill-defined nuclei no generally accepted nomenclature is available, although the subdivision proposed by Stephan and Andy [127] into a dorsal, ventral, caudal and medial group seems to be acceptable. This medial group can be further

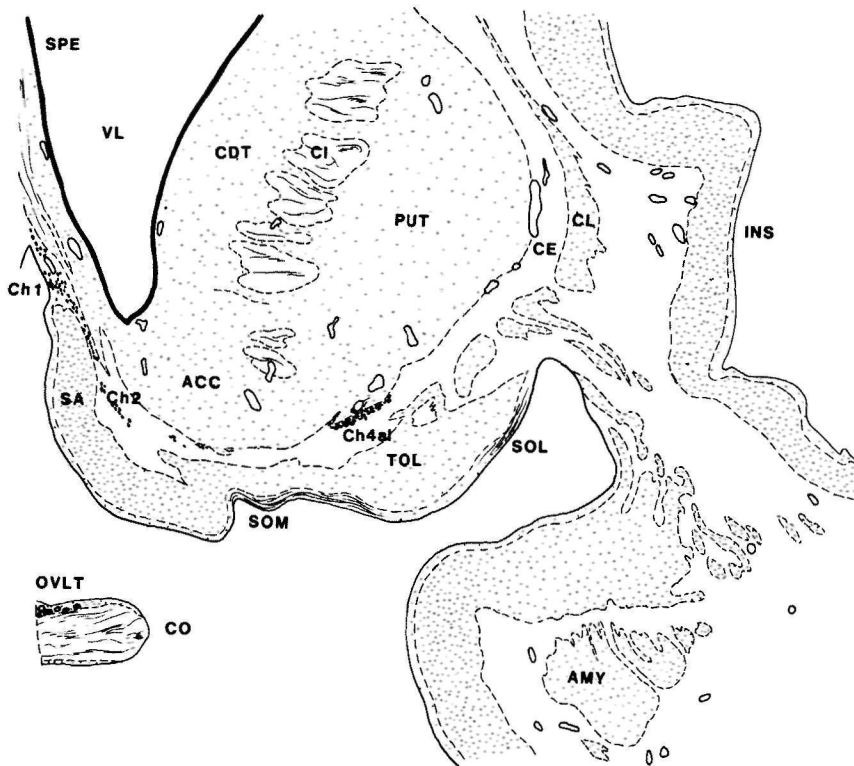


Fig. 2.2a Section through head of caudate nucleus and putamen

subdivided into "the septal component", a small-celled dorsal extension of the most dorsal part of the nucleus of the diagonal band of Broca, and the nucleus septalis medialis consisting of even smaller sized neurons. Only "the septal component" forms part of the NBMC. The parvocellular nucleus septalis medialis has multiple, confusing synonyms in different species in the literature:

- noyau hyperchromatique du septum [33];
- nucleus diagonalis septalis [16];
- nucleus medialis septi [68, 92];
- nucleus parolfactorius medialis [105];
- nucleus septalis medialis [4, 39];
- nucleus septi medialis [6];
- nucleus substantiae innominatae rostralis ascendens [42]; Ch1 [76], the cholinergic neurons in the medial septal nucleus.

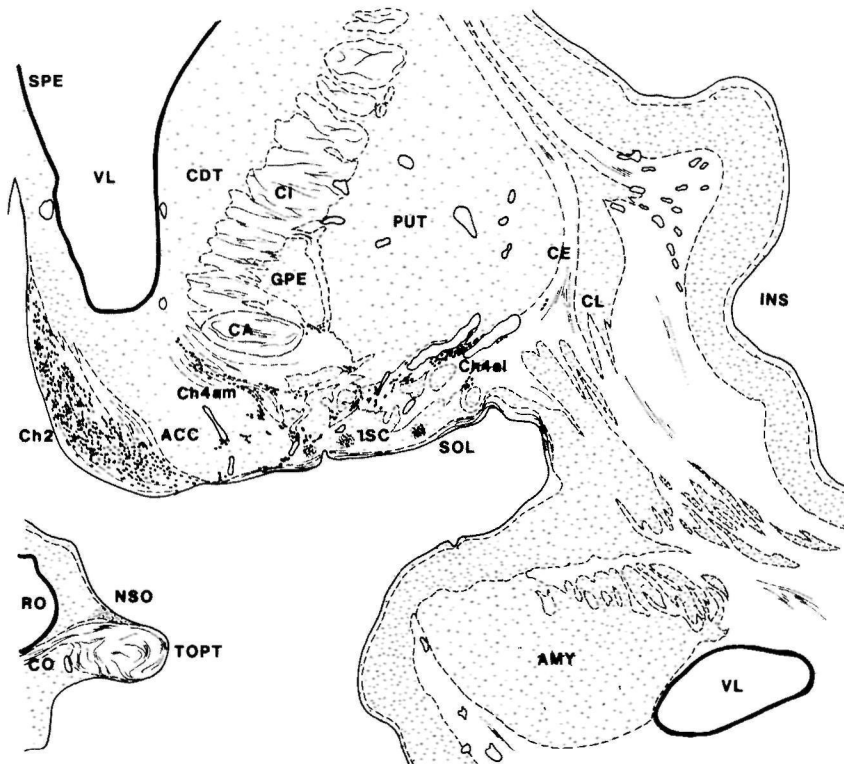


Fig. 2.2b Section through main body of Ch2 and rostral Ch4

The subsequent subdivision of the NBMC is the nucleus of the diagonal band of Broca. This nucleus has a ventrocaudal course, and is delimited by the following structures (Fig. 2.2b):

- dorsal: the medial septal nucleus (Ch1). Its rostradorsal boundary is rather arbitrarily located at the level of the anterior commissure [27];
- medial: subcallosal area and the subarachnoidal space;
- lateral: nucleus accumbens;
- the ventrocaudal boundary of the nucleus of the diagonal band of Broca has been disputed on as well as on the division in subnuclei. Brockhaus [16] distinguished parvocellular and magnocellular nuclei. Other studies subdivided the diagonal band nucleus into a vertical limb nucleus and a horizontal limb nucleus [2, 92]. The horizontal limb nucleus is described as a small band beneath the vertical limb nucleus, extending

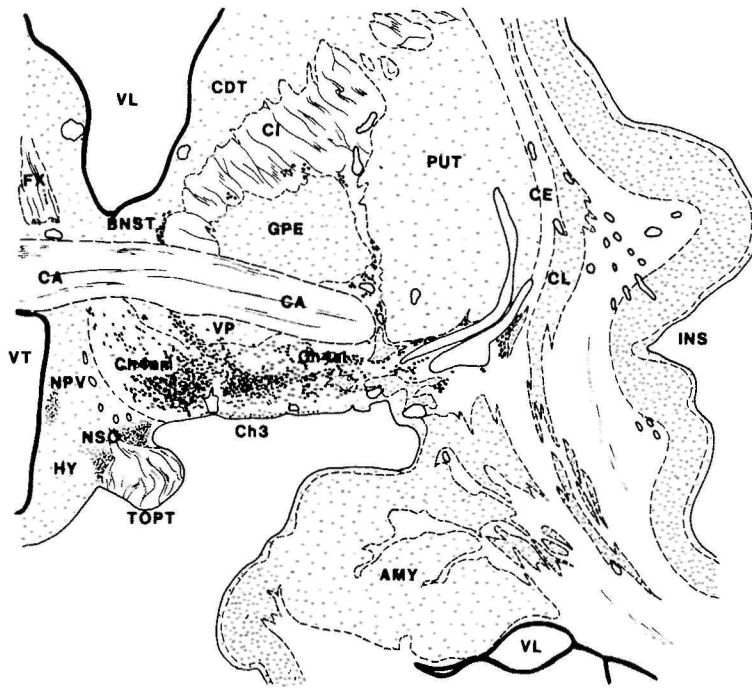


Fig. 2.2c Section through the anterior commissure and Ch4a

caudolaterally and having its greatest expansion between the preoptic region and the amygdaloid region [27, 34, 101]. Meibach and Siegel [72], however, considered the ventral part of the vertical limb nucleus as belonging to the horizontal limb nucleus, whereas De Olmos [27] defined this area as the pars ventralis of the vertical limb nucleus. Mesulam [76] designated the group of cholinergic neurons in the vertical limb nucleus (without the ventral part of this vertical limb nucleus) as Ch2 (Fig. 2.2b), and the cholinergic neurons in the horizontal limb nucleus (defined as a small band without the ventral part of the vertical limb nucleus) as Ch3. This Ch3 group extends caudolaterally to the amygdaloid region (Figs. 2.2c and 2.2d).

The pars ventralis of the vertical limb nucleus of the diagonal band of Broca [27] has been given several synonyms in the literature:

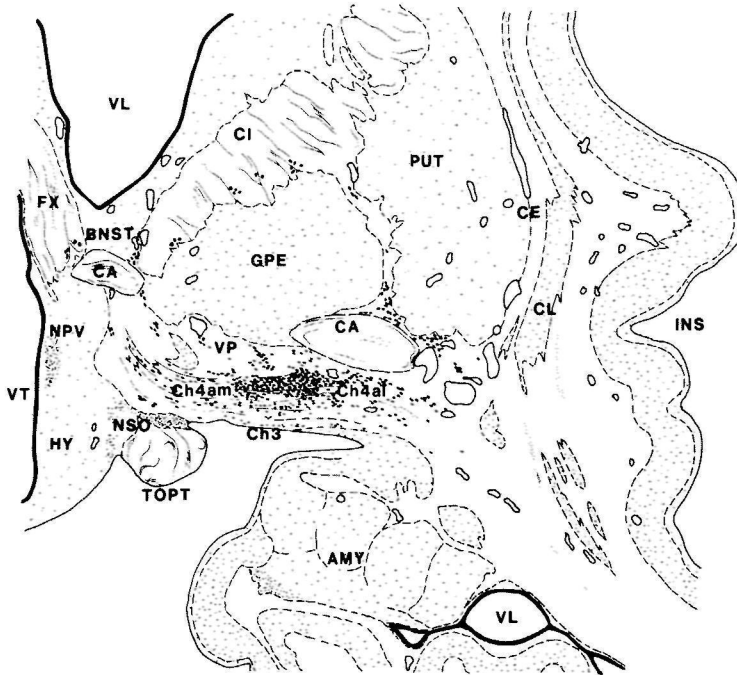


Fig. 2.2d Section through caudal Ch4a

- nucleus diagonalis angularis [16];
 - nucleus substantiae innominatae rostralis angularis [42];
 - segment interstitiel de la bande diagonale de Broca [109];
 - Ch4am [76], the group of cholinergic neurons in the anteromedial part of the nucleus basalis of Meynert (Ch4).
The Ch4am region extends caudally to the ansa lenticularis and is bordered by the following structures:
 - caudal: ansa lenticularis and the Ch4i region (see below);
 - lateral rostral: the olfactory tubercle;
 - lateral caudal: the Ch4al region (see below);
 - dorsal: ventral pallidum (beneath the anterior commissure);
 - medial: lateral preoptic nucleus (lateral hypothalamus);
 - ventral: basal olfactory area and Ch3 region.
- Following the rostrocaudal direction, the rostral part of the Ch4am region borders initially on the olfactory tubercle, but

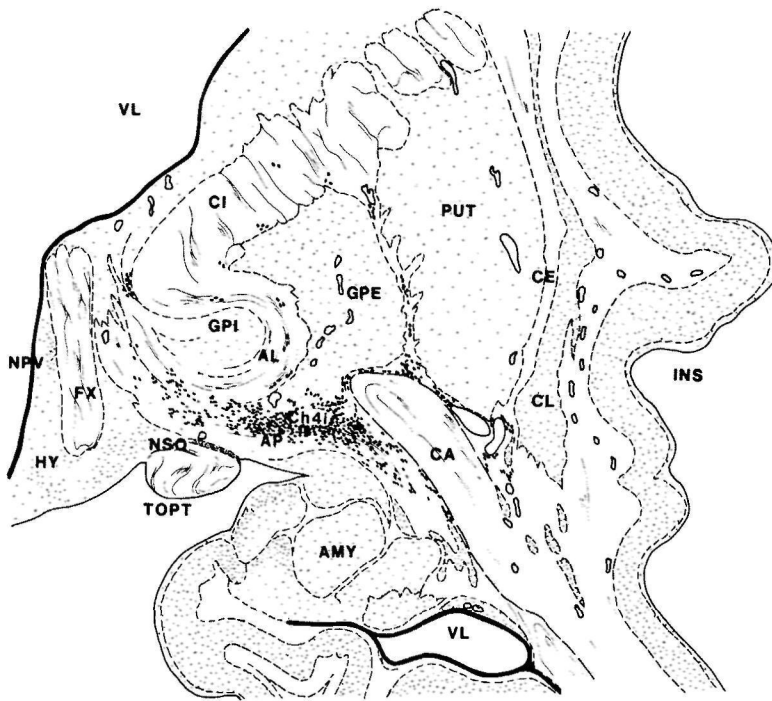


Fig. 2.2e Section through ansa lenticularis and rostral Ch4i

immediately behind the tubercle it extends laterally to the amygdaloid region. This lateral extension of the cholinergic neurons in the the Ch4am region is known as the Ch4al region, the anterolateral part of the nucleus basalis of Meynert [76].

The Ch4al region borders on the following structures:

- rostral: the olfactory tubercle and the basal olfactory area;
- caudal: ansa lenticularis and the Ch4i region (see below);
- lateral: amygdaloid region;
- dorsal: ventral pallidum (beneath the anterior commissure);
- medial: Ch4am group;
- ventral: basal olfactory area and the Ch3 region.

The subdivision of the anterior part of the nucleus basalis of Meynert (Ch4a) into an anteromedial and anterolateral part is rather arbitrarily based upon the presence of a large-sized vessel or a vertically orientated small zone with lower neuron

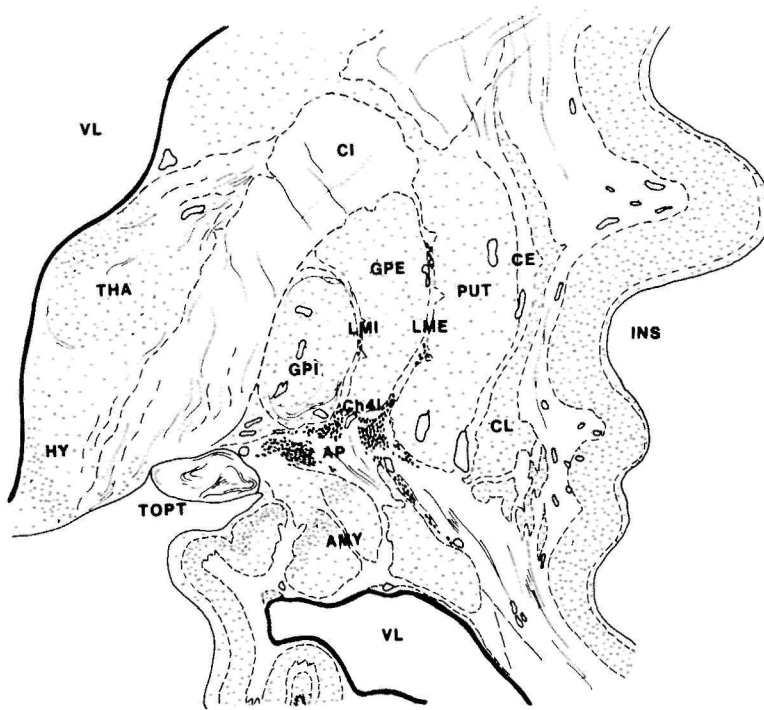


Fig. 2.2f Section through ansa peduncularis and caudal Ch4i

density (Fig. 2.2c). The main characteristic of Ch4a is the high neuron density in the "pars compacta" located in the centre, and the decreasing density towards the periphery of Ch4a, the "pars diffusa" [16, 137]. The most important synonyms for the Ch4a region are:

- nucleus basalis [16];
- nucleus praeopticus magnocellularis [68];
- nucleus substantiae innominatae basalis [42].

The subcommissural part of the substantia innominata (i.e., the ventral pallidum + anterior perforated substance + Ch4a; Figs. 2.2c and 2.2d) extends caudally into the sublenticular part of the substantia innominata (Figs. 2.2e and 2.2f), in which a new subdivision of the NBMC appears extending into caudolateral direction. Again a "pars compacta" and "pars diffusa" can be distinguished (Fig. 2.2e). In the caudal part of this

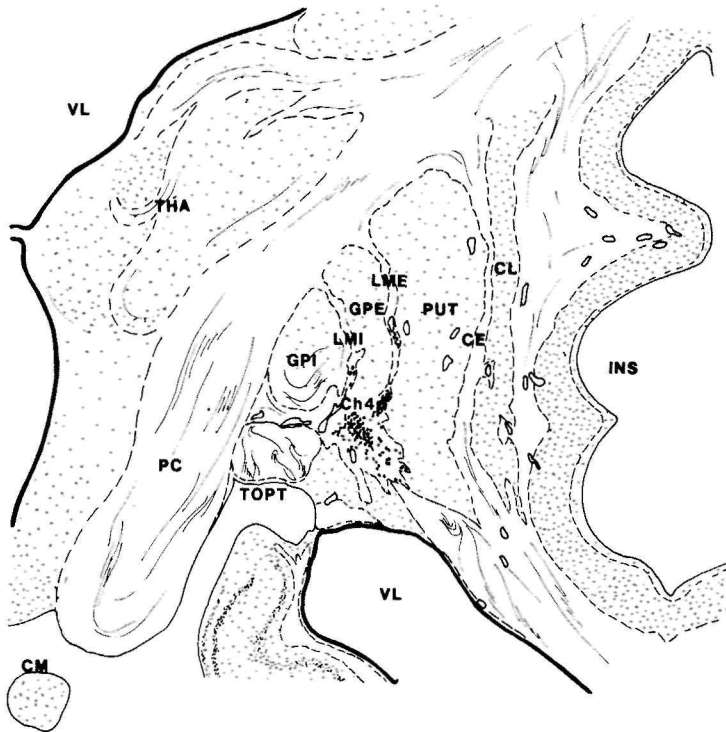


Fig. 2.2g Section through pedunculus cerebri and rostral Ch4p

subdivision the "pars compacta" is being subdivided by the presence of the ansa peduncularis into a ventromedial and a dorsolateral subnucleus (Fig. 2.2f). The boundaries of the sublenticular part of the NBMC are as follows:

- dorsal: globus pallidus (internal and external segment) and the putamen;
- mediorostral: lateral hypothalamic region (Fig. 2.2e);
- mediocaudal: optic tract (Fig. 2.2f);
- ventral: amygdaloid region and amygdala;
- lateral: anterior commissure;
- rostral: Ch4a group;
- caudal: Ch4p group;

This sublenticular part of the NBMC has several synonyms:

- Kern der Linsenkernschlinge [84];
- nucleus ansae peduncularis [9, 92];

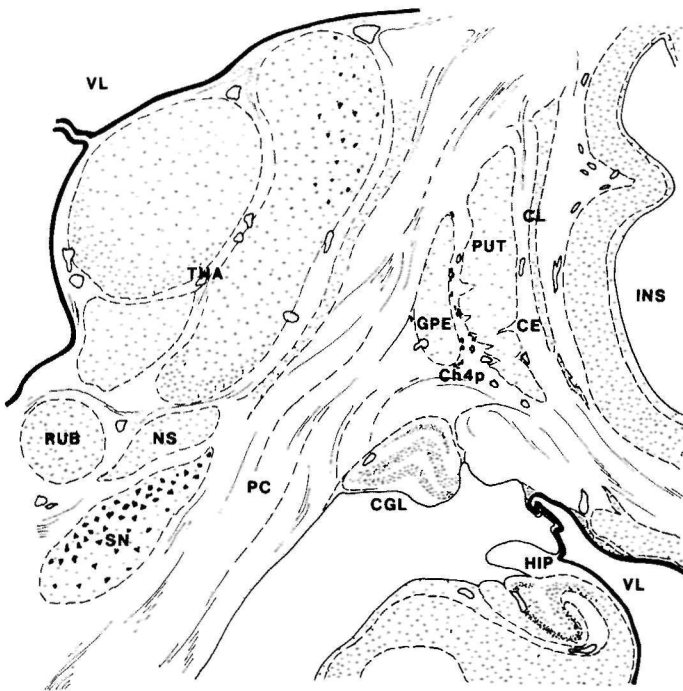


Fig. 2.2h Section through lateral geniculate body and caudal Ch4p

- nucleus substantiae innominatae sublenticularis [42];
- Ch4i [76], the group of cholinergic neurons in the intermediate part of the nucleus basalis of Meynert (Ch4).

The most caudal part of the NBMC is extending caudally from behind the ansa peduncularis to the rostral part of the lateral geniculate body. Even more caudally, small cell clusters are present in the external medullary lamina (Fig. 2.2h). Only Mesulam [76] regarded this posterior part of the NBMC as a separate subdivision and called it the **Ch4p group**, the group of cholinergic neurons in the posterior part of the nucleus basalis of Meynert (Ch4). Others considered this posterior ending of the NBMC as part of respectively the "Kern der Linsenkernschlinge" [84], the "nucleus substantiae innominatae sublenticularis" [42], or the "nucleus ansae peduncularis" [92].

The more-or-less continuous band of cholinergic neurons of

the nucleus basalis Meynert complex (NBMC) has several extensions:

- the most prominent extension is located lateral from the Ch4a1 and extends rostrally beneath the putamen to the frontal plane that shows the rostral beginning of the Ch2 group (Fig. 2.2a). Ayala [10] regarded this extension as a separate nucleus, the subputaminal nucleus.
- another extension from the Ch4a group crosses through the ventral pallidum in a caudodorsal direction, passing the anterior commissure posteriorly to end at the medial edge of the internal capsule (Fig. 2.2c).
- several small extensions of the Ch4 group can be distinguished: the external capsule (Fig. 2.2c), the internal and external medullary laminae (Figs. 2.2c-h) and ventral to the lateral anterior commissure (Figs. 2.2e-f).

Solitary magnocellular neurons showing similar cytology can be demonstrated in the olfactory tubercle (Fig. 2.2b) and the islands of Calleja within the olfactory tubercle [132], the fornix (Fig. 2.2c-d), the internal capsule (Figs. 2.2c-e) and the nucleus accumbens [45] (Fig. 2.2b).

After several initial reports on cholinergic properties of the magnocellular neurons of the human NBMC [36, 86, 95, 98, 113], it was recently demonstrated that 80-90% of the magnocellular neurons in this complex stain positively for choline acetyltransferase in the human brain [82]. In the present study the nomenclature of Mesulam [76] will be adopted. However, it should be explicitly mentioned that, whenever the Ch-prefix is used, not only cholinergic neurons but also noncholinergic neurons are included.

2.1.2 Cytology of the human NBMC

In cresyl-fast violet-staining the characteristic neurons of the Ch1-Ch4 system stand out sharply from their surroundings because of their large size and the intense (hyperchromatic) staining of their Nissl material. Many small neurons are

intermingled between the magnocellular neurons, especially in the Ch1 and Ch2 region.

The Ch1 region (medial septal nucleus) is composed primarily of small to medium sized (10-25 μm in diameter), mostly round neurons. It contains relatively few magnocellular neurons. Many of the smaller neurons are so hyperchromatic in Nissl-stain that their nuclei (and nucleolus) are difficult to distinguish. Only few, large and fusiform neurons, show a clear nucleus with a prominent nucleolus.

The Ch2 region (vertical limb nucleus of the diagonal band of Broca) is also composed primarily of hyperchromatic, but larger neurons with a clearly visible, ellipsoid, eccentric nucleus with a prominent dark nucleolus. The neurons tend to be orientated parallel to the ventrolaterally sweeping fibers of the diagonal band.

Contrary to the Ch4 region, the Ch3 region (horizontal limb nucleus of the diagonal band of Broca) consists of smaller (10-20 μm), more fusiform, relatively hypochromatic, and less densely packed neurons. These neurons are irregularly scattered among the fibers of the diagonal band, which run along the floor of the basal forebrain underlying the Ch4a region.

Both the Ch4a and Ch4i region are cytologically characterized by large and very large (25-50 μm), hyperchromatic neurons with a clearly visible, large (10-15 μm) and eccentric nucleus containing a conspicuous nucleolus. Also small neurons are present. Neuronal shape is distinctly heterogeneous, varying from fusiform and polygonal to predominantly ellipsoid. Aggregates of Nissl material are often located in one or more foci at the periphery of the perikaryon, while smaller deposits occur throughout the rest of the cytoplasm. From the centre of the Ch4a and Ch4i region towards the periphery cell size gradually decreases.

The Ch4p region is primarily composed of hyperchromatic, medium-sized neurons (10-25 μm), that show almost equally intense staining of the cytoplasm and nucleus, among several magnocellular neurons with a clearly visible nucleus and nucleolus.

Using Golgi material, two main classes of neurons have been distinguished within the NBMC, namely medium-sized reticular

neurons and large multipolar neurons [7]). The reticular type was found to be the most predominant. In combined pigment-Nissl preparation, three types of neurons could be defined on behalf of lipofuscin content and cell size [136]. Large neurons with a moderate number of small, faintly stained lipofuscin granules predominated above almost evenly large neurons with dense accumulations of intensely stained lipofuscin granules. The third type showed a small soma size, small amounts of basophilic material, and a few faintly stained lipofuscin granules. The possible importance of morphologic studies [7, 136] describing different neuronal types and their ratios to each other, still have to be evaluated in neurodegenerative diseases such as Alzheimer's and Parkinson's disease associated with dementia.

2.1.3 Chemoarchitecture of the primate and human NBMC

With the use of antibodies to the specific cholinergic marker choline acetyltransferase (ChAT), it has been firmly established that most large neurons in the NBMC are cholinergic [44, 76, 114, 115]. Many large neurons of the NBMC also show galanin-like immunoreactivity [23, 73, 138, 143]. The majority of the cholinergic neurons stain with antibodies for nerve growth factor receptor (NGF-r) in the NBMC in the monkey [61, 119] and human CNS [47, 63, 83]. Intermingled among the cholinergic magnocellular neurons of the NBMC, smaller neurons are present [45, 53, 139], most of which are not cholinergic [76, 143]. In the NBMC of primates it has been shown, that fibers and/or putative nerve terminals on cholinergic neurons, and/or small noncholinergic neurons may demonstrate immunoreactivity against:

- cholecystokinin octapeptide [20];
- enkephalin [20, 40, 41, 143];
- neuropeptide Y [125, 143];
- neurotensin [71, 131, 143];
- oxytocin [20];
- proopiomelanocortin peptides [20, 55];
- somatostatin [12, 20, 143];

- substance P [20, 41];
- vasoactive intestinal polypeptide [20].
- γ -Aminobutyric acid (GABA) containing neurons have been demonstrated in the rat [15] and cat basal forebrain [32], but not in the primate or human NBMC.

No information is yet available on the coexistence of peptides with one another in small neurons of the basal forebrain, as has been demonstrated e.g. for somatostatin and neuropeptide Y in neurons of the hippocampus and cortex [22]. The function of small peptidergic neurons in the NBMC is unclear. The presence of peptidergic axonal "boutons" on cholinergic neurons suggests that small cells could act as local-circuit neurons to possibly regulate the cholinergic activity. The neuropeptidergic fibers in the NBMC could be part of fiber tracts passing through or terminating in the NBMC. These fiber tracts appear to be largely derived from the bed nucleus of the stria terminalis and the amygdala, two centres where many neuropeptide containing cell bodies have been demonstrated [89, 145].

In Alzheimer's disease significant reductions in ChAT enzyme activity in the NBMC correlate with cell counts and reduced cell size in the NBMC [19, 95, 97]. Moreover, a down regulation of cholinergic function of Ch4 has been suggested by galanin hyperinnervation of the remaining cholinergic neurons [24], whereas decreased galanin innervation has been proposed in Ch2 [138]. A further decrease in cholinergic activity in Alzheimer's disease is suggested by selectively reduced gene expression for nerve growth factor receptors within cholinergic neurons of the NBMC [48], nerve growth factor being known to promote growth of NBMC cholinergic neurons and to prevent their atrophy and death [46]. The possible pathogenic role of the small peptidergic, noncholinergic neurons in the NBMC in Alzheimer's disease has been speculated on, but still needs clarification, and remains an important area for future research.

2.1.4 Connections of the nonhuman primate NBMC

Visualization of cholinergic pathways in the brain became possible using histochemical staining methods for acetylcholinesterase (AChE) [54, 58]. For instance, undercutting of the cat cerebral cortex resulted in loss of cortical AChE-positive fibers in the overlying cortex, suggesting the existence of cholinergic neurons extrinsic to the neocortex and probably within the basal forebrain [43, 67, 122]. However, the specificity of AChE as a marker of cholinergic neurons was seriously questioned by the demonstration that catecholaminergic neurons also stained intensely for this enzyme [17]. Direct visualization of cholinergic pathways in the brain by immunocytochemical staining methods for the acetylcholine synthesizing enzyme choline acetyltransferase (ChAT) was hindered by difficulties in obtaining a sufficiently purified preparation of ChAT in order to raise specific monoclonal antibodies. In most mammals ChAT represents only between one millionth and one hundred thousandth of the total brain protein content [107, 108]. Nevertheless, several research groups were able to generate monoclonal antibodies to ChAT [25, 29, 85, 141] and a wealth of information on cholinergic pathways in the brain has now become available in the mammalian brain. In this section the efferent and afferent pathways of the nonhuman primate NBMC will be reviewed, since they are believed to reflect most closely the putative pathways in the human brain.

2.1.4.1 Efferent connections of the nonhuman primate NBMC

In primates, magnocellular AChE-rich and ChAT-immunoreactive neurons are located in the NBMC [44, 76, 77, 114, 115]. Lesions of the NBMC in primates cause significant reductions in ChAT and AChE activities in the cortex [128]. Using retrograde and anterograde transport tracing techniques, anatomical studies in monkeys have shown that the large NBMC neurons project to amygdala [53, 59, 62], hippocampus [2, 53, 59, 76], thalamus [50,

93], caudate nucleus [8], brainstem [93], and in a crudely topographical fashion to the entire neocortex [28, 51, 56, 57, 74, 76, 91, 94, 133, 134, 142, 144].

The subdivisions of the NBMC, the contiguous cell groups Ch1-Ch4, give rise to the following cholinergic projections:

1. Ch1 provides a substantial projection to the hippocampus, especially the Ammon's horn, the dentate gyrus, the subicular complex and the entorhinal cortex [2, 51, 59, 76]. The fibers pass via the fimbria/fornix [57]. Contrary to rats [31], no cholinergic pathway has yet been demonstrated in nonhuman primates via the stria terminalis and the habenulointerpeduncular tract to the interpeduncular nucleus and ventral tegmental area.

2. Ch2 is the major source of cholinergic innervation that the hippocampal formation (Ammon's horn, dentate gyrus, subicular complex, entorhinal cortex) receives from the NBMC [2, 51, 57, 59, 76]. Fibers enter the hippocampus mainly via the ventral pathway, coursing through the entorhinal cortex and subiculum prior to entering the prosubiculum and the hippocampus proper [2, 57, 146]. Ch2 projects heavily to the lateral hypothalamus [76] and several cortical areas [53] as the cingulate cortex [57, 59, 76], the subcallosal area, the parahippocampal gyrus [76] and the visual cortex [134, 144]. Moreover, Ch2 projects to the head of the caudate nucleus [8], to the reticular, mediodorsal, anteroventral/anteromedial and ventromedial (RE, MD, AV/AM, VM) thalamic nuclei [50, 93], and to the pedunculopontine region in the brainstem [93].

3. Ch3 is the major source of cholinergic innervation of the olfactory bulb [76]. Moreover, it has a substantial projection to the magnocellular basal nucleus of the amygdala [3] and minor projections to the head of the caudate nucleus [8], to the hippocampus [59], to the hypothalamus [76], to the reticular and mediodorsal thalamic nucleus [50, 93], and to the pedunculopontine region in the brainstem [93].

4. Ch4_{am}, the anteromedial part of the nucleus basalis of Meynert, projects mainly to the medial surface of the hemispheres, including the cingulate cortex [59, 76]. Lesser, but substantial projections were directed to the hypothalamus,

hippocampal formation, ventral part of somatosensory cortex, ventrolateral orbital, middle insular, peristriate, and parahippocampal regions as well as the inferior parietal lobule [76]. A prominent projection to the amygdala (magnocellular part of the basal nucleus) has been demonstrated [3, 62, 76] as well as minor projections to RE, MD, AV/AM and VM thalamic nuclei [50, 93], the head of the caudate nucleus [8] and to the pedunculopontine region in the brainstem [93].

5. **Ch4al**, the anterolateral part of the nucleus basalis of Meynert, is the principal source of cholinergic projections to frontoparietal opercular regions and to the amygdala [3, 59, 62, 76]. Additional substantial projections were directed to the olfactory bulb, medial frontal pole, dorsomedial motor cortex, ventrolateral orbital cortex, insula, inferotemporal area, and the parahippocampal gyrus [59, 76]. Small projections were directed to RE, MD, AV/AM and VM thalamic nuclei [50, 93], the head of the caudate nucleus [8] and to the pedunculopontine region in the brainstem [93].

6. **Ch4i**, the intermediate part of the nucleus basalis of Meynert, provides prominent cholinergic inputs to ventrolateral orbital, insular, dorsal prefrontal, peristriate, inferotemporal, parahippocampal areas as well as the the inferior parietal lobule [57, 76]. Substantial projections were directed to medial frontal pole, dorsomedial motor cortex, frontoparietal opercular areas, the amygdala, anterior auditory cortex, and the temporal pole [59, 62, 76].

7. **Ch4p**, the posterior part of the nucleus basalis of Meynert, demonstrates rather circumscript projection patterns to the auditory association areas in the superior temporal gyrus, to the temporal pole, and to the entorhinal cortex [76, 80, 82], entering the hippocampal formation via the ventral cholinergic pathway [146]. Substantial projections were directed to inferotemporal and posterior insular regions [76], and minor projections to the amygdala [59].

8. Projections to the contralateral hemisphere are very rare [57, 76, 77, 94, 142]. Only occasional AChE-positive, ChAT-immunoreactive fibers or autoradiographically labeled axons were

demonstrable in the anterior commissure and corpus callosum [57].

The cholinergic efferent projections course through five major pathways to reach their neuronal targets within monkey amygdala, hippocampus and neocortex [57]:

- medial pathway: axons directed rostrally pass through the Ch2 and Ch1 region, bend around the rostrum and genu of the corpus callosum to enter the cingulate bundle, innervating cingulate cortex and medial parts of frontal and parietal cortices.
- lateral pathway: at Ch4a and Ch4i, many fibers assemble laterally beneath the globus pallidus and putamen, transverse the external and extreme capsules, spread out within the corona radiata and innervate parts of the insular and dorsolateral segments of the temporal, parietal and occipital cortices. The medial and lateral pathways have also been described in human brain [113].
- ventral pathway: at Ch4a and Ch4i, axons project ventrally beneath the lateral parts of the anterior commissure to the temporal lobe to innervate the hippocampus and amygdala.
- rostral pathway: via the orbitofrontal fibers cholinergic axons appear in the fasciculus and tractus olfactorius to innervate rostral frontal and olfactory cortices.
- fimbria/fornix pathway: via this pathway NBMC neurons project to the hippocampal formation. The ventral pathway seems to be the major source of cholinergic input to the primate hippocampus [2, 57, 76], whereas in rodents the fimbria/fornix pathway seems to be the most important input pathway [112].

The topographical arrangement of Ch4 connectivity is complex and shows considerable overlap [53, 57, 59, 74, 76, 94, 142]. As compared to the thalamocortical connections, the boundaries of the subdivisions of the NBMC are not as sharply delineated as in the thalamic nuclei, nor does the organization of projection of the Ch4 follow a functional delineation as is the case in thalamocortical projections, where a segregation exists of sensory, motor, association, and limbic connections [88]. The intermingling of NBMC neurons projecting to different cortical areas suggests collateralization. However, no double labeling of cholinergic neurons in the NBMC was observed after tracer

injections in different cortical areas [76, 142]. Nevertheless, double labeled neurons have been demonstrated in the monkey Ch4a, projecting to both the thalamus and pedunculopontine region [93], or projecting to both orbitofrontal cortex and thalamus [50]. In rat, it has been demonstrated that individual NBMC neurons project to very restricted areas of 1-2 mm within the cortex [13, 64, 103, 112] and that these neurons show small clusters of short axon collaterals originating near the perikaryon [64]. This local type of coordination could also be carried out by basal forebrain interneurons [23, 24, 143].

In primates, regional variations in cortical cholinergic innervation are apparent, with the hippocampus, amygdala and piriform regions showing the highest levels of cortical AChE-fibers. The paralimbic regions such as the insula, caudal orbitofrontal cortex, the temporal pole, and the parahippocampal gyrus receive heavier cholinergic innervation than the adjacent association cortical areas [65, 78, 81]. The same AChE-distributions have been demonstrated in the human except for the paralimbic region of the cingulate cortex, that contained high levels of cholinergic markers in the human but not in the monkey [82]. Laminar variations of cortical cholinergic innervation exists among different regions within and across species, but no conclusive remarks can yet be made on this issue [for review: 49]. For instance, in the rat cerebral cortex 13 different laminar patterns of ChAT-staining can be found [70].

In human controls, the ChAT-activity is highest at the level of layers II and IV of the temporal and frontal cortex, whereas in Alzheimer's disease the topographical laminar distribution of ChAT-activity seems completely lost [96, 126]. No data of laminar distribution of ChAT-activity in the parietal and occipital human cortex are available.

2.1.4.2 Afferent connections of the nonhuman primate NBMC

The subdivisions of the NBMC, the contiguous cell groups Ch1-Ch4, receive the following neuronal inputs:

1. In rat, the Ch1 and Ch2 subdivisions, i.e., the medial septal complex comprised of the medial septal nucleus and the vertical limb nucleus of the diagonal band of Broca, receive a massive projection from the lateral septal nucleus [129] and a further wide variety of afferents, including the anterior hippocampus, the hypothalamus, ventral tegmental area, the median raphe, the locus coeruleus, and the dorsal tegmental nucleus [121]. In primates and man, studies of the septal nuclei have been scarce and almost exclusively limited to cytoarchitectonic analyses. In the macaque, hippocampal efferents terminate densely in the medial (Ch1), lateral and dorsal septum, and in the Ch2 region [1]; moreover, innervating amygdalofugal fibers have been demonstrated [1, 110]. In man, the Ch1 and Ch2 region show noradrenergic terminals on cholinergic neurons [35].

2. Ch3, the horizontal limb nucleus of the diagonal band of Broca, receives neuronal input from the central nucleus of the amygdala [38, 102, 110]. Whether the Ch3 region receives substantial input from other structures than the amygdala, is not clear: most studies concerning afferent connections of the cholinergic basal forebrain system are either restricted to the Ch4 region proper or do not differentiate between the Ch4 region and the underlying Ch3 cell group.

3. In primates, the Ch4 region receives neuronal input from a variety of cortical and subcortical sources [52, 53, 66, 79, 90, 102, 110, 111]. The cortical input arises from the orbitofrontal cortex, entorhinal area and perirhinal cortex, the temporopolar and temporosuperior cortex, the prepiriform cortex, and the anterior insula. The subcortical afferents of the Ch4 region originate from the lateral and medial septum complex (Ch1 and Ch2), nucleus accumbens and ventral pallidum, the medial hypothalamus, the thalamus (especially the central and midline thalamic nuclei), the amygdala (particularly the basal nuclei), the peripeduncular nucleus, the pars compacta of the substantia nigra, the mesencephalic raphe nuclei, the parabrachial nuclei, and the locus coeruleus.

4. Concerning the subdivisions of the Ch4 region (Ch4am, Ch4al, Ch4i and Ch4p) the cortical neuronal input patterns to Ch4al and

Ch4i are broadly similar. From the prefrontal and orbitofrontal areas Ch4al and Ch4i receive the highest neuronal input, Ch4am receives less, and Ch4p lacks frontal afferents. From the entorhinal and perirhinal cortex Ch4al and Ch4i receive dense innervation, but the Ch4am and Ch4p lack neuronal input. From temporopolar and superior temporal areas Ch4p receives the highest input, Ch4i less, Ch4al the least, and Ch4am nothing at all. The prepiriform cortex innervates all Ch4 subdivisions except the Ch4p region. The anterior insula innervates all Ch4 subdivisions except the Ch4am region [52, 79]. The subcortical neuronal input to the Ch4 subdivisions is almost similar, except for the medial septal complex (Ch1 and Ch2) that does not innervate the Ch4p region [52, 79].

2.1.5 Functional considerations of the NBMC

From the efferents and the afferents of Ch1 and Ch2, it appears that the septal nuclei (medial and lateral septal nucleus, vertical limb nucleus of the diagonal band of Broca) form part of a number of neuronal loops which also include the hippocampal formation, the hypothalamus and some monoaminergic brain stem nuclei as nodal points [52, 79]. The amygdala, which projects heavily on the Ch4 region, receives itself substantial neuronal input from the Ch4 region [1]. Although the hippocampus sends only very few direct projections to Ch4, it may nevertheless exert considerable indirect effects upon this area, either via the amygdala [100] or via the lateral septum, both of which project heavily throughout the Ch4 [79]. Although the Ch4 complex projects to all parts of the neocortical mantle, the great majority of the Ch4 connections with the neocortex is not reciprocal [52, 79]. The cortical projections into Ch4 arise from orbitofrontal, temporal, prepiriform, anterior insular and entorhinal areas. Additional subcortical projections originate in the amygdala, medial hypothalamus, the septal nuclei and the nucleus accumbens - ventral pallidum complex. The one common characteristic of these neuronal inputs into Ch4 is that they

originate in limbic and paralimbic structures. This connectivity pattern implicates, that the few cortical areas with reciprocal connections to Ch4 can potentially influence not only the level of cholinergic signals they receive but also the cholinergic innervation of other parts of the neocortex.

The responsivity of Ch4 neurons to the sight and taste of food [26, 106] implies that they must be receiving complex sensory information in several modalities. Several potential routes can be indicated for this sensory input. Olfactory information can reach Ch4 neurons from the primary olfactory cortex in the prepiriform region. Gustatory and visceral information might be relayed through projection from the anterior insula into Ch4 [75]. Auditory input could reach Ch4 from the anterior portions of the superior temporal region, and visual information via the medial inferotemporal region. Additional sensory information could be relayed by the amygdala. All the structures that project to the Ch4 region are integrative regions of extensive sensory preprocessing or regions of polysensory convergence [79, 110]. The hodologic organization of the Ch4 complex suggests that it is in a position to act as a cholinergic relay for transmitting predominantly limbic and paralimbic information to the neocortex in a fashion that may influence complex behaviour (integrated motor or emotional responses, learning and memory) according to the prevailing emotional and motivational states encoded by the limbic and paralimbic regions of the brain.

The supposed correlation of the Ch4 complex with higher mental functions is supported by its phylogenesis. From comparative anatomy it is known that the Ch1-Ch4 complex becomes progressively larger and more complex with increasing cerebralization, reaching maximum volume and differentiation in species with the greatest neocortical development such as primates and man [37, 120]. Additionally, pharmacological studies and animal lesion studies of the Ch4 complex support the role of the Ch4 region in higher cognitive function and have led to the formulation of "the cholinergic hypothesis of dementia". Moreover, neuropathological studies demonstrate the involvement of the Ch4 complex in dementing diseases such as Alzheimer's disease.

2.2 Neuroanatomy of the human supraoptic nucleus

In man the supraoptic nucleus (SON) is made up of three parts: a dorsolateral, a dorsomedial and a ventromedial part [16, 30]. The dorsolateral part is the largest of the three, and it is situated most rostrally. Throughout its entire length [5-10 mm, 104, 140] the SON is closely associated with the posterior portions of the optic chiasm and adjacent portions of the optic tract (Figs. 2.2b-e). The SON consists of densely packed multipolar neurons that are evenly dispersed within the limits of the nuclear gray. The SON is extremely vascular. The large SON neurons possess a light, large and eccentric positioned nucleus containing a conspicuous nucleolus. Flocks of Nissl material are often located in one or more foci at the periphery of the perikaryon. Vacuoles of varying size often are present in peripheral portions of the cell body.

The SON projects exclusively along the supraoptico-hypophyseal tract to the posterior pituitary [130], where its neurohormones vasopressin and oxytocin are released into the blood vessels of the neurohypophysis [11].

The afferents to the SON originate from:

- bed nucleus of the stria terminalis [130];
- some catecholaminergic centres in the brain stem (including the noradrenergic locus coeruleus, A1 and A2 cell groups, and the adrenergic C1 and C2 cell groups [117, 118]);
- the hypothalamic dorsomedial nucleus and median preoptic nucleus [116];
- the preoptic region, including the organum vasculosum of the lamina terminalis and the subfornical organ [69, 123].

In summary, it appears that a rather small number of cell groups in the limbic regions of the telencephalon, the brain stem and the hypothalamus provide most of the neural inputs to the SON. The evidence that humoral factors, except in the case for gonadal steroids, directly influence cells in the SON is not so strong [130].

2.3 Neuroanatomy of the human paraventricular nucleus

In man the paraventricular nucleus (PVN) lies closely to the inner surface of the third ventricle as an elongated plate of cells. The rostrocaudal axis of this nucleus is orientated infero-superiorly, extending from the wall of the recessus opticus to the latitude of the interventricular foramen of Monro [16, 30, 87]. Its lateral border is relatively ill-defined. While the SON is made up of uniformly large neurons, the PVN is a composite nucleus composed of cells of diverse size and shape [14]. Cytologically, the Nissl-substance is distributed peripherally in a compact manner. In the cytoplasm vacuoles of varying diameter can be present, giving the neurons an irregular, bulging appearance. The relatively dark nucleus is rather difficult to distinguish, but a large round nucleolus is prominently present in the centre.

In addition to the magnocellular neurosecretory neurons (projecting along the paraventriculo-hypophyseal tract to the posterior pituitary [130], where the neurohormones vasopressin and oxytocin are released into the blood vessels of the neurohypophysis [11]), the PVN contains numerous smaller peptidergic elements, that can be subdivided into:

- a parvocellular neurosecretory system, the fibers of which pass to the external lamina of the median eminence, where their terminals contact the hypophyseal portal capillaries [5]. This subpopulation comprises vasopressinergic neurons and elements containing corticotrophin releasing factor [69];
- and a parvocellular descending projecting system, consisting of thin unmyelinated, mainly oxytocinergic fibers, which innervate a number of autonomic centres in the brain stem and the spinal cord [130].

The afferents to the PVN closely correspond to those to the SON, however, the PVN has additional sources of local hypothalamic input from the suprachiasmatic nucleus, the anterior hypothalamic area, from parts of the lateral hypothalamic area, and from the anterior and ventromedial hypothalamic nuclei [88, 130].

In summary, the primary functions of the SON and PVN are probably best viewed in relation to the magnocellular neurosecretory projections to the posterior lobe of the pituitary: vasopressin is responsible for antidiuresis, promoting reabsorption of water by the kidney, and oxytocin stimulates uterus smooth muscle and mammary glands to contract. In addition, however, the PVN has a second component, which is part of the parvocellular neurosecretory system, that regulates the output of the anterior pituitary, and a third component that modulates autonomic reflexes, which are mediated by circuitry in the brain stem and spinal cord.

2.4 Neuroanatomy of the human organum vasculosum of the lamina terminalis

The organum vasculosum of the lamina terminalis (OVLT) is an unpaired structure situated immediately dorsal to the optic chiasm (Fig. 2.2a). Like the other circumventricular organs as the subfornical organ, the median eminence of the hypothalamus, the neurohypophysis, the pineal body and the area postrema, the OVLT is highly vascularized and lacks a blood-brain barrier [21, 88]. Capillary fenestrations provide specific sites for the transfer of proteins and solutes, irrespective of molecular size and lipid solubility. The neurons in the OVLT are therefore influenced by neuronal afferents, and by substances of the cerebrospinal fluid and plasma-derived substances as well. The OVLT has a role in the control of gonadotrophin secretion [99] and of water-electrolyte balance and blood-pressure regulation [124]. In rats the OVLT receives substantial afferents from the subfornical organ, several hypothalamic nuclei and the locus coeruleus [18, 69]; the OVLT has projections to the dorsomedial, supraoptic and paraventricular hypothalamic nuclei [69, 123].

2.5 References

1. Aggleton JP, Friedman DP and Mishkin M. A comparison between the connections of the amygdala and hippocampus with the basal forebrain in the macaque. *Exp Brain Res* 1987;67:556-8.
2. Amaral DG and Cowan WM. Subcortical afferents to the hippocampal formation in the monkey. *J Comp Neurol* 1980;189:573-91.
3. Amaral DG and Basset JL. Cholinergic innervation of the monkey amygdala: an immunohistochemical analysis with antisera to choline acetyltransferase. *J Comp Neurol* 1989;281:337-61.
4. Andy OJ and Stephan H. The septum in the human brain. *J Comp Neurol* 1968;133:383-410.
5. Antunes JL, Carmel PW and Zimmerman EA. Projections from the paraventricular nucleus to the zona externa of the median eminence of the rhesus monkey: an immunohistochemical study. *Brain Res* 1977;137:1-10
6. Arendt T, Bigl V, Arendt A and Tennstedt A. Loss of neurons in the nucleus basalis of Meynert in Alzheimer's disease, paralysis agitans and Korsakoff's disease. *Acta Neuropathol* 1983;61:101-8.
7. Arendt T, Zvegintseva HG and Leontovich TA. Dendritic changes in the basal nucleus of Meynert and in the diagonal band nucleus in Alzheimer's disease - A quantitative Golgi-investigation. *Neurosci* 1986;19:1265-78.
8. Arikuni T and Kubota K. Substantia innominata projection to caudate nucleus in macaque monkeys. *Brain Res* 1984;302:184- 9.
9. Averbach P. Lesions of the nucleus ansae peduncularis in neuropsychiatric disease. *Arch Neurol* 1981;38:230-5.
10. Ayala G. A hitherto undifferentiated nucleus in the forebrain (nucleus subputaminalis). *Brain* 1915;37:433-48.
11. Bargmann W and Scharrer E. The site of the hormones of the posterior pituitary. *Am Sci* 1951;39:255-9.
12. Bennett-Clarke CA and Joseph SA. Immunocytochemical localization of somatostatin in human brain. *Peptides* 1986;7:877-84.
13. Bigl V, Woolf NJ and Butcher L. Cholinergic projections from the basal forebrain to frontal, parietal, temporal, occipital, and cingulate cortices: a combined fluorescent tracer and acetylcholinesterase analysis. *Brain Res Bull* 1982;8:727-49.
14. Braak H and Braak E. The hypothalamus of the human adult: chiasmatic region. *Anat Embryol* 1987;176:315-30.
15. Brashaer HR, Zaborsky L and Helmer L. Distribution of GABAergic and cholinergic neurons in the rat diagonal band. *Neurosci* 1986;17:439-51.
16. Brockhaus H. Vergleichend-anatomische Untersuchungen über den Basalkern-complex. *J Psychol Neurol.* 1942;51:57-95.
17. Butcher LL, Talbot K and Bilezikjian L. Acetylcholinesterase neurons in dopamine-containing regions of the brain. *J Neural Transm* 1975;37:127-53.
18. Camacho A and Philips MI. Horseradish peroxidase study in rat of neural connections of the organum vasculosum of the lamina terminalis. *Neurosci Lett* 1981;25:201-4.
19. Candy JM, Perry RH, Perry EK, Irving D, Blessed G, Fairbairn AF and Tomlinson BE. Pathological changes in the nucleus of Meynert in Alzheimer's and Parkinson's diseases. *J Neurol Sci* 1983;54:277-89.
20. Candy JM, Perry RH, Thompson JE, Johnson M and Oakley AE. Neuropeptide localisation in the substantia innominata and adjacent regions of the human brain. *J Anat* 1985;140,2:309- 27.
21. Carpenter MB and Sutin J. Human neuroanatomy, ed. 8. Williams & Wilkins,

- Baltimore 1983.
22. Chan-Palay V. Somatostatin immunoreactive neurons in the human hippocampus and cortex shown by immunogold/silver intensification on vibratome sections: coexistence with neuropeptide Y neurons, and effects in Alzheimer-type dementia. *J Comp Neurol* 1987;260:201-23.
 23. Chan-Palay V. Neurons with galanin innervate cholinergic cells in the human basal forebrain and galanin and acetylcholine coexist. *Brain Res Bull* 1988;21:465-72.
 24. Chan-Palay V. Galanin hyperinnervates surviving neurons of the human basal nucleus of Meynert in dementias of Alzheimer's and Parkinson's Disease: a hypothesis for the role of Galanin in accentuating cholinergic dysfunction in dementia. *J Comp Neurol* 1988;273:543-57.
 25. Crawford GD, Correa L and Salvaterra PM. Interaction of monoclonal antibodies with mammalian choline acetyltransferase. *Proc Natl Acad Sci USA* 1982;79:7031-5.
 26. DeLong MR. Activity of pallidal neurons during movement. *J Neurophysiol* 1971;34:414-27.
 27. De Olmos J, Hardy H and Heimer L. The afferent connections of the main and the accessory olfactory bulb formations in the rat: an experimental HRP study. *J Comp Neurol* 1978;181:213-44.
 28. Divac I. Magnocellular nuclei of the basal forebrain project to neocortex, brain stem, and olfactory bulb. Review of some functional correlates. *Brain Res* 1975;93:385-98.
 29. Eckenstein F and Thoenen H. Production of specific antisera and monoclonal antibodies to choline acetyltransferase: characterization and use for identification of cholinergic neurons. *EMBO J* 1982;1:363-8.
 30. Feremutsch K. Strukturanalyse des menschlichen Hypothalamus. *Mtschr Psychiat Neurol* 1955;130:1-85.
 31. Fibiger HC. The organization and some projections of cholinergic neurons of the mammalian forebrain. *Brain Res Rev* 1982;4:327-88.
 32. Fisher RS, Levine MS, Adinolfi AM, Hull CD and Buchwald NA. Postnatal development of GABA neurons in the cat: ventral forebrain, peripallidal regions and ventral tegmental area. *Soc Neurosci Abst* 1983;9:660.
 33. Foix CE, Nicolesco J. Anatomie cérébrale; les noyaux gris centraux et la région mésencéphaloso-optique; suivi d'un appendice sur l'anatomie pathologique de la maladie de Parkinson. Paris, Masson & Cie, 1925.
 34. Friedemann M. Die Cytoarchitektur des Zwischenhirns der Cercopitheken mit besonderer Berücksichtigung des Thalamus opticus. *J Psychol Neurol* 1911;18:309-78.
 35. Gaspar P, Berger B, Alvarez C, Vigny A and Henry JP. Catecholaminergic innervation of the septal area in man: immunocytochemical study using TH and DBH antibodies. *J Comp Neurol* 1985;241:12-33.
 36. German DC, Bruce G and Hersh LB. Immunohistochemical staining of cholinergic neurons in the human brain using a polyclonal antibody to human choline acetyltransferase. *Neurosci Lett* 1985;61:1-5.
 37. Gorry JD. Studies on the comparative anatomy of the ganglion basale of Meynert. *Acta Anat* 1963;55:51-104.
 38. Grove EA. Neural associations of the substantia innominata in the rat: afferent connections. *J Comp Neurol* 1988;277:315-46.
 39. Gurdjian ES. The diencephalon of the Albino rat. *J Comp Neurol* 1927;43:1-114.
 40. Haber S and Elde R. The distribution of enkephalin immunoreactive fibers and terminals in the monkey central nervous system: an immunohistochemical study. *Neurosci* 1982;7:1049-95.
 41. Haber S and Watson SJ. The comparative distribution of enkephalin,

- dynorphin and substance P in the human globus pallidus and basal forebrain. *Neurosci* 1985;14:1011-24.
42. Hassler R. Zur Pathologie der Paralysis agitans und des postencephalitischen Parkinsonismus. *J Psychol Neurol* 1938;48:388-474.
 43. Hebb CO, Krnjevic K and Silver A. Effect of undercutting on the acetylcholinesterase and choline acetyltransferase activity in the cat cerebral cortex. *Nature* 1963;198:692-3.
 44. Hedreen JC, Bacon SJ, Cork LC, Kitt CA, Crawford GD, Salvaterra PM and Price DL. Immunocytochemical identification of cholinergic neurons in the monkey central nervous system using monoclonal antibodies to choline acetyltransferase. *Neurosci Lett* 1983;43:173-7.
 45. Hedreen JC, Struble RG, Whitehouse PJ and Price DL. Topography of the magnocellular basal forebrain system in human brain. *J Neuropathol Exp Neurol* 1984;43:1-21.
 46. Hefti F and Weiner WJ. Nerve growth factor and Alzheimer's disease. *Ann Neurol* 1986;20:275-81.
 47. Hefti F and Mash DC. Localization of nerve growth factor receptors in the normal human brain and in Alzheimer's disease. *Neurobiol Aging* 1989;10:75-87.
 48. Higgins GA and Mufson EJ. NGF receptor gene expression is decreased in the nucleus basalis in Alzheimer's disease. *Exp Neurol* 1990: in press.
 49. Hohmann C, Antuono P and Coyle JT. Basal forebrain cholinergic neurons and Alzheimer's disease. In: Iversen LL and Iversen SD, eds. *Handbook of psychopharmacology*. Vol 20. *Psychopharmacology of the aging nervous system*. New York. Plenum Press 1988;pp69-130.
 50. Hreib KK, Rosene DL and Moss MB. Basal forebrain efferents to the medial dorsal thalamic nucleus in the rhesus monkey. *J Comp Neurol* 1988;277:365-90.
 51. Insausti R, Amaral DG and Cowan WM. The entorhinal cortex of the monkey: III. Subcortical afferents. *J Comp Neurol* 1987;264:396-408.
 52. Irle E and Markowitsch HJ. Afferent connections of the substantia innominata/basal nucleus of Meynert in Carnivores and Primates. *J Hirnforsch* 1986;27:343-67.
 53. Jones EG, Burton H, Saper CB and Swanson LW. Midbrain diencephalic and cortical relationships of the basal nucleus of Meynert and associated structures in primates. *J Comp Neurol* 1976;167:385-420.
 54. Karnovsky MJ and Roots L. A "direct-coloring" thiocholine method for cholinesterase. *J Histochem Cytochem* 1964;12:219-21.
 55. Khachaturian H, Lewis ME, Haber SN, Akil H and Watson SJ. Proopiomelanocortin peptide immunocytochemistry in rhesus monkey brain. *Brain Res Bull* 1984;13:785-800.
 56. Kievit J, Kuypers HGJM. Basal forebrain and hypothalamic connections to the frontal and parietal cortex of the monkey. *Science* 1975;187:660-2.
 57. Kitt CA, Mitchell SJ, DeLong MR, Warner BH and Price DL. Fiber pathways of basal forebrain cholinergic neurons in monkeys. *Brain Res* 1987;406:192-206.
 58. Koelle GB and Friedenwald JS. A histochemical method for localizing cholinesterase activity. *Proc Soc Exp Biol Med* 1949;70:617-22.
 59. Koliatsos VE, Martin LJ, Walker LC, Richardson RT, DeLong MR and Price DL. Topographic, non-collateralized basal forebrain projections to amygdala, hippocampus, and anterior cingulate cortex in the rhesus monkey. *Brain Res* 1988;463:133-9.
 60. Kolliker A. *Handbuch der Gewebelehre des Menschen*. Fur Aerzte und Studierende, 6th ed. Vol 2. Leipzig, Engelmann W, 1896.
 61. Kordower JH, Bartus RT, Bothwell M, Schatteman G and Gash DM. Nerve

- growth factor receptor immunoreactivity in the non-human primate (*Cebus apella*): distribution, morphology and colocalization with cholinergic enzymes. *J Comp Neurol* 1988;277:465-86.
62. Kordower JH, Bartus RT, Marciano FF and Gash DM. Telencephalic cholinergic system of the new world monkey (*Cebus apella*): morphological and cytoarchitectonic assessment and analysis of the projection to the amygdala. *J Comp Neurol* 1989;279:528-45.
 63. Kordower JH, Gash DM, Bothwell M, Hersh L and Mufson EJ. Nerve growth factor receptor and choline acetyltransferase remain colocalized in the nucleus basalis (Ch4) of Alzheimer's patients. *Neurobiol Aging* 1989;10:67-74.
 64. Kristt DA, McGowan RA Jr, Martin-MacKinnon N and Solomon J. Basal forebrain innervation of rodent neocortex: studies using acetylcholinesterase histochemistry, Golgi and lesion strategies. *Brain Res* 1985;337:19-39.
 65. Lehmann J, Struble RG, Antuono PG, Coyle JT, Cork LC and Price DL. Regional heterogeneity of choline acetyltransferase activity in primate neocortex. *Brain Res* 1984;322:361-4.
 66. Leichnetz GR and Astruc J. The course of some prefrontal corticofugals to the pallidum, the substantia innominata, and amygdaloid complex in monkeys. *Exp Neurol* 1977;54:104-9.
 67. Lewis PR and Shute CCD. The cholinergic limbic system: projections to the hippocampal formation, medial cortex, nuclei of the ascending cholinergic reticular system and the subfornical organ and supraoptic crest. *Brain Res* 1967;90:521-40.
 68. Loo YT. The forebrain of the opossum *Didelphis virginiana*. Part II. Histology. *J Comp Neurol* 1931;52:1-148.
 69. Luiten PGM, Ter Horst GJ and Steffens AB. The hypothalamus, intrinsic connections and outflow pathways to the endocrine system in relation to the control of feeding and metabolism. *Prog Neurobiol* 1987;28:1-54.
 70. Lysakowski A, Wainer BH, Bruce G and Hersh LB. An atlas of the regional and laminar distribution of choline acetyltransferase immunoreactivity in rat cerebral cortex. *Neurosci* 1989;28:291-336.
 71. Mai JK, Triepel J and Metz J. Neurotensin in the human brain. *Neurosci* 1987;22:499-524.
 72. Meibach RC and Siegel A. Efferent connections of the septal area in the rat: an analysis utilizing retrograde and anterograde transport methods. *Brain Res* 1977;119:1-26.
 73. Melander T and Staines WA. A galanin-peptide coexists in putative cholinergic somata of the septum-basal forebrain complex and in acetylcholinesterase-containing fibers and varicosities within the hippocampus in the owl monkey (*Aotus trivirgatus*). *Neurosci Lett* 1986;68:17-22.
 74. Mesulam M-M and VanHoesen GW. Acetylcholinesterase-rich projections from the basal forebrain of the rhesus monkey to neocortex. *Brain Res* 1976;109:152-7.
 75. Mesulam M-M and Mufson EJ. Insula of the old world monkey. Part III. Efferent cortical output and comments on function. *J Comp Neurol* 1982;212:38-52.
 76. Mesulam M-M, Mufson EJ, Levey AI and Wainer BH. Cholinergic innervation of cortex by the basal forebrain: cytochemistry and cortical connections of the septal area, diagonal band nuclei, nucleus basalis (substantia innominata) and hypothalamus in the rhesus monkey. *J Comp Neurol* 1983;214:170-97.
 77. Mesulam M-M, Mufson EJ, Levey AI and Wainer BH. Atlas of cholinergic neurons in the forebrain and upper brainstem of the macaque based on

- monoclonal choline acetyltransferase immunohistochemistry and acetylcholinesterase histochemistry. *Neurosci* 1984;12:669-86.
78. Mesulam M M, Rosen A and Mufson EJ. Regional variations in cortical cholinergic innervation: chemoarchitectonics of acetylcholinesterase-containing fibers in the macaque brain. *Brain Res* 1984;311:245-58.
 79. Mesulam M-M and Mufson EJ. Neural inputs into the nucleus basalis of the substantia innominata (Ch4) in the rhesus monkey. *Brain* 1984;107:253-74.
 80. Mesulam M-M, Mufson EJ and Wainer BH. Three-dimensional representation and cortical projection topography of the nucleus basalis in the macaque: concurrent demonstration of choline acetyltransferase and retrograde transport with a stabilized tetramethylbenzidine method for HRP. *Brain Res* 1986;367:301-8.
 81. Mesulam M-M, Volicic L, Marquis JK, Mufson EJ and Green RC. Systematic regional difference in the cholinergic innervation of the primate cerebral cortex: distribution of enzyme activities and some behavioral implications. *Ann Neurol* 1986;19:144-51.
 82. Mesulam M-M and Geula C. Nucleus basalis (Ch4) and cortical cholinergic innervation in the human brain: observations based on the distribution of acetylcholinesterase and choline acetyltransferase. *J Comp Neurol* 1988;275:216-40.
 83. Mesulam M-M, Geula C, Bothwell MA and Hersh LB. Human reticular formation: cholinergic neurons of the pedunculopontine and laterodorsal tegmental nuclei and some cytochemical comparisons to forebrain cholinergic neurons. *J Comp Neurol* 1989;281:611-33.
 84. Meynert T. Vom Gehirn der Säugetiere. In: Stricker S, ed. *Handbuch der Lehre von den Geweben des Menschen und der Thiere*. Leipzig, Engelmann W, 1872:694-808.
 85. Nagai T, Pearson F, Peng F, McGeer EG and McGeer PL. Immunohistochemical staining of the human forebrain with monoclonal antibody to human choline acetyltransferase. *Brain Res* 1983;265:300-6.
 86. Nagai T, McGeer PL, Peng JH, McGeer EG and Dolman CE. Choline-acetyltransferase immunohistochemistry in brains of Alzheimer's disease patients and controls. *Neurosci Lett* 1983;36:195-9.
 87. Nauta WJH and Haymaker W. Hypothalamic nuclei and fiber connections. In: Haymaker W, Anderson E and Nauta WJH, eds. *The hypothalamus*. Springfield, CC Thomas Publisher, 1969;pp. 136-209.
 88. Nieuwenhuys R, Voogd J and Van Huijzen Chr. *The human central nervous system. A synopsis and atlas*. Third ed. Berlin: Springer Verlag, 1988.
 89. Nieuwenhuys R, Veening JG and Van Domburg P. Core and paracores; some new chemoarchitectural entities in the mammalian neuraxis. *Acta Morphol Neerland Scand* 1989;26:131-63.
 90. Norgren R. Gustatory afferents to ventral forebrain. *Brain Res* 1974;81:285-95.
 91. Ogren M and Hendrickson A. Pathways between striate cortex and subcortical regions in *Macaca mulatta* and *Saimiri sciureus*: evidence for a reciprocal pulvinar connection. *Exp Neurol* 1976;53:780-800.
 92. Papez JW and Aronson LR. Thalamic nuclei of *Pithecus* (*Macacus*) rhesus; ventral thalamus. *Arch Neurol Psychiatr* 1934;32:1-26.
 93. Parent A, Paré D, Smith Y and Steriade M. Basal forebrain cholinergic and noncholinergic projections to the thalamus and brainstem in cats and monkeys. *J Comp Neurol* 1988;277:281-301.
 94. Pearson RCA, Gatter KC, Brodal P and Powell TPS. The projection of the basal nucleus of Meynert upon the neocortex in the monkey. *Brain Res* 1983;259:132-6.
 95. Pearson RCA, Sofroniew MV, Cuello AC, Powell TPS, Eckenstein F, Esiri MM

- and Wilcock GK. Persistence of cholinergic neurons in the basal nucleus in a brain with senile dementia of the Alzheimer's type demonstrated by immunohistochemical staining for choline acetyltransferase. *Brain Res* 1983;289:375-9.
96. Perry EK, Atack JR, Perry RH, Hardy JH, Dodd PR, Edwardson JA, Blessed G, Tomlinson BE and Fairbairn AF. Intralaminar neurochemical distributions in human midtemporal cortex: comparison between Alzheimer's disease and the normal. *J Neurochem* 1984;42:1402-10.
 97. Perry RH, Candy JM, Perry EK, Irving D, Blessed G, Fairbairn AF and Tomlinson BE. Extensive loss of choline acetyltransferase activity is not reflected by neuronal loss in the nucleus of Meynert in Alzheimer's disease. *Neurosci Lett* 1982;33:311-5.
 98. Perry RH, Candy JM, Perry EK, Thompson J and Oakley AE. The substantia innominata and adjacent regions in the human brain: histochemical and biochemical observations. *J Anat* 1984;138:713-32.
 99. Piva F, Limonta P and Martini L. Role of the organum vasculosum laminae terminalis in the control of gonadotrophin secretion in rats. *J Endocrinol* 1982;93:355-64.
 100. Poletti CE and Sujatanond M. Evidence for a second hippocampal efferent pathway to hypothalamus and basal forebrain comparable to fornix system: a unit study in the awake monkey. *J Neurophysiol* 1980;44:514-31.
 101. Price JL and Powell TPS. An experimental study of the origin and course of the centrifugal fibers to the olfactory bulb in the rat. *J Anat* 1970;107:215-37.
 102. Price JL and Amaral DG. An autoradiographic study of the projections of the central nucleus of the monkey amygdala. *J Neurosci* 1981;1:1242-59.
 103. Price JL and Stern R. Individual cells in the nucleus basalis-diagonal band complex have restricted axonal projections to the cerebral cortex in rat. *Brain Res* 1983;269:352-6.
 104. Rasmussen AT. Effects of hypophysectomy and hypophysial stalk resection on the hypothalamic nuclei of animals and man. *Assn Res Nerv Ment Diss* 1940;20:245-69.
 105. Rioch DM. Studies on the diencephalon of the Carnivora. I. The nuclear configuration of the thalamus, epithalamus and hypothalamus of the dog and cat. *J Comp Neurol* 1929;49:1-119.
 106. Rolls ET, Sanghera MK and Roper Hall A. The latency of activation of neurones in the lateral hypothalamus and substantia innominata during feeding in the monkey. *Brain Res* 1979;161:121-35.
 107. Rossier J. Choline acetyltransferase: a review with special reference to its cellular and subcellular localization. *Int Rev Neurobiol* 1977;20:283-337.
 108. Rossier J. On the mapping of cholinergic neurons by immunocytochemistry. *Neurochem Int.* 1984;6:183-4.
 109. Roussy G and Mosinger M. La substance innominée de Reichert et ses connexions. *Rev Neurol (Paris)* 1934;41:873-5.
 110. Russchen FT, Amaral DG and Price JL. The afferent connections of the substantia innominata in the monkey, macaca fascicularis. *J Comp Neurol* 1985;242:1-27.
 111. Saper CB, Swanson LW and Cowan WM. Some efferent connections of the rostral hypothalamus in the squirrel monkey (*Saimiri sciureus*) and cat. *J Comp Neurol* 1979;184:205-42.
 112. Saper CB. Organization of the cerebral cortex afferent systems in the rat. I. Magnocellular basal nucleus. *J Comp Neurol* 1984;222:313-42.
 113. Saper CB and Chelmsky TC. A cytoarchitectonic and histochemical study of nucleus basalis and associated cell groups in the normal human brain.

- Neurosci 1984;13:1023-37.
114. Satoh K and Fibiger HC. Distribution of central cholinergic neurons in the baboon (*Papio papio*): I. General morphology. *J Comp Neurol* 1985;236:197-214.
 115. Satoh K and Fibiger HC. Distribution of central cholinergic neurons in the baboon (*Papio papio*): II. A topographic atlas correlated with catecholamine neurons. *J Comp Neurol* 1985;236:215-33.
 116. Sawchenko PE and Swanson LW. The distribution and cells of origin of some afferent projections to the paraventricular and supraoptic nuclei in the rat. *Soc Neurosci Abstr* 1981;7:325.
 117. Sawchenko PE and Swanson LW. Central noradrenergic pathways for the integration of hypothalamic neuroendocrine and autonomic responses. *Science* 1981;214:685-7.
 118. Sawchenko PE and Swanson LW. The organization of noradrenergic pathways from the brainstem to the paraventricular and supraoptic nuclei in the rat. *Brain Res Rev* 1982;4:275-325.
 119. Schatteman GC, Gibbs L, Lanahan AA, Claude P and Bothwell M. Expression of NGF receptor in the developing and adult primate central nervous system. *J Neurosci* 1988;8:860-73.
 120. Schober W, Brauer K, Werner L and Luth H-J. Lage und Ausdehnung der magnozellularen Kerne im basalen Vorderhirn von Nagetieren und Hasenartigen. *J Hirnforsch* 1988;29:443-59.
 121. Segal M and Landis SC. Afferents to the septal area of the rat studied with the method of retrograde axonal transport of horseradish peroxidase. *Brain Res* 1974;82:263-8.
 122. Shute CCD and Lewis PR. The ascending cholinergic reticular system: neocortical, olfactory and subcortical projections. *Brain* 1967;90:497-520.
 123. Silverman AJ, Hoffman DL and Zimmerman EA. The descending afferent connections of the paraventricular nucleus of the hypothalamus (PVN). *Brain Res Bull* 1981;6:47-61.
 124. Simpson JB. The circumventricular organs and the central actions of angiotensin. *Neuroendocrinology* 1981;32:248-56.
 125. Smith Y, Parent A, Kerkérian L and Pelletier G. Distribution of neuropeptide Y immunoreactivity in the basal forebrain and upper brainstem of the squirrel monkey (*Saimiri sciureus*). *J Comp Neurol* 1985;236:71-89.
 126. Sorbi S, Piacentini S and Amaducci L. Intralaminar distribution of neurotransmitter-related enzymes in cerebral cortex of Alzheimer's disease. *Gerontology* 1987;33:197-202.
 127. Stephan H and Andy OJ. Cytoarchitectonics of the septal nuclei in old world monkeys (*Cercopithecus* and *Colobus*). *J Hirnforsch* 1964;7:1-23.
 128. Struble RG, Lehmann J, Mitchell SJ, McKinney M, Price DL, Coyle and DeLong MR. Basal forebrain neurons provide major cholinergic innervation of primate neocortex. *Neurosci Lett* 1986;66:215-20.
 129. Swanson LW and Cowan WM. The connections of the septal region in the rat. *J Comp Neurol* 1979;186:621-55.
 130. Swanson LW and Sawchenko PE. Hypothalamic integration: organization of the paraventricular and supraoptic nuclei. *Ann Rev Neurosci* 1983;6:269-324.
 131. Szigethy E and Beaudet A. Selective association of neurotensin receptors with cholinergic neurons in the rat basal forebrain. *Neurosci Lett* 1987;83:47-52.
 132. Talbot K, Woolf NJ and Butcher LL. Feline islands of Calleja complex: II. Cholinergic and cholinesterasic features. *J Comp Neurol* 1988;275:

133. Tigges J, Tigges M, Cross NA, McBride RL, Letbetter WD and Ansel A. Subcortical structures projecting to visual cortical areas in squirrel monkey. *J Comp Neurol* 1982;209:29-40.
134. Tigges J, Walker LC and Tigges M. Subcortical projections to the occipital and parietal lobes of the chimpanzee brain. *J Comp Neurol* 1983;220:106-15.
135. Ulfing N. Configuration of the magnocellular nuclei in the basal forebrain of the human adult. *Acta Anat* 1989;134:100-5.
136. Ulfing N and Braak H. Neuronal types and their percent distribution within the magnocellular nuclei of the human basal forebrain. *Acta Anat* 1989;134:237-41.
137. Vogels OJM and Ter Laak HJ. The isodensity method for morphologic investigation of the human basal forebrain cholinergic system (BFCS). Leipzig. Abstractbook ESN-IBRO satellite symposium "Structural-functional properties of the Basal Forebrain Cholinergic System". 1987;p69.
138. Vogels OJM, Renkawek K, Broere CAJ, Ter Laak HJ and Van Workum F. Galanin-like immunoreactivity within Ch2 neurons in the vertical limb nucleus of the diagonal band of Broca in aging and Alzheimer's disease. *Acta Neuropathol* 1989;78:90-5.
139. Vogels OJM, Broere CAJ, Ter Laak HJ, Ten Donkelaar HJ, Nieuwenhuys R and Schulte BPM. Cell loss and shrinkage in the nucleus basalis Meynert complex in Alzheimer's disease. *Neurobiol Aging* 1990;12(1): in press.
140. Vogels OJM, Broere CAJ, Nieuwenhuys R. Neuronal hypertrophy in the human supraoptic and paraventricular nucleus in aging and Alzheimer's disease. *Neurosci Lett* 1990: in press
141. Wainer BH, Levey AI, Mufson EJ and Mesulam M-M. Cholinergic systems in mammalian brain identified with antibodies against choline acetyltransferase. *Neurochem Int* 1984;6:163-82.
142. Walker LC, Kitt CA, DeLong MR and Price DL. Noncollateral projections of basal forebrain neurons to frontal and parietal neocortex in primates. *Brain Res Bull* 1985;15:307-14.
143. Walker LC, Koliatsos VE, Kitt CA, Richardson RT, Rokaeus Å and Price DL. Peptidergic neurons in the basal forebrain magnocellular complex of the Rhesus monkey. *J Comp Neurol* 1989;280:272-80.
144. Winfield DA, Gatter KC and Powell TPS. Certain connections of the visual cortex of the monkey shown by the use of horseradish peroxidase. *Brain Res* 1975;92:456-61.
145. Woodhams PL, Roberts GW, Polak JM and Crow TJ. Distribution of neuropeptides in the limbic system of the rat: the bed nucleus of the stria terminalis, septum and preoptic area. *Neurosci* 1983;8:677-704.
146. Zola-Morgan S, Squire LR and Amaral DG. Lesions of the hippocampal formation but not lesions of the fornix or the mamillary nuclei produce long-lasting memory impairment in monkeys. *J Neurosci* 1989;9:897-912.

MATERIAL AND METHODS**3.1 Brain material****3.1.1 Cases**

Twelve cases of Alzheimer's disease (AD) were selected, one case of Parkinson's disease (PD), and ten nondemented controls. The twelve AD cases could be subdivided in five early-onset AD cases (first symptoms of the disease manifested before 65 years of age) and seven late-onset AD cases.

The clinical diagnosis of probable Alzheimer's disease was confirmed neuropathologically using Khachaturian's criteria [11], that include minimum numbers of senile plaques and neurofibrillary tangles per age category in hippocampal and cortical brain areas. The clinical diagnosis of Parkinson's disease was neuropathologically confirmed by the characteristic lesions in the substantia nigra consisting of cell loss, degenerative cell changes, gliosis and the presence of Lewy inclusion bodies [12]. The control patients showed clinically and neuropathologically no evidence of neurological or psychiatric disease. Data on the available brain material are summarized in Table 3.1.

3.1.2 Brain regions of interest

The whole nucleus basalis Meynert complex (NBMC) and its surrounding structures were removed in toto from both hemispheres using the polus temporalis and the corpus geniculatum laterale as borders for the rostral and caudal cutting plane, respectively. These cutting planes were orientated perpendicularly to the hippocampal axis and to the imaginary plane throughout the

TABLE 3.1
Characteristics of brain material

case	dia- gnosis	sex	age (y)	brain weight (g)	NBMC	SON	PVN	OVL	fix. time (m)	p.m. delay (h)	cause of death	duration dementia (y)
1	C	F	60	1162	L+R	--	--	+	5	14	sepsis	
2	C	M	62	1351	L+R	- R	--	+	5	<24	aorta rupture	
3	C	M	65	1570	L+R	L+R	L+R	+	2	36	pneumonia	
4	C	M	69	1200	L+R	L+R	- R	+	9	50	trauma	
5	C	F	70	1185	--	L+R	--	+	5	40	sepsis	
6	C	M	71	1346	L+R	--	L -	+	7	<24	cardiac arrest	
7	C	F	75	1250	L+R	L+R	L+R	+	6	36	carcinoma	
8	C	M	80	1475	L+R	L+R	L+R	+	7	48	cardiac arrest	
9	C	M	86	1290	--	L+R	--	+	5	36	cachexia	
10	C	M	91	1288	L+R	L+R	L+R	+	5.5	36	carcinoma	
11	AD	F	65	865	L+R	- R	--	+	9	<12	sepsis	3
12	AD	M	66	1136	L+R	L+R	--	+	5	<24	sepsis	4
13	AD	F	69	1105	L+R	L+R	L+R	+	5	<12	sepsis	?
14	AD	M	69	1077	L+R	L+R	L+R	+	<1	<12	cachexia	12
15	AD	F	76	970	L+R	L+R	--	+	<1	6	cachexia	14
16	AD	F	76	1275	- R	- R	- R	+	5	4	status epilepticus	5
17	AD	F	76	?	--	- R	--	+	4	5	renal failure	?
18	AD	M	77	985	L+R	L+R	L+R	+	<1	2.5	pneumonia	11
19	AD	M	82	1353	--	- R	--	+	5	<14	cardiac failure	6
20	AD	F	90	1100	- R	L+R	L+R	+	12	<12	pneumonia	6
21	AD	M	90	1160	- R	- R	--	+	6	<12	sepsis	3
22	AD	F	93	842	L+R	L+R	L+R	-	7	<12	pneumonia	16
23	PD	F	74	1370	L+R	L+R	--	+	<1	8	cardiac arrest	

Neuropathological diagnosis, sex, age, brain weight, fixation time, postmortem delay, cause of death, and duration of dementia. AD, Alzheimer's disease; C, control; F, female; L, left hemisphere; M, male; PD, Parkinson's disease; R, right hemisphere; h, hours; m, months; y, years; g, grams; ?, unknown; -, not available or incomplete; +, present; cases 11-15, early onset AD; cases 16-22, late onset AD.

rostrocaudal extent of both tractus optici, which resulted in an approximate 20-25 degrees difference with respect to the coronal plane.

The following subdivisions of the NBMC were investigated:

- Ch1 and Ch2 were considered as one subdivision, because their adjacent boundaries are not readily identifiable and because both regions project to the hippocampus [14];
- Ch3 as recently delineated [15];
- Ch4 as a whole (nucleus basalis of Meynert);
- the three Ch4 subdivisions: Ch4 anterior (Ch4a), Ch4 intermediate (Ch4i), and Ch4 posterior (Ch4p).
- both Ch4a subdivisions: Ch4 anteromedial (Ch4am) and Ch4 anterolateral (Ch4al).

Moreover, to verify if the NBMC is selectively affected in AD, two more nuclei in the immediate vicinity of the NBMC were investigated: the entire supraoptic nucleus (SON) and the whole paraventricular nucleus (PVN).

In addition, the organum vasculosum of the lamina terminalis was studied because this region is devoid of a blood-brain barrier, and could therefore serve as a "natural model" to verify whether amyloid deposits in AD are of systemic origin or whether amyloid is produced in the brain itself.

3.1.3 Histological procedure

All 23 brains were fixed in toto in 4% formaldehyde for at least 5 months except for six brains that were processed earlier (Table 3.1). A fixation time of 5 months has been recommended, because after this time, variation in tissue swelling and shrinkage due to fixation has ceased and a stable volume has been obtained [8, 9, 18]. Different tissue processing may result in different tissue shrinkage and different volumes of brain structures. Moreover, the pathological process itself can also affect volume. As a consequence, for determination of total neuron numbers only those brain structures of interest (NBMC, SON and PVN) that were present in toto in the available brain

material, were processed. It needs to be stressed that the parameter of total neuron number (instead of neuron number per unit volume) is not susceptible to any volume shrinkage (or expansion) of the NBMC, SON and PVN. Although a fixation time less than 5 months may bias neuron size (less shrinkage), no corrections have been made, while it is not known whether, and to what extent neuron size is really affected.

Postmortem delays varied from 2.5 to 50 hours. The postmortem interval between death and fixation or freezing of brain tissue is not only important for neurochemistry (compound levels quickly drop in a few hours and some even in a few seconds), but may also affect morphological parameters. For instance, autolysis is a common artefact from delayed fixation in Nissl-stained sections, and leads to the more confusing microscopic sponginess as a result of cellular desintegration. All brains listed in Table 3.1 showed no autolysis in Nissl and Klüver-Barrera-staining and were suitable for examination. Only one brain (not listed) showed severe autolysis after a postmortem delay of 72 hours.

After embedding in paraffin serial sections with a thickness of 10 or 20 μm were cut using a Jung 2050 microtome. Sections were stained at regular intervals throughout the entire rostro-caudal extent of the NBMC, SON and PVN. The Klüver-Barrera-stained sections were used for identification of the NBMC and its subdivisions Ch1-Ch4, and the adjacent Nissl-stain was used for counting and measuring purposes. If the brain structures of interest (NBMC, SON, PVN) were not entirely present in the available brain material, they were not included in the analysis (see Table 3.1), because availability of the whole structure is an absolute requirement to a sound determination of total neuron numbers.

3.2 Quantitative methods

3.2.1 The nucleolus as sampling item

Nucleoli are regarded as the traditional markers of neurons [22]. Unbiased quantification of neuron numbers using the nucleolus as sampling item can be ascertained under the following assumptions:

1. The neurons of interest contain only one nucleolus;
2. The nucleolus has a spherical shape and therefore the orientation in space is random and independent of the plane of sectioning;
3. The nucleolus is not being transected by the microtome knife and, consequently, does not appear in more than one section.

In the NBMC no neurons were found with more than one nucleolus; however, in the PVN and SON very rarely binucleolated neurons could be demonstrated (± 1 per 1000 neurons, Fig. 3.1). This number of binucleolated neurons is so small, that the generated bias due to this phenomenon is negligible.

To verify whether nucleoli are spherically shaped, 200

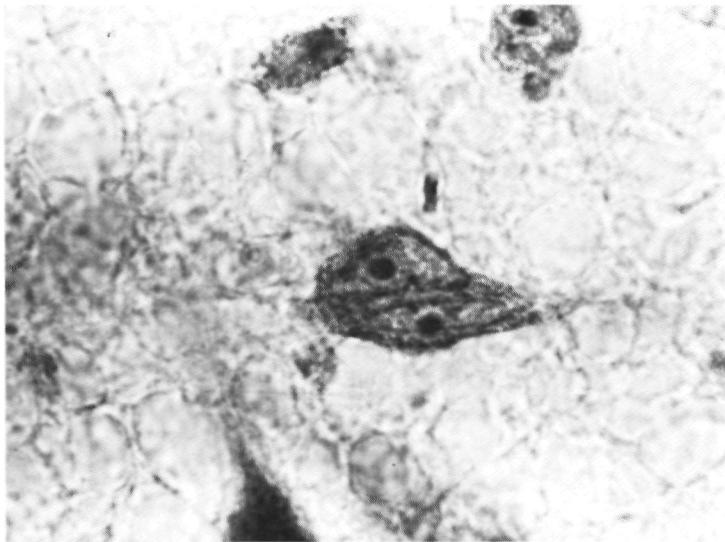


Fig. 3.1 A binucleated and binucleolated neuron in the paraventricular nucleus (x1000 magnification).

nucleoli of NBMC neurons were morphometrically analyzed using a semi-automatic image analysis system (Mopp Videoplan, Kontron): the maximum diameter of the nucleoli was measured at a x1000 magnification ($3.72 \pm 0.07 \mu\text{m}$; mean \pm standard error of the mean, $n=200$) and compared to the mean circular diameter (i.e., the diameter belonging to a virtual circle with an area of the same size as the outlined, actual area occupied by the nucleolus) of the same nucleoli: $3.69 \pm 0.06 \mu\text{m}$. The close similarity between the maximum diameter and the circular diameter demonstrates a spherical shape for the nucleolus.

It has recently been shown, that the nucleolus is not transected but pushed aside by the microtome knife and remains uncut in paraffin sections with a thickness $\geq 10 \mu\text{m}$ [20]. Moreover, when the nucleolus is the particle to be sampled, numerical data do not differ between the conventional counting method (sampling all visible nucleoli throughout the entire thickness of the section) and the unbiased optical disector method [23, 24] provided that paraffin sections $\geq 10 \mu\text{m}$ are used (Chapter 4 of this thesis).

In conclusion, the nucleolus can be used as the sample item without introducing major biases, even when the conventional counting method is applied [20].

All nucleolus counts in the NBMC, SON and PVN were performed at a x400 magnification using an ocular grid with a quadrant sampling field of $250 \times 250 \mu\text{m}^2$, subdivided into 100 squares of $25 \times 25 \mu\text{m}^2$ each. The nucleoli hitting the boundaries of the sampling grid were dealt with according to the exclusion principle of Gundersen [5] (Fig. 3.2).

Neuron size was defined as the maximum diameter (d_{max}). Focussing at the level of the nucleolus, the d_{max} of each nucleolated neuron within the sampling field was measured. Four size categories (0-12.5; 12.5-25.0; 25.0-37.5 and $>37.5 \mu\text{m}$) were deliberately chosen: firstly, the sampling grid with squares of $25 \times 25 \mu\text{m}^2$ could serve as a quick measuring scale, and secondly, mapping studies demonstrated the NBMC-neurons with a $d_{\text{max}} \geq 25 \mu\text{m}$ to be the putative cholinergic neurons [13, 14] and therefore cholinergic and noncholinergic neurons of the NBMC could be

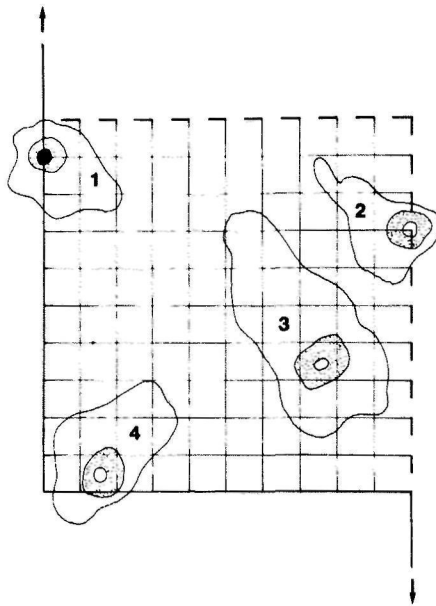


Fig. 3.2 The ocular sampling field with the exclusion principle of Gundersen [5]: all nucleoli (no. 1) that hit the forbidden (solid) line are not counted; the nucleoli entirely inside the sampling frame as well as those hitting the dotted line are counted (nos. 2, 3 and 4). The side length of the frame corresponds to 250 μm at a x400 magnification or to 100 μm at x1000 magnification.

roughly differentiated. However, the use of the d_{max} as a measure for neuron size with the nucleolus being in focus, is biased in two ways. Firstly, the d_{max} depends on the orientation of the neuron in space and therefore on the angle of the section plane. Secondly, the possibility of nucleolus displacement from the centre of the soma is far from theoretical [1], because both the accumulation of lipofuscin in normal aging and the presence of neurofibrillary tangle formations in AD do in fact displace the nucleus and nucleolus towards an eccentric position. However, in order to maintain the possibility of comparison with data from the literature, this bias has not been corrected for.

3.2.2 The sampling design

Taking the nucleolus as the particle to be sampled, the question arises in which way and how many nucleoli have to be sampled to accomplish reliable estimations on total nucleolus numbers in the structures of interest and to minimize the observed variance (variance is defined as s^2 ; s =standard deviation). It should be emphasized that the observed variance (Os^2) in any biological system depends on several variables each contributing to the observed total variance between the subjects. This is particularly true for a multiple stage sampling, consisting of several hierarchical sampling levels, each with its own variance. The sampling strategy of this study consists of three hierarchical levels:

1. population sample (i.e., the subjects used in one population);
2. tissue sample (i.e., the sections used in one structure);
3. field sample (i.e., the fields used in one section);

The observed total variance between subjects (Os^2_{subj}) may be regarded as the sum of the true biological variance (s^2_{subj}) plus the observed variance of the mean of the number n sections at the second lower level (Os^2_{sect} / n_{sect}); similarly, the observed variance of the sections (Os^2_{sect}) may be regarded as the sum of the true variance of the sections (s^2_{sect}) plus the variance of the mean of the number m sampling fields at the third lowest level (s^2_f / m_f). This will result in the following formula:

$$Os^2_{subj} = s^2_{subj} + \frac{1}{n_{sect}} * s^2_{sect} + \frac{1}{n_{sect} * m_f} * s^2_f$$

Os^2_{subj} being the observed total variance of the subjects;

s^2_{subj} is the true (biological) variance of the subjects;

s^2_{sect} is the true variance of the sections;

s^2_f is the true variance of the sampling fields;

n_{sect} is the number of n sections;

m_f is the number of m fields.

From this formula it can be deduced, that major reductions in the observed total variance can be most efficiently accomplished by increasing the number of subjects and sections but not by increasing the number of fields per section. For instance, it is appropriate to investigate more subjects (10 instead of 5 subjects) and less sections per subject (5 instead of 10 sections) than vice versa; it is also worthwhile to study more sections and less fields per section than vice versa. Alternatively speaking, by "doing more less well" it is possible to optimize the sampling design and to reduce the observed total variance [6], whereas the workload remains the same (for example, 10 fields in each of the 5 sections per subject instead of 50 fields in only one section per subject).

In order to obtain a representative sample of the structure of interest and to prevent any bias, the sampling of sections and fields within sections should be basically randomized. This procedure, that postulates that the samples should be taken independently from each other, is called "simple random sampling" [22]. However, independent samples are prone to cluster in certain regions, whereas other regions are undersampled (Fig. 3.3a: so-called 0-dimensional-sampling design). This disadvantage of simple random sampling can be overcome by spacing the samples in a more or less regular fashion in order to get a more representative sample of the entire structure. This systematic approach with a random start is called the "systematic random sampling" method, that is both theoretically [3] and experimentally [4] proven to be superior to simple random sampling. These studies have shown that the standard error of the number of nucleoli within one section is nearly ten times as large when the microscope fields are obtained by simple random (Fig. 3.3a) rather than systematic sampling (Fig. 3.3b). A further decrease in the standard error can be effectuated by investigating equidistant systematic sections (Fig. 3.4a). The most representative sample of the entire structure can be obtained when all samples are positioned systematically along three perpendicular directions (Fig. 3.4b). In such a sampling system all the samples are dependent on each other: the first

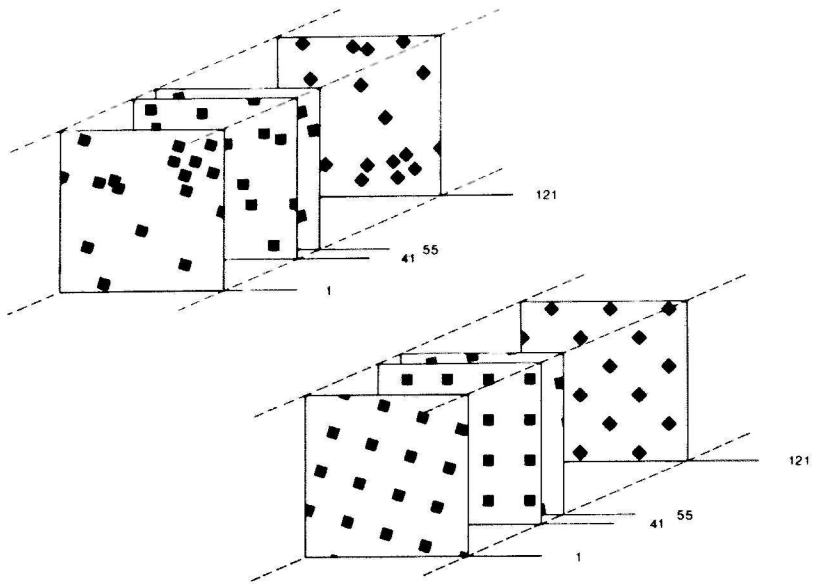


Fig. 3.3a 0-dimensional simple random sampling design
 b 1-dimensional systematic random sampling design
 black squares represent sample fields; numbers indicate sections

sample, that is randomly chosen somewhere in the structure, automatically defines the positions of all other samples throughout the entire specimen. The whole structure of interest is now evenly appreciated and bias to clustering of sample fields is fully absent. However, if the structure itself contains a certain periodicity which coincides with that of the sampling fields, variance may be dramatically increased. The three structures of interest in this study (NBMC, SON and PVN) do not have such periodicities, like, for instance, a layered structure as the neocortex, or the parallel bundling of elongated elements like myofibrils in skeletal muscle and nerve fibers in nerve tracts. Therefore, periodicity bias is unlikely to occur.

Considering all the sampling pitfalls mentioned above, efficient and reliable sampling schemes for the NBMC, SON and PVN could be designed. Equidistant sections were sampled at intervals of 800 μm , with a random start of the first section somewhere between 0 and 800 μm . For the rostrocaudal extent of

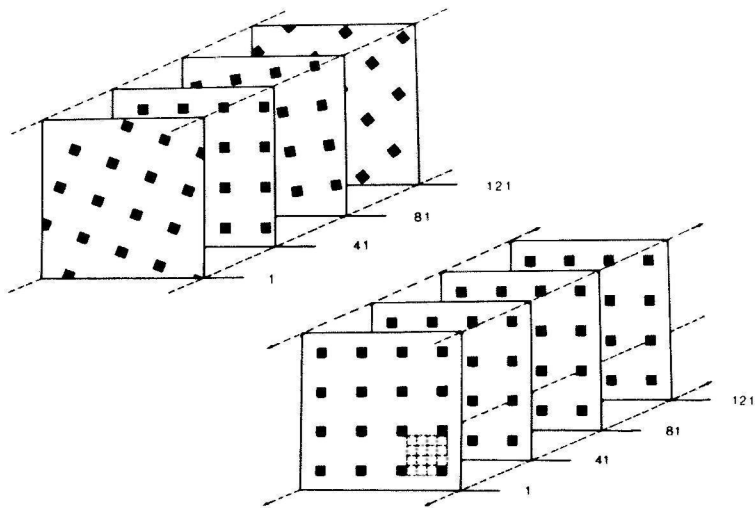


Fig. 3.4a 2-dimensional systematic random sampling design
 b 3-dimensional systematic random sampling design
 black squares represent sample fields; numbers indicate sections

both the entire SON and PVN, this resulted in an amount of 9.5 sections, and for the NBMC as a whole in approximately 25 sections. This is an amply sufficient large amount of sections to accomplish reliable results with a low variance [7]. The latter study proved experimentally and theoretically, that each systematic randomly performed count in any structure will have an estimated coefficient of error (CE) below 5% provided that at least eight equidistant sections are used (the CE is a measure of the reliability of the count; a CE of 0.05 or 5% corresponds to a 95% reliability of the count; this means that the true number is somewhere in between the counted number +5% and -5%). Considering the magnitude of variation among subjects in most stereological studies a CE of 10% or better is nearly always sufficient.

Gundersen and Jensen [7] developed formulae to predict the validity of 2-dimensional (Fig. 3.4a) and 3-dimensional (Fig. 3.4b) systematic sampling designs. Using these formulae, it became possible to optimize the sampling scheme of the NBMC, SON

and PVN, and to co-relate the CE with the minimum number of nucleoli, that had to be sampled. For both the SON and PVN this resulted in a 2-dimensional-sampling scheme, in which 4 sampling fields per mm^2 were taken systematically; at a x400 magnification the area of 1 sampling field corresponds to $250 \times 250 \mu\text{m}^2$. Using this design, it could be shown for both the SON and PVN, that an amount of ≥ 200 sampled nucleoli always resulted in a CE of less than 10%, or alternatively speaking in a reliability of $\geq 90\%$ (Figs. 3.5a and b).

The NBMC as a whole has sufficient sections for a 2-dimensional-sampling scheme, even when only 1 sampling field per mm^2 is taken. However, its subdivisions Ch3, Ch4i and sometimes also Ch4a and Ch4p span less than 8 sections, resulting in an increase of the CE (Fig. 3.6a). Therefore, the 3-dimensional-sampling system was applied on the subdivisions of the NBMC as well as on the NBMC as a whole, in order to reduce the CE. Using this 3-dimensional-sampling system and taking only 1 sampling field per mm^2 , an amount of ≥ 200 systematically sampled nucleoli always resulted in a CE less than 5%, or a reliability of $\geq 95\%$. Already 50 nucleoli ensure a reliability of $\geq 90\%$ (Fig. 3.6b).

Because the whole procedure of sampling is in fact nothing else than fractionating the total structure of interest, total nucleolus number can be easily calculated. At first, 20 μm sections are investigated at regular distances of 800 μm , the section fraction being 1/40th (only 1 out of every 40 sections is sampled). Secondly, taking only 1 sampling field of $250 \times 250 \mu\text{m}^2$ per mm^2 throughout the entire structure area of the section, only 1/16th of the area is sampled, the area fraction being 1/16th. Therefore, the total sampling fraction of the entire structure is $1/40 \times 1/16 = 1/640$. Total nucleolus number is obtained by multiplying the sampled nucleolus number (e.g., 1800 for a NBMC) with the inverse of the sampling fraction (640) resulting in a total number of $1.800 \times 640 = 1.152.000$ nucleoli.

For the SON and PVN the section fraction is the same (1/40), but the area fraction is smaller (1/4). The sampled nucleolus number (e.g. 350 for a SON) must now be multiplied with 160 (40×4) to a total number of $350 \times 160 = 56.000$ nucleoli.

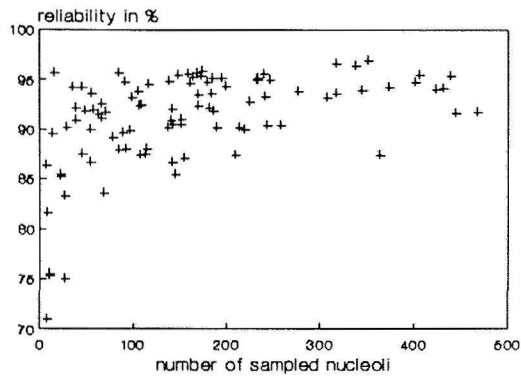


Fig. 3.5a Relation between the numbers of 2-dimensionally sampled nucleoli in the supraoptic nucleus and the corresponding reliabilities expressed as %

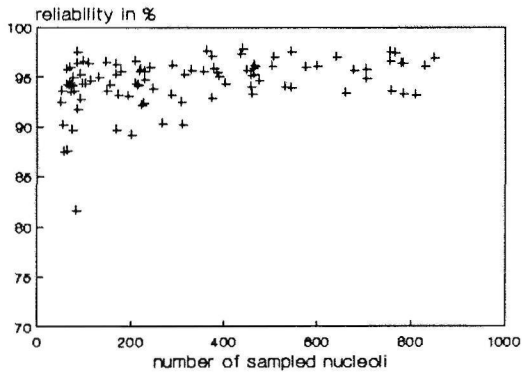


Fig. 3.5b Relation between the numbers of 2-dimensionally sampled nucleoli in the paraventricular nucleus and the corresponding reliabilities expressed as %

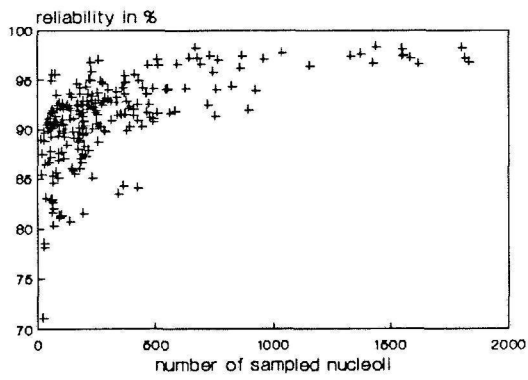


Fig. 3.6a Relation between the numbers of 2-dimensionally sampled nucleoli in the nucleus basalis Meynert complex and the corresponding reliabilities expressed as %

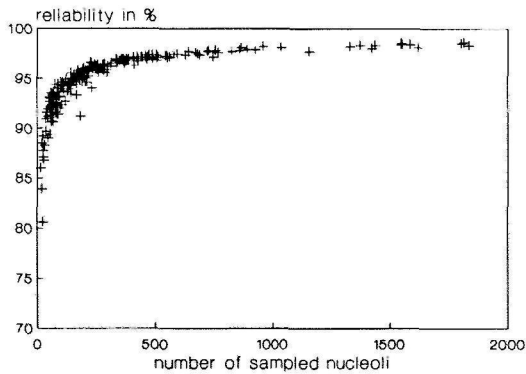


Fig. 3.6b Relation between the numbers of 3-dimensionally sampled nucleoli in the nucleus basalis Meynert complex and the corresponding reliabilities expressed as %

3.3 Qualitative methods

The qualitative methods concern classical staining methods and immunohistochemical staining methods.

As regards the staining methods Congo red [16, 17] and thioflavine-S [19] were chosen to describe the neuropathology in normal aging and AD (granulovacuolar degeneration, senile plaques, neurofibrillary tangles and congophilic angiopathy) as observed in the NBMC, the SON and PVN and the OVLT. For details about these methods see Chapter 7 of this thesis.

Concerning the immunohistochemical staining methods the antibodies to galanin were used and visualized with the avidin-biotin-peroxidase complex method [10]. The antibody galanin was chosen because of its co-localization with choline acetyltransferase in the cholinergic neurons of the basal forebrain in monkey [21] and human [2]. Galanin could therefore serve as a marker for cholinergic neurons. For details about the galanin immunohistochemistry see Chapter 8 of this thesis.

3.4 References

1. Born DE, Carman CS and Rubel EW. Correcting errors in estimating neuron area caused by the position of the nucleolus. *J Comp Neurol* 1987;255:146-52.
2. Chan-Palay V. Galanin hyperinnervates surviving neurons of the human basal nucleus of Meynert in dementias of Alzheimer's and Parkinson's Disease: a hypothesis for the role of Galanin in accentuating cholinergic dysfunction in dementia. *J Comp Neurol* 1988;273:543-57.
3. Cochran WC. Sampling techniques. Wiley and Sons, New York, 1953.
4. Ebbeson SOE and Tang DB. A comparison of sampling procedures in a structured cell population. In: *Stereology. Proceedings 2nd International Congress for Stereology*, Elias H, ed. Springer Verlag, Berlin-Heidelberg-New York: 1967:131-2.
5. Gundersen HJG. Notes on the estimation of the numerical density of arbitrary profiles: the edge effect. *J Microsc* 1977;111:219-23.
6. Gundersen HJG and Osterby R. Optimizing sampling efficiency of stereological studies in biology: or "Do more less well!". *J Microsc* 1981;121:65-73.
7. Gundersen HJG and Jensen EB. The efficiency of systematic sampling in stereology and its prediction. *J Microsc* 1987;147:229-63.
8. Haug H, Kühl S, Mecke E, Sass N-L and Wasner K. The significance of morphometric procedures in the investigation of age changes in cytoarchitectonic structures of human brain. *J Hirnforsch* 1984;25:353-74.

9. Haug H. Gibt es Nervenzellverluste während der Alterung in der menschlichen Hirnrinde? Ein morphometrischer Beitrag zu dieser Frage. *Nervenheilk* 1985;4:103-9.
10. Hsu S-M, Raine L and Fanger H. Use of Avidin-Biotin-Peroxidase Complex (ABC) in immunoperoxidase techniques: a comparison between ABC and unlabeled antibody (PAP) procedures. *J Histochem Cytochem* 1981;29:577-80.
11. Khachaturian ZS. Diagnosis of Alzheimer's Disease. *Arch Neurol* 1985;42:1097-1105.
12. Lewy FH. Zur pathologischen Anatomie der Paralysis Agitans. *Deutsch Zeitschr Nervenheilk* 1913;50:50-5.
13. McGeer PL, McGeer EG, Suzuki J, Dolman CE and Nagai T. Aging, Alzheimer's Disease, and the cholinergic system of the basal forebrain. *Neurol* 1984;34:741-5.
14. Mesulam M-M, Mufson EJ, Levey AI and Wainer BH. Cholinergic innervation of cortex by the basal forebrain: cytochemistry and cortical connections of the septal area, diagonal band nuclei, nucleus basalis (substantia innominata) and hypothalamus in the rhesus monkey. *J Comp Neurol* 1983;214:170-97.
15. Mesulam M-M and Geula C. Nucleus basalis (Ch4) and cortical cholinergic innervation in the human brain: observations based on the distribution of Acetylcholinesterase and Choline Acetyltransferase. *J Comp Neurol* 1988;275:216-40.
16. Puchtler H, Sweat F and Levine M. On the binding of Congo red by amyloid. *J Histochem Cytochem* 1962;10:355-64.
17. Puchtler H and Sweat F. Congo red as a stain for fluorescence microscopy of amyloid. *J Histochem Cytochem* 1965;13:693-4.
18. Sass N-L. The age-dependent variation of the embedding-shrinkage of neurohistological sections. *Microskopie* 1982;39:278-81.
19. Schwartz P. Amyloid degeneration and tuberculosis in the aged. *Gerontologia* 1972;18:321-62.
20. Vogels OJM, Ter Laak HJ and Broere CAJ. The nucleolus in quantitative morphology. *J Comp Neurol*, submitted 1989
21. Walker LC, Koliatsos VE, Kitt CA, Richardson RT and Price DL. Galanin-containing somata in the primate nucleus basalis/diagonal band complex. *Neurosci Abstr* 1987;273:13.
22. Weibel ER. *Stereological Methods, Vol 1: Practical Methods for Biological Morphometry*. London: Academic Press, 1979
23. Williams RW and P Rakic. Three-dimensional counting: an accurate and direct method to estimate numbers of cells in sectioned material. *J Comp Neurol* 1989;278:344-52.
24. Williams RW and P Rakic. Erratum and Addendum. Three-dimensional counting: an accurate and direct method to estimate numbers of cells in sectioned material. *J Comp Neurol* 1989;281:335.

THE NUCLEOLUS IN QUANTITATIVE MORPHOLOGY

O.J.M. Vogels, H.J. ter Laak and C.A.J. Broere
(submitted for publication)

4.1 Abstract

This study compares numerical data obtained from biased conventional counting methods with unbiased numerical data obtained from the disector. Three lines of evidence (conventional counting, physical disector and optical disector) indicate that the nucleolus is not transected but pushed aside by the microtome knife and remains uncut in paraffin sections with a thickness ≥ 10 μm . As a consequence, when the nucleolus is the particle to be quantified, numerical data do not differ between biased conventional counting methods and the unbiased disector. This study shows, that the conventional counting methods in the past have not led to seriously false results with regard to numerical data, provided that the nucleolus was quantified in paraffin sections with a thickness of at least 10 μm .

4.2 Introduction

Estimates of total numbers of particles (e.g. nucleoli, nuclei and nerve cell somata) in various regions of the human brain have been carried out for many decades using a variety of indirect and biased methods. Recently developed stereological tools as the physical disector [17], the optical disector [7, 12, 19, 20], the selector [4], and the fractionator [7] have enabled morphologists to quantify total numbers of particles in an unbiased way without assumptions upon shape, size, and orientati-

on of the investigated particles and without assumptions upon overprojection and capping. Because this chapter deals with the physical and optical disector and not with the selector and fractionator, readers interested on the latter subjects are referred to three review articles by Gundersen et al. [7, 9, 10].

The most frequently used conventional method for counting particles was developed by Abercrombie [1]: in a defined area of one single section with a certain section thickness (t) all particles are counted, including those particle fragments that are transected by the microtome knife in the upper and lower surfaces of the section; consequently, this counted particle number is too large and depends on the height of the particles (h) and the section thickness (t). The thinner the section and the larger the particle height, the larger the counting error. Abercrombie [1] postulated a formula (1) to correct for this overcount:

$$\text{true particle number} = \text{counted particle number} * \frac{t}{h + t} \quad (1)$$

However, Abercrombie's method [1] has five limitations:

1. Particle size distribution, shape and orientation are not taken into account.
2. To determine particle height, the particle diameter in sections cut precisely at a right angle to the remainder of the tissue, has to be measured [Abercrombie, 1]; in practice this is almost impossible, and height will be easily mixed up with particle diameter.
3. Actual section thickness varies considerably within one individual section [11].
4. Small particle fragments are difficult to be identified as such ("lost caps").
5. It is not known to what extent particles are indeed transected by the microtome knife and whether or not they are pushed aside by the knife and remain uncut.

All these limitations are in fact the consequences of using

one single section, and can be overcome by the disector [17]. The central idea of the physical disector is that arbitrarily shaped particles with an arbitrary orientation in space can be counted unambiguously by using two consecutive sections with thickness (t), which is smaller than the minimum particle height. Because large particles have an increased chance of being hit by the section plane in comparison to small particles, the number of particle profiles seen in one section has no known relationship to the number of particles in the 3-dimensional space or reference volume $V(\text{ref})$. However, the probability that a particle is hit by a section and at the same time is not hit by the parallel section is identical for both small and large particles. Therefore, total number of particles (N) can be estimated using the following equation (2):

$$N = \frac{\sum_{i=1}^n \bar{Q}_i}{t * \sum_{i=1}^n a(\text{fra})_i} * V(\text{ref}) \quad (2)$$

- \bar{Q}_i is the number of particles that is counted in the first section minus the number of particles present in both sections;
- $a(\text{fra})_i$ is the area of the sampling frame (Fig. 4.1), in which particles are sampled according to the exclusion principle of Gundersen [6];
- Σ is the summation that is carried out over $i=1,2,\dots,n$ systematic randomly positioned disectors (i.e., at equidistant positions with a random start) in the reference volume $V(\text{ref})$;
- t represents the section thickness. In this approach it is not necessary anymore to measure t , since:

$$V(\text{ref}) = t * \sum_{j=1}^m A_j \quad (3)$$

ΣA_j being the estimated total sectional area of all m sections.

Substituting equation (3) into (2), the t in the numerator cancels the t in the denominator [16]. In practice, not all m sections but only a certain fraction (f) will be used (e.g., every 50th section is measured, f being $1/50$), resulting in the following equation:

$$V(\text{ref}) = 1/f * t * \Sigma A_j \quad (4)$$

The central idea of the optical disector [7, 12, 19, 20] is the use of one relatively thick section, in which two parallel thin optical sections can be indicated by moving the plane of focus up or down. Total particle number was obtained by using equation (2) in which t now represents the height of the optical disector (the distance between the two optical planes of focus, e.g. $10 \mu\text{m}$ in a $20 \mu\text{m}$ thick section). For the purpose of optical dissectioning a microcator was attached to the microscope to measure the movements of the stage in the z -axis. The smallest possible focal depth was reached by using high numerical aperture oil immersion lenses. As compared to the physical disector, the optical disector in one relatively thick physical section has one main advantage: the most time consuming step of aligning the two physically separate sections in order to obtain two coinciding fields of view in two identical microscopes, is eliminated. Moreover, densely packed cells like the dentate granule cells of the hippocampus are almost impossible to count in physical disectors (overprojection), whereas the optical disector solves this problem.

The results of numerous quantification studies obtained in the past using conventional counting methods [like Abercrombie's method, 1] are biased to an unknown extent. The aim of this study is to investigate whether and to what extent these conventional data have led to seriously false conclusions in the past. The particle of interest in this study is the nucleolus, because it is regarded as the traditional marker for neurons [18]. Moreover, the nucleolus has a spherical shape, and therefore the orientation in space is independent of the plane of sectioning. To investigate to what extent nucleoli are indeed

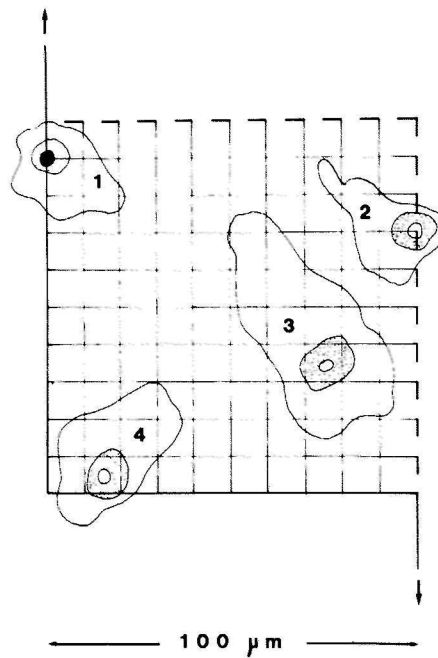


Fig. 4.1 The ocular sampling grid with the exclusion principle of Gundersen [6]: all profiles (black nucleolus, no. 1) that hit the forbidden (solid) line are not counted; the profiles entirely inside the sampling frame as well as those hitting the dotted line are counted (open nucleoli, nos. 2, 3 and 4). The side length of the frame corresponds to 100 μm at a x1000 magnification.

being transected by the microtome knife and whether or not they are pushed aside by the knife and remain uncut, three different approaches are used:

1. Comparison of the number of nucleoli in 10 and 20 μm sections, obtained with conventional methods; if transection of nucleoli does occur, the counts in 10 μm sections will be relatively higher than those in 20 μm sections.
2. Using the physical disector, fragments of the same nucleolus in two physically separated 10 μm sections can be traced.
3. Comparison of the nucleolus count using the optical disector

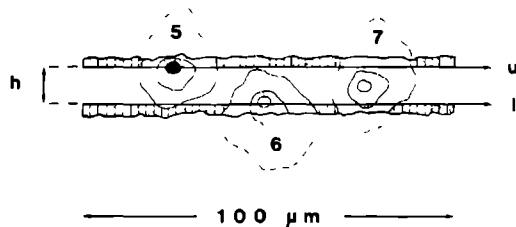


Fig. 4.2 Schematic representation of the optical disector with height ($h=10\ \mu\text{m}$) in a nominal $20\ \mu\text{m}$ section, with upper and lower guard zone (dotted/hatched areas; $\pm 2\ \mu\text{m}$), and the upper (u) and lower (l) focus plane of the optical disector. Nucleoli (black, no. 5) hitting the upper focus plane are not counted, but those nucleoli entirely inside the optical disector (no. 7) or in the lower focus plane (no. 6) are sampled.

with a height of $10\ \mu\text{m}$ within a section of nominal thickness of $20\ \mu\text{m}$, with the conventional nucleolus count in exactly the same area throughout the entire section thickness (both counts expressed as number per unit volume).

4.3 Material and methods

4.3.1 Histological methods

The structure of interest is the human nucleus basalis of Meynert in the basal forebrain because of its large constituent, putative cholinergic neurons ($>25\ \mu\text{m}$) [14, 15] showing relatively large nucleoli ($\pm 3.5\ \mu\text{m}$) that can be easily recognized as prominent, round structures in the nuclei. After fixation in 4% formaldehyde and embedding in paraffin, 27 serial sections were cut on a Jung 2050 microtome with varying thickness resulting in 6 series of a total thickness of $60\ \mu\text{m}$, consisting of alternate $6 \times 10\ \mu\text{m}$ sections and $3 \times 20\ \mu\text{m}$ sections (totally 18 sections of $10\ \mu\text{m}$ and 9 sections of $20\ \mu\text{m}$ thickness). Sections were stained according to Nissl.

4.3.2 Stereological methods

The conventional counts were carried out on the 10 and 20 μm sections throughout the entire thickness of the sections at a $\times 400$ magnification using an ocular grid with a quadrant sampling area of $250 \times 250 \mu\text{m}^2$, subdivided into 100 squares of $25 \times 25 \mu\text{m}^2$ each. The nucleoli hitting the boundaries of the grid were dealt with according to the exclusion principle of Gundersen [6] (Fig. 4.1). All other visible nucleoli in the sampling grid were counted, whether they were transected or not. As counting of all nucleoli is a rather elaborate task, one sample of $250 \times 250 \mu\text{m}^2$ per each 1mm^2 was systematically taken throughout the whole area of each section. This sampling scheme provided a sufficiently large amount of samples to ensure a high validity ($>95\%$) of the counting data [8]. Only large, putative cholinergic neurons with a maximum diameter of $>25 \mu\text{m}$ were considered because of their relatively large and prominent nucleoli. Because determination of nucleolus number can be influenced by the actual section thickness of nominal 10 μm and 20 μm sections (due to possible inaccuracy of the microtome, variation in temperature, and histological processing), the thickness of all sections was measured at 4 different positions within each section. These measurements were carried out at $\times 1000$ magnification (oil immersion lens, numerical aperture of 1.4) using the microcator attached to the light microscope.

The physical disector approach was not used to quantify nucleoli in an unbiased way [17] in this study, but to verify whether actual transectioning of nucleoli did occur. In two adjacent 10 μm sections 200 nuclei and nucleoli were investigated at a $\times 1000$ magnification (oil immersion lens, numerical aperture of 1.4) to determine the number of neurons showing nuclei and nucleoli in both sections.

The optical disector approach was compared to the conventional counting method. Firstly, in an area of $1000 \times 4500 \mu\text{m}^2$ in a section with nominal thickness of 20 μm , 72 samples of $250 \times 250 \mu\text{m}^2$ were taken meanderlike (4 vertically versus 18 horizontally) at a $\times 400$ magnification and all visible nucleoli throughout the whole

section thickness were counted. Secondly, in each of the 72 samples the actual section thickness was measured using the microcator at a x1000 magnification. Thirdly, in exactly the same area of $1000 \times 4500 \mu\text{m}^2$ of the same section 450 consecutive optical disectors (disector area: $100 \times 100 \mu\text{m}^2$; height disector: $10 \mu\text{m}$) were taken meanderlike (10 vertically versus 45 horizontally) at a x1000 magnification. Because the cut-surface of the section is irregular, an upper guard zone of about $2 \mu\text{m}$ under the cut-surface was taken into account to ensure that the upper plane of the optical disector was fully present within the section. All nucleoli, that were sharply focused were not counted, and while focusing down along $10 \mu\text{m}$ of the z-axis all new nucleoli coming into focus were being counted including those that were in focus in the lower plane of the optical disector (Fig. 4.2). The nucleoli that hit the boundaries of the sampling frame were dealt with according to the exclusion principle of Gundersen [6] (Fig. 4.1).

4.4 Results

Results include the conventional counts in 10 and 20 μm sections, the physical disector to verify actual transectioning of the nucleolus, and the comparison between the counting data obtained with the optical disector and the data obtained with conventional counting.

The nominal 10 and 20 μm thick sections appeared to be actually $8.6 \pm 0.1 \mu\text{m}$ (mean \pm standard error of the mean; $n=72$) and $17.1 \pm 0.2 \mu\text{m}$ ($n=36$), respectively. This change in section thickness did not significantly differ between 10 and 20 μm sections. Secondly, to exclude a possible change in nucleolus number along the extent of the 27 sections investigated, nucleoli counts of all eighteen 10 μm sections were added and compared with the total nucleolus number of all nine 20 μm sections. In the 10 μm sections a total of 944 nucleoli were sampled versus 953 in the 20 μm sections (difference: $<1\%$). This result suggests either the absence of nucleolar transectioning, or an

equal number of nucleolar splitting, that may be due to a more severe compression during the cutting of the 10 μm sections.

To verify whether actual transectioning of nucleoli and nuclei did occur, the physical disector was applied on a 10 μm section pair. Only 21 nuclei from the 200 nuclei present in the first section only 21 nuclei could also be detected in the adjacent second section (10.5%). All of these 21 transected nuclei showed an intact nucleolus present in either of the two nucleus halves. Moreover, each of the 200 nuclei contained only 1 nucleolus. These results indicate the absence of nucleolus transectioning in 10 μm thick paraffin sections.

The approach of the optical disector (450 consecutive disectors of $100 \times 100 \times 10 \mu\text{m}^3$ in an area of $1000 \times 4500 \mu\text{m}^2$ at a $\times 1000$ magnification) resulted in an unbiased number of 259 sampled nucleoli. The actual section thickness of this area was $14.23 \pm 0.17 \mu\text{m}$ ($n=72$). The biased conventional count (72 consecutive samples of $250 \times 250 \mu\text{m}^2$ in exactly the same area of $1000 \times 4500 \mu\text{m}^2$ throughout the whole thickness of the section, at a $\times 400$ magnification) resulted in a sampled number of 370 nucleoli. If no nucleolus transectioning does occur, the number of nucleoli sampled in the biased manner should equal the number of nucleoli obtained from the optical disector (259) multiplied with the volume-fraction of the two sampling methods ($1000 \times 4500 \times 14.23 \mu\text{m}^3 / 1000 \times 4500 \times 10 \mu\text{m}^3$), i.e., $259 \times 1.423 = 368.55$ nucleoli. The conventional count mounted up to 370 nucleoli (difference: $< 1\%$). The latter finding indirectly points out to an absence of nucleolus transectioning.

4.5 Discussion

The results show three lines of evidence, that the nucleoli of neurons of the human nucleus basalis of Meynert are not transected but pushed aside by the microtome knife, and remain uncut in paraffin sections with a thickness $\geq 10 \mu\text{m}$. As a consequence, when the nucleolus is the particle to be quantitated, the numerical data obtained from biased conventional

counting methods do not differ from the unbiased numerical data obtained from the optical disector. It is therefore tempting to extrapolate this finding on conventional biased data of the past, and to state cautiously that these former quantification studies have not led to seriously false conclusions, provided that paraffin sections with a thickness of $\geq 10 \mu\text{m}$ were used and that the nucleolus was being quantified. Larger particles like the nuclei or the neurons themselves would never give similar results in both the biased conventional counting methods and the unbiased stereological techniques, because several assumptions have to be made upon transectioning, shape, size-distribution and orientation in space. While counting nerve cells (not nucleoli) in the neocortex, Bok en Van Erp Taalman Kip [2] previously faced this problem of overcounting due to transectioning of the cell soma, and developed a kind of predecessor of the physical disector. They performed cell counts in both 15 and 30 μm sections; subsequently, the difference between the two counts was reckoned to be the number of nerve cells present in an imaginary section the thickness of which was equal to the difference between the thicknesses of the two sections used.

The small percentage of transected nuclei (10.5%) may be due to compression and (temporary, elastic) deformation of the nucleus during the cutting procedure. It can be hypothesized that nuclei are behaving like water balloons with a smooth surface and are pushed aside by the microtome knife into one or the other of the two sections. A splitting error of 10% for nuclei has already been reported previously [5], however, section thickness was not mentioned. A neglectable nucleolus splitting in 6 up to 12 μm thick sections has been demonstrated by Jones [13], who postulated that the nucleolus was harder than the surrounding tissues and the paraffin like intact peanuts in peanut-butter. This hypothesis was indirectly supported by the demonstration of artifactual displacement of intact nucleoli in the direction of cutting [3], sometimes even through the nuclear membrane into the cytoplasm. However, in the present study no nucleolar displacement was found, because of the small probability for the nucleolus of being transected by the microtome as a

direct consequence of the low percentage of nucleus transectioning.

In conclusion, biased quantification studies in the past, that used the nucleolus as quantifiable particle in paraffin sections with a thickness ≥ 10 μm , have not led to seriously false conclusions. However, it can not be excluded that nucleoli of neurons in pathological conditions are indeed susceptible to transectioning. Therefore, the (optical) disector approach may turn out to be superior to any conventional counting method.

4.6 References

1. Abercrombie M. Estimation of nuclear populations from microtome sections. *Anat Rec* 1946;94:239-47.
2. Bok ST and Van Erp Taalman Kip MJ. The size of the body and the size and the number of the nerve cells in the cerebral cortex. *Acta Neerl Morphol* 1939;3:1-22.
3. Cammermeyer J. Artifactual displacement of neuronal nucleoli in paraffin sections. *J Hirnforsch* 1967;9:209-24.
4. Cruz-Orive L-M. Particle number can be estimated using a disector of unknown thickness: the selector. *J Microsc* 1987;145:121-42.
5. Guild SR, Crowe SJ, Bunch CC and Polvogt LM. Correlations of differences in the density of innervation of the organ of Corti with differences in the acuity of hearing, including evidence as to the location in the human cochlea of the receptors of certain tones. *Acta Oto-laryng (Stockholm)* 1931;15:269-308.
6. Gundersen HJG. Notes on the estimation of the numerical density of arbitrary profiles: the edge effect. *J Microsc* 1977;111:219-23.
7. Gundersen HJG. Stereology of arbitrary particles. A review of unbiased number and size estimators and the presentation of some new ones, in memory of William R Thompson. *J Microsc* 1986;143:3-45.
8. Gundersen HJG and Jensen EB. The efficiency of systematic sampling in stereology and its prediction. *J Microsc* 1987;147:229-63.
9. Gundersen HJG, Bendtsen TF, Korbo L, Marcussen N, Moller A, Nielsen K, Nyengaard JR, Pakkenberg B, Sorensen FB, Vesterby A and West MJ. Some new, simple and efficient stereological methods and their use in pathological research and diagnosis. *APMIS* 1988;96:379-94.
10. Gundersen HJG, Bagger P, Bendtsen TF, Evans SM, Korbo L, Marcussen N, Moller A, Nielsen K, Nyengaard JR, Pakkenberg B, Sorensen FB, Vesterby A and West MJ. The new stereological tools: disector, fractionator, nucleator and point sampled intercepts and their use in pathological research and diagnosis. *APMIS* 1988;96:857-81.
11. Helander KG. Thickness variations within individual paraffin and glycol methacrylate sections. *J Microsc* 1983;132:223-7.
12. Howard V, Reid S, Baddeley A and Boyde A. Unbiased estimation of particle density in the tandem scanning reflected light microscope. *J Microsc* 1985;138:203-12.

13. Jones RL. Split nucleoli as a source of error in nerve cell counts. *Stain Technol* 1937;12:91-5.
14. McGeer PL, McGeer EG, Suzuki J, Dolman CE and Nagai T. Aging, Alzheimer's Disease, and the cholinergic system of the basal forebrain. *Neurol* 1984;34:741-5.
15. Mesulam M-M, Mufson EJ, Levey AI and Wainer BH. Cholinergic innervation of cortex by the basal forebrain: cytochemistry and cortical connections of the septal area, diagonal band nuclei, nucleus basalis (substantia innominata) and hypothalamus in the rhesus monkey. *J Comp Neurol* 1983;214:170-97.
16. Pakkenberg B and Gundersen HJG. Total number of neurons and glial cells in human brain nuclei estimated by the disector and the fractionator. *J Microsc* 1988;150:1-20.
17. Sterio DC. The unbiased estimation of number and sizes of arbitrary particles using the disector. *J Microsc* 1984;134:127-36.
18. Weibel ER. *Stereological Methods. Vol. 1: Practical Methods for Biological Morphometry.* Academic Press, London, 1979.
19. Williams RW and Rakic P. Three-dimensional counting: an accurate and direct method to estimate numbers of cells in sectioned material. *J Comp Neurol* 1988;278:344-52.
20. Williams RW and Rakic P. Erratum and Addendum. Three-dimensional counting: an accurate and direct method to estimate numbers of cells in sectioned material. *J Comp Neurol* 1989;281:335.

**CELL LOSS AND SHRINKAGE IN THE NUCLEUS BASALIS MEYNERT COMPLEX IN
ALZHEIMER'S DISEASE**

O.J.M. Vogels, C.A.J. Broere, H.J. ter Laak, H.J. ten Donkelaar,
R. Nieuwenhuys and B.P.M. Schulte

(Neurobiology of Aging 1990;12:1)

5.1 Abstract

Marked neuron loss in the nucleus basalis of Meynert complex (NBMC) in Alzheimer's disease has repeatedly been reported in the literature. However, most of these studies quantitated only magnocellular, hyperchromatic (putative cholinergic) neurons of just a small part of the NBMC, and counts were expressed as numerical density. Applying a 3-dimensional-sampling design throughout the entire rostrocaudal extent of the NBMC and sampling neurons regardless of their size and staining characteristics, an overall neuron loss of only 15.5% was demonstrated for the whole NBMC. Neuron loss varied from 0% rostrally in the NBMC up to 36% in the most caudal part of the nucleus basalis of Meynert. Moreover, a significant increase in the number of small-sized neurons and a significant decrease in the number of large, putative cholinergic neurons could be detected, suggesting that apart from neuron loss neuron shrinkage appears to be another characteristic neuropathological feature of this degenerating cholinergic NBMC system. Preservation of these magnocellular cholinergic neurons in shrunken form renders it likely that cholinergic dysfunction, characteristic of Alzheimer's disease, may be responsive to neurotrophic influences.

5.2 Introduction

There has been considerable debate during the last years regarding the extent of neuronal loss during normal aging and in dementing diseases. This is particularly true for the nucleus basalis of Meynert complex (NBMC) in the basal forebrain (medial septal nucleus, nucleus of Broca's diagonal band, nucleus basalis of Meynert). Based on the distribution of choline acetyltransferase positive neurons and their respective fiber connections, the NBMC can be subdivided into four regions [33, 34]: the Ch1 region (corresponding to the medial septal nucleus), the Ch2 region (vertical limb nucleus of the diagonal band of Broca), the Ch3 region (horizontal limb nucleus of the diagonal band of Broca) and the Ch4 region (nucleus basalis of Meynert), which latter can be further subdivided into an anteromedial (Ch4am), an anterolateral (Ch4al), an intermediate (Ch4i) and a posterior part (Ch4p), that ends at the rostral level of the corpus geniculatum laterale.

In normal aging a linear decline in neuronal number of the NBMC starting shortly after birth has been reported, showing cell loss ranging from 23% [29] up to 70% [32]. However, other investigators claimed stability of neuronal number in this complex [5, 8] during normal aging (Table 5.1).

In Alzheimer's disease (AD) and Senile Dementia of Alzheimer's Type (SDAT) the reported variation in cell loss is even greater, ranging from apparent persistence of cholinergic neurons [37] to a 90% cell loss in a patient with a familial form of AD [51]. This considerable variation in neuron number and cell loss of the NBMC does not result from different patient selection criteria and inconsistency in tissue processing, but is mainly due to counting procedures applied.

Concerning tissue processing, an age-dependent embedding-shrinkage of brain tissue could have influenced data on neuronal densities [42], although this is not a universal problem, and may even be isolated to the use of methylbenzoate for paraffin embedding. Together with a secular acceleration in body and brain size [21] both these variables may significantly affect

morphometric evaluation of neuronal densities (number per unit volume) during aging.

A closer look at the counting procedures applied reveals three sources of bias (Table 5.1):

1. Most studies [1, 7, 8, 10, 11, 30, 35, 37, 39, 41, 48, 51, 52, 55, 56] examined only a small region of one or more of the subdivisions of the NBMC, especially the subcommissural region,

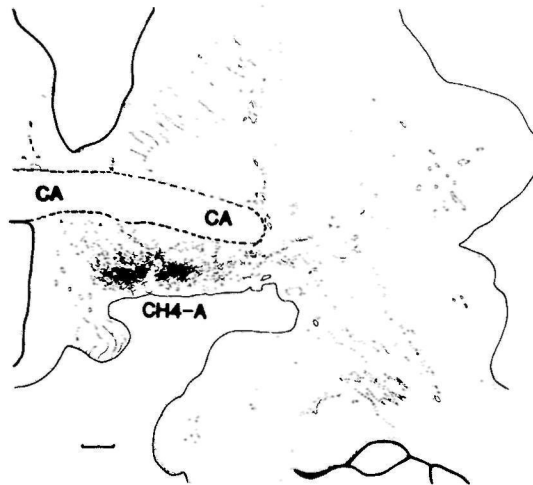


Fig. 5.1 The subcommissural Ch4a region. Note the absence of sharply delineated boundaries. Abbreviations: CA = Commissura Anterior; Ch4a: anterior part of the nucleus basalis of Meynert.

i.e., the anterior part of the nucleus basalis of Meynert (Ch4a; see Fig. 5.1). However, the NBMC of the human brain is a large, complex, and highly differentiated structure that is characterized by a marked irregularity in arrangement and distribution of its constituent cholinergic and noncholinergic neurons. Therefore, an investigation of the entire rostrocaudal extent of the NBMC and its subdivisions is an inevitable requirement for a sound analysis.

2. Neuron number has usually been expressed as numerical density, i.e., neuron number per unit volume (or per unit area). This parameter can only be used appropriately under the assumption that the total volume of the brain structure of interest is not affected by pathological conditions nor by (differential) embedding shrinkage. Therefore, it seems more suitable to express neuron numbers as absolute total neuron numbers.

3. Most studies [3, 4, 5, 7, 8, 10, 11, 13, 29, 30, 32, 35, 39, 48, 51, 52, 55, 56] introduced two criteria for neurons to be counted: a minimum size criterion (magnocellular neurons, usually larger than 30 μm) and a subjective staining criterion (hyperchromatic neurons showing "abundance of Nissl substance"). Mapping studies demonstrated these hyperchromatic, magnocellular neurons to be the putative cholinergic neurons [32, 33]. It is not known whether neuronal loss is restricted to large neurons and whether shrinkage of cells prior to death might lead to inaccurate impressions of the loss of large neurons. The decreased functional state of the NBMC cholinergic neurons in Alzheimer's disease is reflected by strongly reduced levels of choline acetyltransferase in the NBMC itself [39, 7] and by dissolution of the Nissl substance in the cytoplasm of the NBMC neurons. Therefore, an immunohistochemical stain for choline acetyltransferase or the use of another staining criterion such as "abundance of Nissl substance" make these parameters less reliable as markers for the NBMC in Alzheimer's disease, because these parameters are subjected to the disease process itself. Moreover, absence of transmitter-associated enzyme staining (choline acetyltransferase and acetylcholinesterase) is not an absolute indicator of death of cholinergic neurons [27]. Consequently, it appears to be necessary to count all neurons irrespective of their size and staining characteristics, and thus irrespective of their cholinergic properties. Quantitative studies that did not use a minimum size criterion, but instead counted all neurons, showed an increase in small-sized neurons [1, 37, 41, 53], indeed indicating neuronal shrinkage. However, these studies were either restricted to a small part of the NBMC [1, 37, 41, 53], or used the perikaryon instead of the nucleolus

TABLE 5.1

Neuron numbers of NBMC in normal aging and Alzheimer's disease

Reference	Region	N	Technique	Criteria	Expressed As	Results
Normal Aging						
Chui <i>et al</i> (8)	Ch4a	17	histology (CV)	>25 μm nucleolus	maximum density	cell density \leftrightarrow (25-87 y)
Mann <i>et al</i> (30)	Ch4a	20	histology (CV)	>30 μm hyperchromatic nucleolus	mean density	cell density \downarrow 35% (40-90 y)
McGeer <i>et al</i> (32)	Ch4	10	immunochem. histology (ChAT + CV)	>35 μm perikaryon nucleolus	total neuron number	ChAT cell No. \downarrow 70% (1-95 y) (475,000 \rightarrow 150,000)
Bigl <i>et al</i> (5)	Ch1, Ch2 Ch4	8	histology (CV)	>20 and >30 μm hyperchromatic nucleolus	total neuron number	cell No \leftrightarrow (36-85 y) (Ch1+2+4 \pm 225,000)
Lowes-Hummel <i>et al</i> (29)	Ch4	16	histology (CV + HE)	>35 μm nucleolus	total neuron number	cell No \downarrow 23% (0-90 y) (150,000 \rightarrow 114,000)
Alzheimer's Disease						
Whitehouse <i>et al</i> (51)	Ch4	1	histology (CV + HE)	large neurons hyperchromatic nucleolus	maximum density	cell density \downarrow 90%
Whitehouse <i>et al</i> (52)	Ch4	5	histology (CV)	>30 μm hyperchromatic nucleolus	maximum density	cell density \downarrow 73%
Perry <i>et al</i> (39)	Ch4	6	histochem (AChE)	large neurons	density	cell density \downarrow 33%
Wilcock <i>et al</i> (55)	Ch4	6	histology (CV)	>30 μm hyperchromatic nucleolus	maximum density	cell density \downarrow 50%
Arendt <i>et al</i> (3)	Ch1, Ch2 Ch4	14	histology (CV)	>20 μm hyperchromatic nucleolus	maximum density	cell density \downarrow 70%
Candy <i>et al</i> (7)	Ch4	5	histology (CV)	large neurons nucleolus	mean density	mean density \downarrow 35%
Nagu <i>et al</i> (35)	Ch4	3	immunochem. (ChAT)	>30 μm perikaryon	mean density	density ChAT \downarrow 66%
Pearson <i>et al</i> (37)	Ch4a	1	immunochem. histochem (ChAT + AChE)	all sizes perikaryon	mean density	density ChAT \downarrow 18% (n.s.) density AChE \downarrow 14% (n.s.) soma area \downarrow 26%
Tagliavini and Pillen (48)	Ch4	9	histology (CV)	large neurons nucleolus	mean density	cell density \downarrow 44-76%
Whitehouse <i>et al</i> (52)	Ch4	7	histology (CV)	all sizes perikaryon or nucleolus?	mean density	large neurons \downarrow small neurons \uparrow
Mann <i>et al</i> (30)	Ch4a	22	histology (CV)	>30 μm hyperchromatic nucleolus	mean density	cell density \downarrow 59% nucleolus diam. \downarrow 33%
McGeer <i>et al</i> (32)	Ch4	6	immunochem histology (ChAT + CV)	>35 μm perikaryon nucleolus	total neuron number	ChAT cell No. \downarrow 75%

TABLE 5.1

Continued

Reference	Region	N	Technique	Criteria	Expressed As	Results
Arendt <i>et al</i> (4)	Ch1, Ch2, Ch4am, Ch4i Ch4al, Ch4p	5	histology (CV)	>20 and >30 μ m hyperchromatic nucleolus	total neuron number	cell No. \downarrow 57%, Ch4p most affected
Doucette <i>et al</i> (10)	Ch4a, Ch4i Ch4p	8	histology (CV)	medium and large neurons nucleolus	mean density	cell density Ch4a \downarrow \pm 60% Ch4i \downarrow \pm 55%, Ch4p \downarrow \pm 60%
Euene <i>et al</i> (11)	Ch2, Ch4a Ch4i	10	histology (CV)	>30 μ m hyperchromatic nucleolus	mean density	cell density Ch2 \downarrow 70% Ch4a \downarrow 73%, Ch4i \downarrow 87% soma size \leftrightarrow
Gertz <i>et al</i> (13)	Ch1, Ch2	7	histology (CV)	>20 and >30 μ m nucleus	total neuron number	cell No. Ch1 + Ch2 \downarrow 46%
Rinne <i>et al</i> (41)	Ch4a	7	histology (CV)	all sizes nucleolus	mean density	cell density Ch4a \downarrow 22% mean cell size Ch4a \downarrow 25%
Allen <i>et al</i> (1)	Ch4i	7	immunohem. (NSE)	all sizes penkaryon	mean density	cell density \downarrow 29%, small \uparrow 59%, large \downarrow 61%
Wilcock <i>et al</i> (56)	Ch2, Ch4a Ch4i, Ch4p	13	histology (CV)	>20 and >30 μ m hyperchromatic nucleolus	maximum density	cell density Ch2 \downarrow 39%, Ch4am \downarrow 13%, Ch4al \downarrow 52%, Ch4i \downarrow 41%, Ch4p \downarrow 57%

N, number of subjects; n.s., not significant; y, years; CV, cresyl violet; HE, hematoxylin eosin; ChAT, choline acetyltransferase; AChE, acetylcholine esterase; NSE, neuron specific enolase.

as the counting item [1, 37, 53] and were therefore biased by overcounting due to splitting error.

As Table 5.1 shows, no quantitative studies on the NBMC in normal aging and in Alzheimer's disease have yet appeared in the literature that at once made allowance for all three methodological sources of bias as mentioned above by: in toto analysis of the NBMC (or of its subdivisions), determination of total neuron numbers, absence of size or staining restrictions.

This paper deals with an efficient and reliable sampling scheme for the NBMC as a whole, as well as for its subdivisions (Ch1-4), in order to determine total neuron numbers. Neurons to be counted were not subjected to any size or staining criterion; thus cholinergic and noncholinergic neurons were included.

Moreover, the NBMC-neurons were subdivided into four size categories, in order to detect a possible shift from large neurons into shrunken ones. To our knowledge no study has appeared in the literature that accounts for estimation of total neuron number regardless of size and staining properties and of neuron number per size category throughout the entire rostrocaudal extent of the NBMC and of its subdivisions in age-matched controls and Alzheimer's disease.

5.3 Material and methods

Five cases of early onset Alzheimer's disease, five cases of late onset Alzheimer's disease, one case of Parkinson's disease without cognitive impairment, and eight nondemented controls were obtained. The clinical diagnosis of probable Alzheimer's disease was confirmed neuropathologically using Khachaturian's criteria [25]. The clinical diagnosis of Parkinson's disease was neuropathologically confirmed by the characteristic lesions in the substantia nigra consisting of cell loss, degenerative cell changes, gliosis and the presence of Lewy inclusion bodies. The control patients showed no evidence of neurological or psychiatric disease. Clinical and pathological data are summarized in Table 5.2.

The whole NBMC was removed from both hemispheres using the *polus temporalis* and the *corpus geniculatum laterale* as borders for the rostral and caudal cutting plane, respectively. These cutting planes were orientated perpendicularly to the hippocampal axis, which resulted in an approximate 20-25 degree difference with respect to the coronal plane. The following subdivisions of the NBMC were investigated:

- Ch1 and Ch2 were taken together, because the boundaries between them are rather arbitrary and because both regions project to the hippocampus [33];
- Ch3 as recently delineated [34];
- Ch4 as a whole (nucleus basalis of Meynert);
- the three Ch4 subdivisions: Ch4 anterior (Ch4a), Ch4 interme-

TABLE 5.2
Brain material

case	dia- gnosis	sex	age (y)	brain weight (g)	hemi- sphere	fix. time (m)	p.m. delay (h)	cause of death	duration dementia (y)
1	C	F	60	1162	L+R	5	14	sepsis	
2	C	M	62	1351	L+R	5	<24	aorta rupture	
3	C	M	65	1570	L+R	2	36	pneumonia	
4	C	M	69	1200	L+R	9	50	trauma	
5	C	M	71	1346	L+R	7	<24	cardiac arrest	
6	C	F	75	1250	L+R	6	36	carcinoma	
7	C	M	80	1475	L+R	7	48	cardiac arrest	
8	C	M	91	1288	L+R	5.5	36	carcinoma	
9	AD	F	65	865	L+R	9	<12	sepsis	3
10	AD	M	66	1136	L+R	5	<24	sepsis	4
11	AD	F	69	1105	L+R	5	<12	sepsis	?
12	AD	M	69	1077	L+R	<1	<12	cachexia	12
13	AD	F	76	970	L+R	<1	6	cachexia	14
14	AD	F	76	1275	- R	5	4	status epilepticus	5
15	AD	M	77	985	L+R	<1	2.5	pneumonia	11
16	AD	F	90	1100	- R	12	<12	pneumonia	6
17	AD	M	90	1160	- R	6	<12	sepsis	3
18	AD	F	93	842	L+R	7	<12	pneumonia	16
19	PD	F	74	1370	L+R	<1	8	cardiac arrest	

Characteristics of brain material with neuropathological diagnosis, sex, age, brain weight, hemispheres available, fixation time, postmortem delay, cause of death, and duration of dementia. AD, Alzheimer's disease; C, control; F, female; L, left hemisphere; M, male; PD, Parkinson's disease; R, right hemisphere; h, hours; m, months; y, years; g, grams; ?, unknown; -, not available. P.M.: cases 9-13, early onset AD; cases 14-18, late onset AD.

- diate (Ch4i), and Ch4 posterior (Ch4p);
- both Ch4a subdivisions: anteromedial (Ch4am) and anterolateral (Ch4al).

5.3.1 Histological methods

Brains were fixed in toto in 4% formaldehyde. Postmortem delays varied from 2.5 to 50 hours. After embedding in paraffin serial sections with a thickness of 10 or 20 μm were cut using a Jung 2050 microtome. Sections were stained at regular intervals of 800 μm throughout the entire rostrocaudal extent of the NBMC. The Nissl-stain was used for counting and measuring purposes and the adjacent Klüver-Barrera-stained sections were used for identification of the NBMC and its subdivisions Ch1-Ch4.

5.3.2 Stereological methods

Morphometric analysis was carried out by counting the nucleoli, the traditional markers of neurons [50], and by measuring the maximum diameter of neurons that contained a nucleolus. Nucleolus counts were made at a 400x magnification using an ocular grid with a quadrant area of 250x250 μm^2 , subdivided into 100 squares of 25x25 μm^2 each. The nucleoli hitting the boundaries of the grid were dealt with according to the exclusion principle of Gundersen [18]. Focussing at the level of the nucleolus the maximum diameter of every nucleolated neuron (regardless of size or staining property) was measured. Four size categories (0-12.5; 12.5-25.0; 25.0-37.5 and over 37.5 μm) were chosen and the squared eyepiece graticule served as measuring scale. Medium- and large-sized neurons could easily be identified by their cytoplasm (with or without abundant Nissl substance) and their relatively pale, large, round or oval nucleus with a prominent nucleolus. In Nissl-stain small-sized neurons (<12.5 μm) could be distinguished from oligodendrocytes and astrocytes on their distribution pattern and on the morpholo-

gy of their nuclei [14]:

- macroglia, especially the oligodendroglia, are often grouped together in small clusters or chains;
- the nuclei of oligodendroglia are round or oval and small ($\leq 5\mu\text{m}$), relatively darker stained, and with many deep-blue spots;
- the nuclei of astrocytes are larger (4-10 μm), irregular and lighter stained, and with many light-blue spots, some of which (>1) are prominent, resembling nucleoli;
- apart from their somewhat Nissl-positive cytoplasm small-sized neurons contain large (5-10 μm), regular nuclei with fewer light-blue spots and with precisely one prominent nucleolus. Small-sized neurons were always larger than $\pm 7\mu\text{m}$ in their largest diameter.

A 3-dimensional-sampling scheme was used throughout the whole NBMC and its surroundings. Samples were taken systematically along three mutually perpendicular directions at intervals of 1.0 mm within the sections and 0.8 mm between the sections (see Fig. 5.2a). These three directions corresponded to three mutually perpendicular planes: the median plane, the plane through both "hippocampal axes" and the plane at an angle of 25 degrees to the frontal plane perpendicular to both former planes. For the NBMC this means about 25 equidistant sections at regular intervals of 800 μm throughout its entire rostrocaudal extent. In this 3-dimensional-sampling scheme the sampling fraction is either 1/640 (only 1 out of 40 serial 20 μm sections is considered, the section fraction = 1:40; each sample of 250x250 μm^2 represents 1/16 part of 1 mm^2 , the area fraction = 1:16) or 1/1280 (when only 1 out of 80 serial 10 μm sections is considered, the section fraction being 1:80; the area fraction remaining 1:16). Actual nucleolus number was obtained by multiplication of the number of counted nucleoli with the inverse of the sampling fraction, i.e., x640 or x1280.

The rostrocaudal length of the NBMC and its subdivisions in age-matched controls and AD was defined as the mean number of sections transecting the NBMC (or each of its subdivisions)

multiplied by the distance between the sections, i.e., x0.8 millimeters.

5.3.3 Sampling design and statistical methods

In general statistics the coefficient of error (CE) is a measure of accuracy of the average of several independent observations. The CE is statistically defined as $CV/n^{1/2}$, in which CV is defined as $SD/mean$ (abbreviations: CV = coefficient of variation; n = number of independent observations; SD = standard deviation; mean = the mean or average of n observations; $n > 1$). The lower this calculated CE, the more accurate is the average of several independent observations. From the definition of the CE it can be deduced that the accuracy (or reliability) does not depend on the standard deviation (SD remains constant in a given distribution) but on the number, n, of observations: the higher the number n, the lower the CE.

In a strict 3-dimensional-sampling scheme the position of 1 sample automatically defines the position of all other samples (see Fig. 5.2a); this first sample is the only randomly chosen sample. This dependency between all samples makes it theoretically possible to estimate the coefficient of error (CE) of each total nucleolar count ($n=1$), that is in fact a summation of several samples. CE estimation formulae have been developed [20] that can give an impression of the reliability of just 1 nucleolar count (and not of n independent counts) of a certain brain region based on the strict dependent position of all samples taken 3-dimensionally throughout the whole extent of that particular brain structure. This opens the opportunity to detect a relationship between nucleolar counts and their respective estimated CE's, and to optimize the sampling scheme.

Differences in neuron counts in AD and age-matched controls were all statistically analyzed applying the distribution-free, nonparametric Mann-Whitney U-test. Comparisons were made at the hemisphere level:

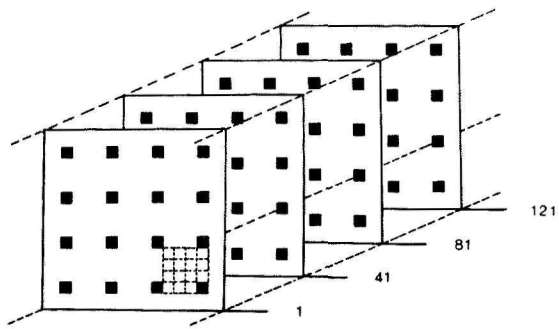


Fig. 5.2a 3-Dimensional-sampling design with section fraction of 1:40 and area fraction of 1:16. The black squares represent the counting fields of $250 \times 250 \mu\text{m}^2$. The numbers indicate sections

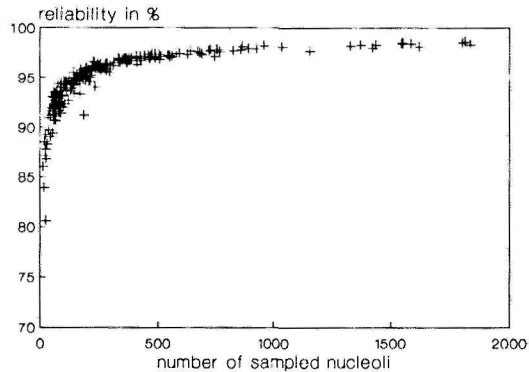


Fig. 5.2b Relation between number of neurons sampled in a 3-dimensional-sampling design and reliability expressed as % $([1-CE] \times 100\%)$

- left hemisphere : 5 young (cases 1-5) versus
3 old age-matched controls (cases 6-8);
5 early onset AD versus 2 late onset AD;
7 AD versus 8 age-matched controls;
- right hemisphere: 5 young versus 3 old age-matched controls;
5 early onset AD versus 5 late onset AD;
10 AD versus 8 age-matched controls;
- left-right : 8 left versus 8 right age-matched controls;
7 left versus 7 right AD.

In both early and late onset AD correlations were made between the duration of dementia and the total numbers of putative cholinergic neurons ($>37.5 \mu\text{m}$ and $>25.0 \mu\text{m}$) and smaller neurons ($<25.0 \mu\text{m}$).

5.4 Results

Results concern the efficiency of the 3-dimensional-sampling method, total neuron numbers of the NBMC and its subdivisions, total neuron numbers as a function of neuron size, left-right comparisons, the rostrocaudal length of the NBMC and its subdivisions in age-matched controls and in AD, and correlations between total numbers of putative cholinergic neurons and duration of dementia. Neuron counts of the left and right hemisphere of one Parkinson's disease brain will be shown.

5.4.1 The efficiency of the 3-dimensional-sampling method

For the counts of the whole NBMC, its subdivisions and of size categories each time the coefficient of error (CE) is determined, using CE estimation formulae [20]. Concerning the 3-dimensional-sampling design (sampling fraction: $1/640$; see Figs. 5.2a and 5.2b) a strict relationship between number of neurons sampled and reliability (expressed as $(1-CE)*100\%$) can be indicated: it seems not necessary to count more than 200 neurons in order to ensure a reliability of 95% ; if a reliability of 90%

suffices, not more than 50 neurons have to be sampled systematically (Fig. 5.2b). For the NBMC as a whole this 3-d-sampling scheme resulted in a mean number of 1897 sampled neurons in normal aging versus 1604 in AD; for the Ch1+Ch2 region a mean of 350 neurons was sampled in age-matched controls versus 348 in AD; for the Ch3 subdivision 100 versus 85 neurons in AD; for the Ch4a1 subdivision 262 versus 221; for Ch4am 487 neurons in age-matched controls versus 409 in AD; for Ch4i 503 versus 413 and for Ch4p 195 sampled neurons versus 124 in AD.

5.4.2 Neuron numbers of the NBMC in young and old controls

No significant differences in mean neuron numbers between young (case 1-5) and old age-matched controls (case 6-8) could be demonstrated. Therefore all age-matched controls were considered as one homogeneous group for further statistical analysis.

5.4.3 Neuron numbers of the NBMC in early and late onset AD

No significant differences in mean neuron numbers between early (case 9-13) and late onset AD (case 14-18) could be indicated. Therefore the early and late onset AD cases were considered as one group for further statistical analysis.

5.4.4 Neuron numbers of the NBMC and its subdivisions in age-matched controls and AD

Total neuron numbers in age-matched controls (young and old taken together) and AD (early and late onset together) indicated neuron loss for the NBMC as a whole and for all its subdivisions in AD except for the Ch1+Ch2 region, in which stability of neuron number was found (see Figs. 5.3a and 5.3b). Applying the Mann-Whitney U-test, significant neuron loss was demonstrated for the left (L) and right (R) NBMC as a whole (15 and 16%, L+R:

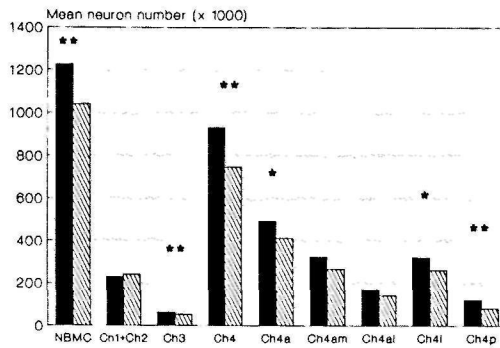


Fig. 5.3a Total number of neurons (x 1000) of the whole NBMC and subdivisions in normal aging (black bars) and Alzheimer's disease (hatched bars) of the left hemisphere. *, $p < 0.05$; **, $p < 0.01$; ***, $p < 0.001$, according to Mann-Whitney U-test.

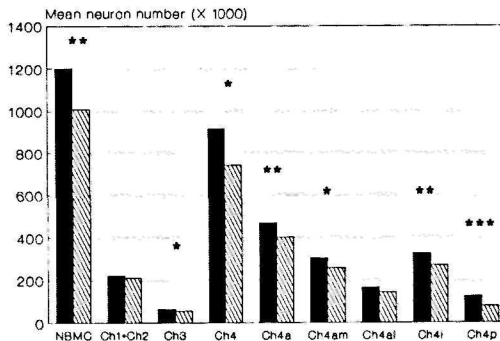


Fig. 5.3b Total number of neurons (x 1000) of the whole NBMC and subdivisions in normal aging (black bars) and Alzheimer's disease (hatched bars) of the right hemisphere. *, $p < 0.05$; **, $p < 0.01$; ***, $p < 0.001$, according to Mann-Whitney U-test.

$p < 0.01$), the nucleus basalis of Meynert as a whole (Ch4-L, 20%: $p < 0.01$; R, 19%: $p < 0.05$), the anterior part of the nucleus basalis of Meynert (Ch4a-L, 16%: $p < 0.05$; Ch4a-R, 14%: $p < 0.01$), the intermediate part (Ch4i-L, 18%: $p < 0.05$; Ch4i-R, 17%: $p < 0.01$) and the posterior part (Ch4p-L, 35%: $p < 0.01$; Ch4p-R, 37%: $p < 0.001$).

5.4.5 Neuron number as a function of neuron size

In AD the whole NBMC and all subdivisions showed a considerable loss of absolute neuron numbers of large, putative cholinergic neurons ($>25 \mu\text{m}$) and an increase of neurons of the smallest size category ($<12.5 \mu\text{m}$). Applying the Mann-Whitney U-test, a significant increase in absolute neuron numbers of the smallest size category ($<12.5 \mu\text{m}$) was demonstrated for the NBMC as a whole and for almost all its subdivisions: left hemisphere, ranging from 38 to 79% increase ($p < 0.05$, or $p < 0.01$); right hemisphere, ranging from 9 to 48% ($p > 0.05$, or $p < 0.05$). Neuron loss in the size categories 25-37.5 μm and $>37.5 \mu\text{m}$ proved to be significant for the whole left and right NBMC as well as for all left and right subdivisions (probability ranging from $p < 0.05$ to $p < 0.001$), except for R-Ch3 in size class 25-37.5 μm ($p = 0.09$).

5.4.6 Left and right hemispheric counts

Comparisons between neuron numbers of 8 left and 8 right hemispheres of age-matched controls showed no statistical difference at all; comparisons between 7 left and 7 right AD hemispheres were also not significantly different. Neuron numbers and p-values are given in Table 5.4.

5.4.7 Rostrocaudal length of the NBMC and its subdivisions

In AD the length of both the left and right NBMC was significantly reduced: $p < 0.001$. The subdivision that accounted for this

TABLE 5.3

Mean neuron numbers expressed in thousands (\pm SEM)
of the NBMC and its subdivisions as well as per size class
in age matched controls (3A)

	12.5 μ m	12.5-25.0 μ m	25.0-37.5 μ m	37.5 μ m	all cells					
3A										
NORMAL AGING										
	L	R	L	R	L	R	L	R	L	R
	(n=8)	(n=8)	(n=8)	(n=8)	(n=8)	(n=8)	(n=8)	(n=8)	(n=8)	(n=8)
NBMC	164 \pm 20	172 \pm 16	522 \pm 17	511 \pm 25	344 \pm 13	339 \pm 14	195 \pm 24	179 \pm 16	1225 \pm 17	1201 \pm 31
- Ch1+Ch2	39 \pm 4	44 \pm 5	110 \pm 9	107 \pm 9	59 \pm 2	51 \pm 4	21 \pm 2	19 \pm 2	229 \pm 10	221 \pm 14
- Ch3	12 \pm 2	15 \pm 2	35 \pm 1	34 \pm 1	14 \pm 2	12 \pm 1	3 \pm 0.5	3 \pm 0.3	64 \pm 2	64 \pm 3
- Ch4-total	113 \pm 15	113 \pm 12	377 \pm 18	370 \pm 16	271 \pm 12	276 \pm 10	171 \pm 22	157 \pm 16	932 \pm 19	916 \pm 20
- Ch4a	53 \pm 10	54 \pm 7	196 \pm 10	183 \pm 9	141 \pm 8	140 \pm 7	102 \pm 13	90 \pm 9	492 \pm 14	467 \pm 17
- Ch4am	36 \pm 8	35 \pm 6	130 \pm 8	124 \pm 9	90 \pm 5	87 \pm 7	66 \pm 9	56 \pm 4	322 \pm 14	302 \pm 16
- Ch4al	17 \pm 2	19 \pm 3	66 \pm 6	59 \pm 5	51 \pm 6	53 \pm 5	36 \pm 6	34 \pm 6	170 \pm 16	165 \pm 15
- Ch4i	44 \pm 6	42 \pm 4	132 \pm 10	135 \pm 9	93 \pm 5	98 \pm 5	50 \pm 7	50 \pm 4	319 \pm 15	325 \pm 11
- Ch4p	16 \pm 2	17 \pm 2	49 \pm 3	52 \pm 3	37 \pm 4	38 \pm 4	19 \pm 5	17 \pm 3	121 \pm 9	124 \pm 8
3B										
ALZHEIMER'S DISEASE										
	(n=7)	(n=10)	(n=7)	(n=10)	(n=7)	(n=10)	(n=7)	(n=10)	(n=7)	(n=10)
NBMC	160**	134*	102	100	57**	60***	26**	38***	85**	84**
- Ch1+Ch2	179**	121	115	103	61**	73**	41**	58*	105	96
- Ch3	138*	109	83**	90	48**	69	16**	29**	83**	88*
- Ch4-total	156*	142*	100	100	57**	57***	25**	35***	80**	81*
- Ch4a	158*	141*	109	107	62**	64***	27**	41**	84*	86**
- Ch4am	150*	143*	107	107	63**	60***	27**	41***	83	85*
- Ch4al	175*	137	111	108	60*	70*	27**	41**	84	86
- Ch4i	150*	148*	98	100	57**	56***	26**	34***	82*	83**
- Ch4p	164*	134	75*	75*	38**	37***	9**	17***	65**	63***
3C										
PARKINSON'S DISEASE										
	(n=1)	(n=1)	(n=1)	(n=1)	(n=1)	(n=1)	(n=1)	(n=1)	(n=1)	(n=1)
NBMC	109	114	103	115	95	97	97	94	100	106

Mean neuron numbers in Alzheimer's disease (3B) and Parkinson's disease (3C) are expressed as percentage of age-matched controls (3A). L, left hemisphere, R, right hemisphere; SEM, standard error of the mean; *, $p < 0.05$; **, $p < 0.01$; ***, $p < 0.001$, according to Mann-Whitney U-test.

TABLE 5.4

Mean neuron numbers of NBMC of left and right hemispheres expressed in thousands (\pm SEM) in age-matched controls and Alzheimer's disease

size class (μ m)	Normal aging		Alzheimer's disease	
	L (n=8)	R (n=8)	L (n=7)	R (n=7)
<12.5	164 \pm 20	172 \pm 16	262 \pm 16	249 \pm 12
12.5-25.0	522 \pm 17	511 \pm 25	534 \pm 30	520 \pm 28
25.0-37.5	344 \pm 13	339 \pm 14	197 \pm 13	204 \pm 12
>37.5	195 \pm 24	179 \pm 16	51 \pm 5	55 \pm 3
all cells	1225 \pm 17	1201 \pm 31	1044 \pm 38	1028 \pm 31

L, left hemisphere; R, right hemisphere; SEM, standard error of the mean; p-values according to Mann-Whitney U-test ranged from 0.53 to 0.90.

for this shortening, is the Ch4p (L:p<0.01; R:p<0.001), whereas the other subdivisions Ch4i, Ch4a, Ch3 and Ch1+Ch2 demonstrated no significant changes in length (Table 5.5).

5.4.8 Correlations between neuron numbers and duration of dementia

Although no differences were detected in both the mean neuron numbers and in the mean duration time of dementia between early (8.25 years \pm 2.8 (SEM)) and late onset AD (8.2 \pm 2.4) applying the Mann-Whitney U-test, rather strong negative correlation coefficients could be demonstrated in late onset AD patients between duration of dementia and total numbers of putative cholinergic neurons (>37.5 μ m: r=-0.80, p=0.06; >25.0 μ m: r=-0.61, p=0.15), whereas weak correlations were found in early onset AD patients (>37.5 μ m: r=0.16, p=0.71; >25.0 μ m: r=0.19,

TABLE 5.5

Rostrocaudal length (mm \pm SEM) of the NBMC and its subdivisions
in normal aging and Alzheimer's disease

structure	Normal aging		Alzheimer's disease	
	L (n=8)	R (n=8)	L (n=7)	R (n=10)
NBMC	19.6 \pm 0.6	20.0 \pm 0.7	17.6 \pm 0.2***	16.8 \pm 0.4***
- Ch1+Ch2	8.2 \pm 0.4	8.8 \pm 0.4	7.9 \pm 0.4	8.3 \pm 0.4
- Ch3	4.0 \pm 0.3	4.3 \pm 0.3	4.3 \pm 0.2	4.2 \pm 0.2
- Ch4-total	19.0 \pm 0.5	18.9 \pm 0.6	17.0 \pm 0.3*	16.3 \pm 0.5**
- Ch4a	7.2 \pm 0.3	7.3 \pm 0.4	7.0 \pm 0.3	7.5 \pm 0.2
- Ch4am	7.2 \pm 0.3	7.3 \pm 0.4	7.0 \pm 0.3	7.5 \pm 0.2
- Ch4al	6.5 \pm 0.3	6.9 \pm 0.4	6.2 \pm 0.3	6.6 \pm 0.2
- Ch4i	4.1 \pm 0.2	4.1 \pm 0.2	4.1 \pm 0.2	4.1 \pm 0.2
- Ch4p	7.7 \pm 0.2	7.5 \pm 0.4	5.8 \pm 0.2**	4.8 \pm 0.3***

L, left hemisphere; R, right hemisphere; mm, millimeter; SEM, standard error of the mean; *, p < 0.05; **, p < 0.01; ***, p < 0.001, according to Mann-Whitney U-test.

p=0.66). Small-sized neurons showed only weak correlations with duration of dementia (-0.29 < r < 0.33). However, none of these correlations was significant, probably due to the limited number of cases studied rather than to lack of a relationship.

5.4.9 Neuron numbers and sizes in Parkinson's disease

All neuron numbers per size category and per size class fell within the range of neuron numbers of age-matched controls. Because just one left and right hemisphere of the same Parkinson brain have been investigated, only the counting data of the whole NBMC are illustrated (Table 5.3c).

5.5 Discussion

It is obvious that the large variation in neuron counts in the NBMC in AD as reported in the literature has to be attributed not only to differences in methodology (Table 5.1), but also to the disease process itself: variation exists in which subdivisions are affected [4, 11, 56, this paper]; additionally, increasing age at onset of the AD cases is inversely related to the loss of large neurons [48]; and lastly, the duration of dementia may turn out to be another important variable affecting neuronal loss [this paper].

5.5.1 Discussion on methodology

This paper points out that methodology has a major effect whether all neurons are counted irrespective of their size and staining characteristics, or whether only magnocellular, hyperchromatic (presumptive cholinergic) neurons are counted. Secondly, this paper shows that the subdivisions of the NBMC are differently affected in AD with respect to cell loss and cell shrinkage; therefore, it certainly does not suffice to investigate only a small part of the NBMC, especially because the NBMC is a large, complex, and highly differentiated structure characterized by a marked irregularity in arrangement and distribution of its constituent neurons. Moreover, if neuron counts have not been performed systematically throughout the entire extent of the NBMC and its subdivisions, and therefore had to be expressed as numerical densities (i.e., neuron numbers per unit volume), possible changes in length or volume of the NBMC could not have been taken into account. As this paper demonstrates (Table 5.5), the length of the NBMC in AD is significantly shorter, and this finding itself makes the cell loss even more severe than is indicated by decreased density alone.

Until now, only two studies [4, 5] performed neuron counts systematically throughout the entire rostrocaudal extent of the NBMC, as was done too for the nucleus basalis of Meynert [29,

32]; however, in these studies only large, hyperchromatic neurons were counted. Quantitative studies that did count all neurons irrespective of size and staining characteristics, showed an increase in small-sized neurons [1, 37, 41, 53], indicating neuronal shrinkage. However, these studies were possibly biased by either the use of mean densities instead of total neuron numbers [1, 37, 41, 53], or by overcounting due to splitting error of the perikaryon [1, 37, 53] that was used as counting item instead of the nucleolus (Table 5.1).

All studies but those that performed systematic counts expressed neuron numbers as numerical densities i.e., number per unit volume. Use of this parameter is only permitted under the assumption of stability of total volume of the brain structure of interest under pathological conditions. However, recent studies [36, 47] clearly demonstrated changes in total volume of particular brain structures in various neurological and psychiatric disorders. The present study revealed a significant decrease in the total length (and probably in volume, too) of the Ch4p region of the NBMC. Since neuropathologists so far have almost exclusively used numerical densities in their search for changes in the brain in relation to various neurological and psychiatric conditions, alterations in total neuron numbers may have been underestimated or exaggerated. Therefore, numerical densities are parameters to avoid. This bias generated by using numerical density and by investigating only a small part of the NBMC, can be avoided by applying the Cavalieri's principle [9, 20, 31, 49] upon the whole NBMC or any structure in general. The Cavalieri's principle can be used as a total volume estimator: the total volume of any arbitrary object can be estimated by summation of the cross-sectional areas of systematically taken (i.e., at regular intervals with a random start) equidistant sections, multiplied with the distance between two sections (see Fig. 5.4). If at least eight systematic sections are used, the total volume can be estimated with a coefficient of error (CE) less than five percent [20]. Total cell number can be obtained by multiplying the total volume by the mean numerical density. However, reliable determination of cross-sectional areas demands

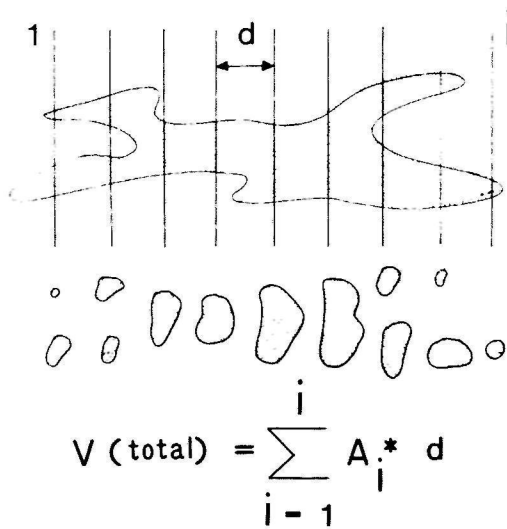


Fig. 5.4: Cavalieri's principle to estimate total volume of any arbitrary object on at least 8 systematical sections, resulting in a reliability of >95%.

sharply delineated boundaries of the structure of interest, a requirement the NBMC cannot fulfill because of its indistinct boundaries (see Fig. 5.1). We developed a 3-dimensional-sampling scheme through a dissected part of the brain large enough to contain the whole NBMC, under the necessity that it is possible to identify unambiguously each neuron belonging to the NBMC [19]. Bias can then be eliminated by sampling neurons (regardless of their size and staining characteristics) systematically throughout the length of the whole NBMC. Theoretically, such a 3-dimensional-sampling design can be applied to any arbitrary object independent of its shape without homogeneity assumptions and without regard to distinct or indistinct boundaries [20]. Although the 3-d-sampling method seems to be elaborate because samples at several levels have to be taken through the whole

extent of the structure, it is not as time consuming and inefficient as expected at first glance: as Fig. 5.2b points out, it can be realized that counting more than 200 neurons is not worth the effort: a tenfold increase in workload (2000 neurons instead of 200) only enhances the reliability from 95 to 98%. It is the sampling step that is time consuming, but not the counting step since 200 neurons always suffice for a reliability of 95% in a 3-d-sampling design. The workload is largely dependent on the number of subdivisions and size categories investigated, since in each subdivision or size category per subdivision 200 neurons have to be sampled to reach 95% reliability or 50 neurons for 90% reliability. If one is only interested in total neuron numbers (not classified into size classes) of the whole NBMC, sampling and counting will take no more than 2 hours per hemisphere. However, for making statements about all subdivisions including size categories, two days workload are necessary to maintain a reliability of at least 90% for each of the 24 constituting subsets in our analysis (four size categories per Ch1+Ch2; per Ch3; Ch4am; Ch4al; Ch4i and Ch4p). An exact 3-dimensional-sampling scheme cannot strictly be realized in practice, but can at best be approximated. Therefore the value of the estimated CE of each neuron number will in fact be slightly higher. So, sampling more than 200 neurons does not per se imply a reliability of over 95%. However, this certainly does not mean any release from applying a 3-d-sampling scheme as carefully as possible.

For determination of neuron size the maximum diameter was measured with the nucleolus being in focus. This approach is biased in two ways: firstly, maximum diameter is dependent on the orientation of the neuron in space and therefore on the angle of the section plane; secondly, focussing at the level of the nucleolus and measuring the maximum diameter does not ensure the real maximum diameter of the neuron [6]. The possibility of nucleolus displacement from the centre of the soma is far from theoretical, because accumulation of lipofuscin in normal aging and moreover presence of neurofibrillary tangle formations in Alzheimer's disease in fact do displace the nucleus and nucleolus

towards an eccentric position. However, to maintain the possibility of comparison with data from the literature, no correction for this bias has been made.

The effect of different section thickness (10 or 20 μm) upon probable nucleolus splitting in paraffin sections [e.g. 10, 11] is of no significant influence [submitted, 1989]: using the disector [46] to trace actual splitting of nucleoli in two adjacent sections only 10.5% of 100 nuclei and none of the nucleoli were split in 10 μm sections. Therefore, it was justified to use both 10 μm and 20 μm serially sectioned brains in the same series, if the nucleolus is the counting item.

5.5.2 Discussion of results

The counting data obtained by this 3-dimensional-sampling method represent the first unbiased total neuron numbers of the NBMC and its subdivisions. For the nucleus basalis of Meynert (Ch4) the total neuron number per hemisphere was 164.000 neurons larger than 37.5 μm and 274.000 neurons sized between 25.0 and 37.5 μm in the normal aged brain. This is not considerably different from the 200.000 neurons larger than 30 μm [4] and almost similar to the 150.000 [32] and 120.000 [29] neurons larger than 35 μm in control patients over the age of 65 years [32] and in the 9th decade respectively [29]. For the first time neuron numbers in Ch3 are determined: 3000 neurons larger than 37.5 μm on a total of 64.000 neurons.

In AD an overall neuron loss of only 15.5% for the whole NBMC and 19.5% for Ch4 was demonstrated. This is in full agreement with another study [37], in which antibodies to choline acetyltransferase were used and that reported an 18% neuron loss of the Ch4a in one AD brain without taking a minimum size criterion for neurons into account. Moreover, neuron numbers clearly reveal a differential involvement in the pathology of the subdivisions of the NBMC in AD: whereas the rostral Ch1+Ch2 region shows no neuron loss at all, Ch3, Ch4a, Ch4i and especially Ch4p are significantly affected. Ch4p is the only subdivision with a

rather circumscript projection pattern to monkey temporopolar and superior temporal cortex [33] and therefore it would be interesting to investigate cholinergic changes in these cortical areas in AD patients in order to indirectly verify anatomical connectivity between Ch4p and these cortical structures in human.

Total neuron numbers per size category unequivocally detect a shift from large into small neurons resulting in a significant increase of small-sized neurons ($<12.5 \mu\text{m}$) for the NBMC as a whole and for all the subdivisions, ranging from 9 to 48% for the right hemisphere, and from 38 to 79% for the left (no significant differences could be detected between neuron numbers of left and right hemispheres in both AD and age-matched controls). Many investigators (Table 5.1) reported a marked loss of magnocellular neurons in the NBMC in AD; our results support these reports: we found a 68% reduction in neurons with a maximum diameter $>37.5 \mu\text{m}$ for the whole NBMC and a 70% reduction for Ch4.

Subdividing the AD patients in early onset ($n=5$) and late onset AD patients ($n=5$) no significant differences were found in either mean total neuron numbers per size category nor in the mean duration of apparent dementia ($8.25 \text{ years} \pm 2.8$ (SEM) versus 8.2 ± 2.4) (Table 5.2). However, in late onset AD a rather strong correlation can be demonstrated between duration of dementia and numbers of large neurons ($>37.5 \mu\text{m}$: $r=-0.80$, $p=0.06$; $>25.0 \mu\text{m}$: $r=-0.61$, $p=0.15$), whereas no correlations can be indicated for early onset ($r=0.16$; $p=0.71$ and $r=0.19$; $p=0.66$, respectively). This finding suggests the possibility of a different disease process for late onset AD, although these data have to be interpreted with caution, because: 1) the validity of the start point of dementia and thus its duration time is difficult to ascertain, 2) the duration time is not necessarily correlated with the degree of dementia (not assessed in this study), 3) the number of brains in this study is limited, and 4) it is methodologically wrong to quantitate only magnocellular neurons, as this paper demonstrates.

Considering the loss of large neurons and the absolute increase in small neurons, our results suggest neuron death and neuron shrinkage as well. In the Ch1+Ch2 region that projects

mainly to the hippocampus, which is heavily affected in AD, only shrinkage seems to occur, possibly suggesting a secondary retrograde degeneration process. In other NBMC subdivisions shrinkage combined with neuron death (to a limited extent) can be found. Whether neuron death has to be interpreted as the ultimate result of shrinkage due to secondary degeneration or as a possible primary degeneration process due to yet unknown factors has to await further future analysis. Atrophy of cholinergic neurons has been described in rat, monkey and man following cortical damage [38, 43, 44, 45], indicating retrograde degeneration. It has been hypothesized that lack of specific neurotrophic factors could be the cause of Alzheimer's disease [2], such as lack of nerve growth factor (NGF) [22]. It is well known, that retrograde transport of NGF to basal forebrain cholinergic neurons occurs from their target zones in hippocampus and cerebral cortex, that NGF exerts a cytoprotective effect on cholinergic cells following fimbrial transection and that NGF elevates choline acetyltransferase activity in vitro and in vivo [54]. Immunocytochemical studies have shown extensive loss of NBMC neurons positive for nerve growth factor-receptors (NGF-r) [23, 26]. In contrast, no change in NGF-r mRNA levels in basal forebrain [17] nor in NGF mRNA levels in cerebral cortex [16] from patients with AD was found using RNA dot-blotting techniques. However, using the more sensitive, quantitative in situ hybridization analysis, it was recently demonstrated that NGF-r gene expression is extensively decreased in the Ch4 region, but not in the Ch1+Ch2 region in AD [24]. The reduction in NGF-r gene expression was most severe in Ch4p, the posterior part of the NBMC. This rostrocaudal decrease in NGF-r gene expression closely matches our findings of increasing cell loss and shrinkage from the anterior Ch1+Ch2 region to the posterior Ch4p. Recent studies suggest that NGF regulates the expression of its own receptor in the central nervous system [12, 28]. Therefore, the decrease in NGF-r gene expression in NBMC neurons in AD may result from a lack of NGF support due to cortical atrophy. Moreover, insulin and insuline-like growth factors I and II (IGF) potentiate the response to NGF by increasing the number of NGF-

receptors by an up-regulation of the NGF-r gene [40]. A possible defect in IGF diffusion from the production sites in neocortex and hippocampus to the axonal endings of the basal forebrain cholinergic neurons may contribute to the lack of NGF as a consequence of mechanical barriers due to amyloid depositions in AD; using in situ hybridization techniques we were able to demonstrate that IGF is produced in the endothelial cells of the vessel wall [Broere and Vogels, unpublished observations]. In AD, amyloid depositions known as congophilic angiopathy may provide such a barrier [15].

In conclusion, our findings that neuron death is limited in the NBMC and that neuron shrinkage is a main neuropathological feature in AD may provide a basis on which the therapeutic aspects of neurotrophic factor(s) can be explored.

5.6 References

1. Allen SJ, Dawbarn D and Wilcock GK. Morphometric immunochemical analysis of neurons in the nucleus basalis of Meynert in Alzheimer's Disease. *Brain Res* 1988;454:275-81.
2. Appel SH. A unifying hypothesis for the cause of amyotrophic lateral sclerosis, Parkinsonism, and Alzheimer's Disease. *Ann Neurol* 1981;10:499-505.
3. Arendt T, Bigl V, Arendt A and Tennstedt A. Loss of neurons in the nucleus basalis of Meynert in Alzheimer's disease, Paralysis agitans and Korsakoff's disease. *Acta Neuropathol (Berl)* 1983;61:101-8.
4. Arendt T, Bigl V, Tennstedt A and Arendt A. Neuronal loss in different parts of the nucleus basalis is related to neuritic plaque formation in cortical target areas in Alzheimer's Disease. *Neurosci* 1985;14:1-14.
5. Bigl V, Arendt T, Fischer S, Fischer S, Werner M and Arendt A. The cholinergic system in aging. *Gerontology* 1987;33:172-80.
6. Born DE, Carman CS and Rubel EW. Correcting errors in estimating neuron area caused by the position of the nucleolus. *J Comp Neurol* 1987;255:146-52.
7. Candy JM, Perry RH, Perry EK, Irving D, Blessed G, Fairbairn AF and Tomlinson BE. Pathological changes in the nucleus of Meynert in Alzheimer's and Parkinson's diseases. *J Neurol Sci* 1983;54:277-89.
8. Chui HC, Bondareff W, Zarow C and Slager U. Stability of neuronal number in the human nucleus basalis of Meynert with age. *Neurobiol Aging* 1984;5:83-8.
9. Cruz-Orive L-M. Estimating volumes from systematic hyperplane sections. *J Appl Prob* 1985;22:518-30.
10. Doucette R, Fisman M, Hachinsky VC and Mersky M. Cell loss from the nucleus basalis of Meynert in Alzheimer's Disease. *Can J Neurol Sci* 1986;13:435-40.

11. Etienne P, Robitaille Y, Gauthier S and Nair NPV. Nucleus basalis neuronal loss and neuritic plaques in advanced Alzheimer's Disease. *Can J Physiol Pharmacol* 1986;64:318-24.
12. Gage FH, Batchelor P, Chen KS, Chin D, Deputy S, Rosenberg MS, Higgins GA, Koh S, Fischer W and Bjorklund A. NGF-receptor re-expression and NGF-mediated cholinergic neuronal hypertrophy in the damaged adult neostriatum. *Neuron* 1989;2:1177-84.
13. Gertz HJ, Cervos-Navarro J and Ewald V. The septohippocampal pathway in patients suffering from senile dementia of Alzheimer's type. Evidence for neuronal plasticity? *Neurosci Lett* 1987;76:228-32.
14. Glees P. Neuroglia. Morphology and function. Oxford: Blackwell Scientific Publications, 1955.
15. Glenner GG, Henry JH and Fujihara S. Congophilic angiopathy in the pathogenesis of Alzheimer's degeneration. *Ann Pathol* 1981;1:120-9.
16. Goedert M, Fine A, Hunt SP and Ullrich A. Nerve growth factor mRNA in peripheral and central rat tissues and in the human central nervous system: lesion effects in the rat brain and levels in Alzheimer's disease. *Molecular Brain Res* 1986;1:85-92.
17. Goedert M, Fine A, Dawbarn D, Wilcock GK and Chao MV. Nerve growth factor receptor mRNA distribution in human brain: normal levels in basal forebrain in Alzheimer's disease. *Molecular Brain Res* 1989;5:1-7
18. Gundersen HJG. Notes on the estimation of the numerical density of arbitrary profiles: the edge effect. *J Microsc* 1977;111:219-23.
19. Gundersen HJG. Stereology of arbitrary particles. A review of unbiased number and size estimators and the presentation of some new ones, in memory of William R Thompson. *J Microsc* 1986;143:3-45.
20. Gundersen HJG and Jensen EB. The efficiency of systematic sampling in stereology and its prediction. *J Microsc* 1987;147:229-63.
21. Haug H. Are neurons of the human cerebral cortex really lost during aging? A morphometric examination. In: Traber J, and Gispen WH, eds. *Senile dementia of the Alzheimer type*. Berlin: Springer, 1985:150-63.
22. Hefti F. Is Alzheimer's Disease caused by lack of nerve growth factor? *Ann Neurol* 1983;13:109-10.
23. Hefti F and Mash DC. Localization of nerve growth factor receptors in the normal human brain and in Alzheimer's disease. *Neurobiol Aging* 1989;10:75-87.
24. Higgins GA and Mufson EJ. NGF receptor gene expression is decreased in the nucleus basalis in Alzheimer's disease. *Exp Neurol*, in press, 1989.
25. Khachaturian ZS. Diagnosis of Alzheimer's Disease. *Arch Neurol* 1985;42:1097-105.
26. Kordower JH, Gash DM, Bothwell M, Hersh L and Mufson EJ. Nerve growth factor receptor and choline acetyltransferase remain colocalized in the nucleus basalis (Ch4) of Alzheimer's patients. *Neurobiol Aging* 1989;10:67-74.
27. Lams BE, Isacson O and Sofroniew MV. Loss of transmitter-associated enzyme staining following axotomy does not indicate death of brainstem cholinergic neurons. *Brain Res* 1988;475:401-6.
28. Larkfors L, Ebendahl T, Whittemore SR, Persson H, Hoffer B and Olson L. Decreased levels of nerve growth factor (NGF) and its messenger RNA in the aged rat brain. *Mol Brain Res* 1987;3:55-60.
29. Lowes-Hummel P, Gertz H-J, Ferszt R and Cervos-Navarro J. The basal nucleus of Meynert revised: the nerve cell number decreases with age. *Arch Gerontol Geriatr* 1989;8:21-7.
30. Mann DMA, Yates PO and Marcyniuk B. Alzheimer's presenile dementia, senile dementia of Alzheimer type and Down's syndrome in middle age form

- an age related continuum of pathological changes. *Neuropathol Appl Neurobiol* 1984;10:185-207.
31. Mattfeldt T. Volume estimation of biological objects by systematic sections. *J Math Biol* 1987;25:685-95.
 32. McGeer PL, McGeer EG, Suzuki J, Dolman CE and Nagai T. Aging, Alzheimer's Disease, and the cholinergic system of the basal forebrain. *Neurol* 1984;34:741-5.
 33. Mesulam M-M, Mufson EJ, Levey AI and Wainer BH. Cholinergic innervation of cortex by the basal forebrain: cytochemistry and cortical connections of the septal area, diagonal band nuclei, nucleus basalis (substantia innominata) and hypothalamus in the rhesus monkey. *J Comp Neurol* 1983;214:170-97.
 34. Mesulam M-M and Geula C. Nucleus basalis (Ch4) and cortical cholinergic innervation in the human brain: observations based on the distribution of Acetylcholinesterase and Choline Acetyltransferase. *J Comp Neurol* 1988;275:216-40.
 35. Nagai T, McGeer PL, Peng JH, McGeer EG and Dolman CE. Choline acetyltransferase immunohistochemistry in brains of Alzheimer's disease patients and controls. *Neurosci Lett* 1983;36:195-9.
 36. Pakkenberg B and Gundersen HJG. Total number of neurons and glial cells in human brain nuclei estimated by the disector and the fractionator. *J Microsc* 1988;150:1-20.
 37. Pearson RCA, Sofroniew MV, Cuellar AC, Powell TPS, Eckenstein F, Esiri MM and Wilcock GK. Persistence of cholinergic neurons in the basal nucleus in a brain with senile dementia of the Alzheimer type demonstrated by immunohistochemical staining for choline acetyltransferase. *Brain Res* 1983;289:375-9.
 38. Pearson RCA, Gatter KC and Powell TPS. Retrograde cell degeneration in the basal nucleus in monkey and man. *Brain Res* 1983;261:321-6.
 39. Perry RH, Candy JM, Perry EK, Irving D, Blessed G, Fairburn F and Tomlinson BE. Extensive loss of choline acetyl transferase activity is not related to neuronal loss in nucleus of Meynert in Alzheimer's disease. *Neurosci Lett* 1982;33:311-5.
 40. Recio-Pinto E and Ishii DN. Insulin and related growth factors: effects on the nervous system and mechanism for neurite growth and regeneration (review). *Neurochem Int* 1988;12:397-414.
 41. Rinne JO, Paljarvi L and Rinne UK. Neuronal size and density in the nucleus basalis of Meynert in Alzheimer's disease. *J Neurol Sci* 1987;79:67-76.
 42. Sass N-L. The age-dependent variation of the embedding-shrinkage of neurohistological sections. *Microscopie* 1982;39:278-81.
 43. Sofroniew MV, Pearson RCA, Eckenstein F, Cuellar AC and Powell TPS. Retrograde changes in cholinergic neurons in the basal forebrain of the rat following cortical damage. *Brain Res* 1983;289:370-4.
 44. Sofroniew MV, Pearson RCA and Powell TPS. The cholinergic nuclei of the basal forebrain of the rat: normal structure, development and experimentally induced degeneration. *Brain Res* 1987;411:310-31.
 45. Stephens PH, Tagari PC and Cuellar AC. Retrograde degeneration of basal forebrain cholinergic neurons after neurotoxin lesions of the neocortex: application of ganglioside GM₁. *Neurochem Int* 1988;12:475-81.
 46. Sterio DC. The unbiased estimation of number and sizes of arbitrary particles using the disector. *J Microsc* 1984;134:127-36.
 47. Swaab DF, Roozendaal B, Ravid R, Velis DN, Gooren L and Williams LS. Suprachiasmatic nucleus in aging, Alzheimer's disease, transsexuality and Prader-Willi syndrome. In: de Kloet ER, Wiegant VM and de Wied D, eds.

- Neuropeptides and Brain Function. Amsterdam: Elsevier Science Publisher BV, Prog Brain Res 1987;72:301-10.
48. Tagliavini F and Pilleri G. Basal nucleus of Meynert. A neuropathological study in Alzheimer's disease, Simple Senile Dementia, Pick's disease and Huntington's chorea. J Neurol Sci 1983;62:243-60.
 49. Uylings HBM, van Eden CG and Hofman MA. Morphometry of size/volume variables and comparison of their bivariate relations in the nervous system under different conditions. J Neurosci Meth 1986;18:19-37.
 50. Weibel ER. Stereological Methods, Vol 1: Practical Methods for Biological Morphometry. London: Academic Press, 1979.
 51. Whitehouse PJ, Price DL, Clark AW, Coyle JT and DeLong MR. Alzheimer disease: evidence for selective loss of cholinergic neurons in the nucleus basalis. Ann Neurol 1981;10:122-6.
 52. Whitehouse PJ, Price DL, Struble RG, Clark AW, Coyle JT and DeLong MR. Alzheimer's Disease and Senile Dementia: loss of neurons in the basal forebrain. Science 215:1982:1237-9.
 53. Whitehouse PJ, Hedreen JC, Jones BE and Price DL. A computer analysis of neuronal size in the nucleus basalis of Meynert in patients with Alzheimer's Disease. Ann Neurol 1983;14:149-50.
 54. Whitemore SR and Seiger Å. The expression, localization and functional significance of β -nerve growth factor in the central nervous system. Brain Res Rev 1987;12:439-64.
 55. Wilcock GK, Esiri MM, Bowen DM and Smith CCT. The nucleus basalis in Alzheimer's disease: cell counts and cortical biochemistry. Neuropathol Appl Neurobiol 1983;9:175-9.
 56. Wilcock GK, Esiri MM, Bowen DM and Hughes AO. The differential involvement of subcortical nuclei in senile dementia of Alzheimer's type. J Neurol Neurosurg Psychiatr 1988;51:842-9.

**NEURONAL HYPERTROPHY IN THE HUMAN SUPRAOPTIC AND PARAVENTRICULAR
NUCLEUS IN AGING AND ALZHEIMER'S DISEASE**

O.J.M. Vogels, C.A.J. Broere and R. Nieuwenhuys
(Neuroscience Letters 1990: in press)

6.1 Abstract

In the literature activation of the hypothalamo-neurohypophyseal system (HNS) in normal aging has been demonstrated in rat and human. This activation might be secondary to an age-related decline in vasopressin binding sites in the kidney, or to cell loss in the supraoptic (SON) and paraventricular nuclei (PVN) and/or to an age-related decline in noradrenergic (NA) innervation of the hypothalamus. This study shows neuronal hypertrophy in SON and PVN in normal aging and an additional hypertrophy in Alzheimer's disease. No cell loss could be demonstrated in both conditions.

6.2 Introduction

It has long been known that the neurohormones vasopressin (AVP) and oxytocin (OXT) are produced in the supraoptic (SON) and paraventricular nucleus (PVN), two centres situated in the anterior hypothalamus [2]. In the SON a predominance of AVP cells was found ranging from 90% [7] to 95% [5]. In the PVN 53% of the magnocellular neurons were shown to be AVP cells [7], whereas others reported 70-80% AVP cells in the PVN [5].

In the aging rat an increased activity of the AVP-cells has been reported [6], and cell numbers of SON and PVN were found to be unchanged [26]. Recently, an age-related increase of the

blood levels of AVP was demonstrated in humans [8,15,24], and an increase in nucleolar [12] and cellular size of human AVP-cells after 80 years of age [7] also indicated an activation of AVP-cells; similar changes in nucleolar and cellular size were found in senile dementia of the Alzheimer type (SDAT) [7]. Three explanations for this activation of the hypothalamo-neurohypophyseal system (HNS) in aging have been indicated in the literature:

1. The activation of the AVP cells could serve as a compensatory mechanism for cell loss in the SON and PVN (cf.[7,12]).
2. The HNS-activation might be secondary to an age-related decline in AVP-binding sites in the kidney as has already been shown in rat [23].
3. Increased HNS-activity might be related to a reduction of noradrenergic (NA) innervation of magnocellular SON and PVN neurons, originating from the locus coeruleus [16]. Evidence for such a reduction has been provided for the aging rat [28,29]; in the aging human brain cell loss in the locus coeruleus has been demonstrated [21,32], and in Alzheimer's disease (AD) cell loss is even much greater [3,18,32], strongly suggesting a reduction in NA hypothalamic input.

Total neuron number in the human PVN was recently found to remain constant in normal aging [11]. Until now, it is not known whether cell loss in the human PVN occurs in AD, nor whether cell loss in the human SON occurs in normal aging or in AD. The aim of this study is to determine total neuron numbers of the SON and PVN in both normal aging and AD, and to determine cell sizes of SON and PVN neurons in both conditions, regarding cell size as a rough measure for functional activity.

6.3 Material and methods

Fifteen normally aged (range 62-91y; mean age \pm SEM (standard error of the mean): 75.5 \pm 2.4y) and 19 AD anterior hypothalami (range 65-93y; 77.3 \pm 2.2y) were processed (Table 3.1). Histological examination showed all control brains (11 men, 4 women) to be essentially normal, and neuropathological study of all AD brains

(9 men, 10 women) confirmed the clinical diagnosis and excluded other structurally identifiable disorders [14]. The duration of illness varied between 3 and 16 years. The immediate cause of death was broadly similar, in $\pm 55\%$ of both groups being associated with hypoxia and hypotension, both of which can influence peripheral release of AVP [1,27]. No conclusive data on medication known to affect AVP secretion were available. Mean postmortem delays (hrs) in age matched controls (AMC) were longer than in AD (33 ± 2.7 versus 11 ± 1.2), whereas fixation times (months) were similar (5.8 ± 0.5 versus 5.2 ± 0.8). In our brain material, the entire rostrocaudal extent of the SON was present in all of these anterior hypothalami; however, the PVN with its long dorsocaudal extension was entirely present in only 10 normally aged (range 65-91y; $76.0 \pm 2.8y$) and 11 AD anterior hypothalami (69-93y; 79.2 ± 3.0).

After fixation in formaldehyde and embedding in paraffin, serial sections with a thickness of $20 \mu\text{m}$ were cut and stained by cresyl-fast violet at regular intervals of $800 \mu\text{m}$. Morphometric analysis was carried out by counting the nucleoli, the traditional markers of neurons [33], and by measuring the maximum diameter (d_{MAX}) of the neurons. Approximately 1 out of 1000 neurons showed double nucleoli, so no corrections were made for overcounting. Nucleolus counts were made at a $\times 400$ magnification using an ocular grid with a quadrant sampling area of $250 \times 250 \mu\text{m}^2$, subdivided into 100 small squares of $25 \times 25 \mu\text{m}^2$ each. The nucleoli hitting the left and lower boundaries of the grid were dealt with according to the exclusion principle of Gundersen [9]. At a $\times 400$ magnification nucleoli were always distinct and clearly visible, and small neurons could be easily distinguished from glia. With the nucleolus in focus, the d_{MAX} of the soma was determined, using the small squares of $25 \times 25 \mu\text{m}^2$ as a measuring scale. The d_{MAX} data were recorded in 4 size categories: $< 12.5 \mu\text{m}$, $12.5 - 25 \mu\text{m}$, $25 - 37.5 \mu\text{m}$ and $> 37.5 \mu\text{m}$ in order to detect a possible shift from small-sized neurons to large-sized neurons indicative for hypertrophy. To determine total cell numbers and cell numbers per size category, we developed an efficient sampling design throughout the entire rostrocaudal extent of the

SON and PVN (1 out of every 40th section, and 1/4 of the section area was sampled systematically, i.e., 4 samples/1 mm²; sampling fraction: 1/160; total cell number = sampled cell number multiplied with 160). This systematic sampling design enabled us to estimate the reliability of each total number of sampled neurons in a particular structure [10]: sampling more than 200 SON or PVN neurons always resulted in a sufficiently high reliability (>90%) (Figs 3.5a and b). Neuron numbers were statistically analyzed using the nonparametric Mann-Whitney U-test.

6.4 Results

Total neuron numbers of PVN did not change after 65 years of age (mean \pm SEM in thousands: 122.3 \pm 4.5; n=10) nor did they differ from total neuron numbers in AD (123.2 \pm 3.6; n=11). However, in AD neuron numbers per size category of the PVN showed a significant decrease (p<0.05) of small-sized neurons (<12.5 μ m) and a significant increase (p<0.05) of large-sized neurons (>37.5 μ m; Table 6.1) as compared to AMC, indicating neuronal hypertrophy of the PVN cells in AD. Although the same trend was present in normal aging after 65 years of age, no significant differences could be demonstrated between "young" (65-75y; n=6) and "old" AMC (76-91; n=4) (Table 6.1).

Total neuron numbers of the SON did not change after 62 years of age (mean \pm SEM in thousands: 58.4 \pm 4.6; n=15) nor did they differ from total neuron numbers in AD (57.0 \pm 2.1; n=19) (Table 6.1). However, in normal aging (after 62 years of age) neuron numbers of size class 25.0-37.5 μ m in "old" AMC (76-91y; n=6) were significantly increased (p<0.05) as compared to "young" AMC (62-75y; n=9), indicating neuronal hypertrophy (Table 6.1). Moreover, in AD neuron numbers per size category of the SON showed a significant decrease (p<0.05) of small-sized neurons (<12.5 μ m) and a significant increase (p<0.01) of large-sized neurons (>37.5 μ m) as compared to AMC, indicating an additional neuronal hypertrophy of the SON in AD (Table 6.1).

TABLE 6.1

Mean neuron numbers \pm SEM per size class of PVN and SON in young and old age-matched controls and Alzheimer's disease

PVN	AMC-y	AMC-o	AMC-t	AD
d_{MAX} (μ m)	(n=6)	(n=4)	(n=10)	(n=11)
<12.5	19.0 \pm 3.0	18.8 \pm 1.6	18.9 \pm 2.5	13.6 \pm 0.8*
12.5-25	68.3 \pm 4.5	68.1 \pm 3.9	68.2 \pm 4.4	66.3 \pm 3.3
25-37.5	24.4 \pm 2.1	28.1 \pm 2.9	25.9 \pm 2.7	31.4 \pm 2.2
>37.5	9.3 \pm 1.8	9.3 \pm 1.5	9.3 \pm 1.7	11.9 \pm 1.3*
all cells	121.0 \pm 4.6	124.3 \pm 4.0	122.3 \pm 4.5	123.2 \pm 3.6
SON	AMC-y	AMC-o	AMC-t	AD
d_{MAX} (μ m)	(n=9)	(n=6)	(n=15)	(n=19)
<12.5	5.4 \pm 1.6	4.4 \pm 1.2	5.0 \pm 1.5	1.8 \pm 0.4*
12.5-25	22.5 \pm 3.3	22.0 \pm 2.9	22.3 \pm 3.3	19.3 \pm 2.4
25-37.5	19.6 \pm 1.9	25.6 \pm 1.5*	22.0 \pm 2.1	22.6 \pm 1.5
>37.5	8.5 \pm 1.2	9.8 \pm 2.1	9.1 \pm 1.6	13.3 \pm 1.5**
all cells	56.1 \pm 4.4	61.7 \pm 2.8	58.4 \pm 4.6	57.0 \pm 2.1

AD, Alzheimer's disease; AMC, age-matched controls; y, young; o, old; t, total; PVN, paraventricular nucleus; SON, supraoptic nucleus; *, p<0.05; **, p<0.01 according to Mann-Whitney U-test.

No significant correlation was present between neuron numbers per size class and either postmortem delay ($r=-0.31$; $p>0.2$) or duration of illness ($r=-0.35$; $p>0.3$). No differences between men and women could be detected. No cytopathological changes could be found in these hypertrophied cells.

6.5 Discussion

Our results confirm the activation of the human HNS in aging as reported by others [7,8,12,15,24]. This activation is not due to a compensatory mechanism for cell loss in the PVN and SON since total neuron numbers remain constant during aging. Moreover, although the PVN and SON do not reveal any cell loss in AD, an additional activation of the HNS can be indicated in AD. Our results and those of others [7,12] are in contrast with a study reporting decreased nuclear and nucleolar volume of neurons in PVN and SON [17]. This difference may be due to the small number of subjects investigated and to the methodology used. We investigated several hundreds of neurons spread over approximately 9 different levels, whereas the other study [17] investigated 40 neurons in 1 section, neglecting the changing distribution of AVP and OXT neurons in the PVN in rostrocaudal direction [7].

The total neuron number of the SON as reported here (58.400) is almost similar to that found in a previous study (52.600) in 5 control persons over the age of 62 years [22], but the total neuron number of the PVN (122.000) is more than twice the number of 55.500 in the same study [22]. The discrepancy in PVN neuron number is probably due to the fact that the latter study quantitated only magnocellular cells in the PVN, that contains also numerous small sized neurons contrary to the SON (Table 6.1). The less pronounced activation of the PVN as a whole in normal aging and in AD as compared to the SON in this study, is probably due to the smaller fraction of AVP cells in the PVN [5,7]: the effect of activation of the AVP cells is "diluted" by the presence of many small-sized, probably non-AVP cells in the PVN. Although OXT neurons in the SON and PVN are reported to be normal in AD [7], they are probably hypertrophied too but to a lesser extent than the AVP cells that might undergo an additional hypertrophy due to an age-related decline in AVP-binding sites in the human kidney as has been demonstrated in rat [23].

The HNS-activation in AD seems conflicting with the reported reduction in cerebrospinal fluid (CSF) AVP-levels in AD [19,31], the latter contrasting with the reported normal brain AVP-

levels (pg/mg protein) in AD [20]. However, apart from the HNS, AVP neurons are also located in the suprachiasmatic nucleus, the bed nucleus of the stria terminalis and the medial amygdaloid nucleus [4], all three nuclei being affected in AD. Moreover, CSF AVP-levels are normal in diabetes insipidus characterized by decreased plasma AVP-levels [13], suggesting two different AVP-systems. Additionally, plasma AVP can not pass the blood-CSF barrier [30], and lastly the reported normal brain AVP-levels in AD are expressed as concentrations [20], leaving the possibility of total AVP amounts being decreased in the atrophied AD brain. Further, in AD the increased CSF volume may also attribute to the decreased AVP CSF-levels.

An age-related decline in AVP-binding sites in the human kidney as has been demonstrated in rat [23] can not be excluded as an explanation for the increased AVP-activity, and needs further clarification. Also, the HNS-activation might be a secondary event due to changes within the central nervous system itself. A decline in the NA innervation of the magnocellular SON and PVN neurons could play a role in this respect [3,18,21,28,29], although no conclusive evidence exists for inhibitory properties of the NA system upon the hypothalamus. Hypothalamic compensatory mechanisms have already been described in the dopaminergic pathways in Parkinson's disease [25]; similarly, the activation of the HNS in AD could may as a compensatory mechanism for decreased noradrenergic inputs in the SON and PVN.

6.6 References

1. Anderson RJ, Pluss RG, Berns AS, Jackson JT, Arnold PE, Schrier RW and McDonald KM. Mechanism of effect of hypoxia on renal water excretion. *J Clin Invest* 1978;62:769-77.
2. Bargmann W and Scharrer E. The site of the hormones of the posterior pituitary. *Am Sci* 1951;39:255-9.
3. Bondareff W, Mountjoy CQ and Roth M. Selective loss of neurons of origin of noradrenergic projection to cerebral cortex (nucleus locus coeruleus) in senile dementia. *Lancet* 1981;1:783-4.
4. De Vries GJ, Buijs RM, Van Leeuwen FW, Caffé AR and Swaab DF. The vasopressinergic innervation of the brain in normal and castrated rats. *J Comp Neurol* 1985;233:236-54.
5. Dierickx K and Vandesande F. Immunocytochemical localization of the

- vasopressinergic and the oxytocinergic neurons in the human hypothalamus
Cell Tiss Res 1977;184:15-27.
6. Fliers E and Swaab DF. Activation of vasopressinergic and oxytocinergic neurons during aging in the Wistar rat. *Peptides* 1983;4:165-70
 7. Fliers E, Swaab DF, Pool CW. and Verwer RWH. The vasopressin and oxytocin neurons in the human supraoptic and paraventricular nucleus; changes with aging and in senile dementia. *Brain Res* 1985;342:45-53.
 8. Frolkis VV, Golovchenko SF, Medved VI and Frolkis RA. Vasopressin and cardiovascular system in aging. *Gerontology* 1982;28:290-302.
 9. Gundersen HJG. Notes on the estimation of the numerical density of arbitrary profiles: the edge effect. *J Microsc* 1977;111:219-23.
 10. Gundersen HJG and Jensen EB. The efficiency of systematic sampling in stereology and its prediction. *J Microsc* 1987;147:229-63.
 11. Hofman MA, Fliers E, Goudsmit E and Swaab DF. Morphometric analysis of the suprachiasmatic and paraventricular nuclei in the human brain: sex differences and age-dependent changes. *J Anat* 1988;160:127-43.
 12. Hoogendijk JE, Fliers E, Swaab DF and Verwer RWH. Activation of vasopressin neurons in the human supraoptic and paraventricular nucleus in senescence and senile dementia. *J Neurol Sci* 1985;69:291-9
 13. Jenkins JS, Mather HM and Ang V. Vasopressin in human cerebrospinal fluid. *J Clin Endocrinol Metab* 1980;50:364-7.
 14. Khachaturian ZS. Diagnosis of Alzheimer's disease. *Arch Neurol* 1985;42:1097-1105.
 15. Kirkland J, Ley M, Goddard C, Vargas E and Davies I. Plasma arginine vasopressin in dehydrated elderly patients. *Clin Endocrinol* 1984;20:451-6.
 16. Loughlin SE. Locus coeruleus projections to cortex - topography, morphology and collateralization. *Brain Res Bull* 1982;9:287-94.
 17. Mann DMA, Yates PO, Bansal DV and DJ Marshall. Hypothalamus and dementia. *Lancet* 1981;1:393-4.
 18. Marcyniuk B, Mann DMA and Yates PO. The topography of cell loss from locus coeruleus in Alzheimer's disease. *J Neurol Sci* 1986;76:335-45.
 19. Mazurek MF, Growdon JH, Beal MF and Martin JB. CSF vasopressin concentration is reduced in Alzheimer's disease. *Neurology* 1986;36:1133-7.
 20. Mazurek MF, Beal MF, Bird ED and Martin JB. Vasopressin in Alzheimer's disease: a study of postmortem brain concentrations. *Ann Neurol* 1986;20:665-70.
 21. McGeer EG. Aging and neurotransmitter metabolism in the human brain. In R Katzman, RD Terry and KL Bick, eds. *Aging, Volume 7, Alzheimer's disease, senile dementia and related disorders*. Raven Press, New York 1978;427-40.
 22. Morton A. A quantitative analysis of the normal neuron population of the hypothalamic magnocellular nuclei in man and of their projections to the neurohypophysis. *J Comp Neurol* 1969;136:143-58.
 23. Ravid R, Swaab DF and Pool CW. Immunocytochemical localization of vasopressin binding sites in the rat kidney. *J Endocrinol* 1985;105:133-40.
 24. Rondeau E, De Lima J, Caillens H, Ardailou R, Vahanian A and Acar J. High plasma antidiuretic hormone in patients with cardiac failure: influence of age. *Mineral Electrolyte Metab* 1982;8:267-74.
 25. Sandyk R. Hypothalamic compensatory mechanisms in Parkinson's disease. *Intern J Neurosci* 1989;44:135-42.
 26. Sartin JL and Lamperti AA. Neuron numbers in hypothalamic nuclei of young, middle-aged and aged male rats. *Experientia* 1985;41:109-11.
 27. Share L and Levy MN. Carotid sinus pulse pressure, a determinant of

- plasma antidiuretic hormone concentration. *Am J Physiol* 1966;211:721-4.
28. Sladek JR, Khachaturian H, Hoffman GE and Scholer J. Aging of central endocrine neurons and their aminergic afferents. *Peptides* 1980;1:Suppl; 1:141-57.
 29. Sladek JR, Schöler J and Armstrong WE. Norepinephrine-vasopressin interactions during aging. In: Y Sano, Y Iyata and EA Zimmerman, eds. *Structure and function of peptidergic and aminergic neurons*. Japan Scientific Societies Press, Tokyo 1983;289-98.
 30. Sorensen PS, Vilhardt H, Gjerris F and Warberg J. Impermeability of the blood-cerebrospinal fluid barrier to 1-deamino-8-D-arginine-vasopressin (DDAVP) in patients with acquired, communicating hydrocephalus. *Eur J Clin Invest* 1984;14:435-9.
 31. Sorensen PS, Gjerris A and Hammer M. Cerebrospinal fluid vasopressin in neurological and psychiatric disorders. *J Neurol Neurosurg Psychiatr* 1985;48:50-7.
 32. Tomlinson BE, Irving D and Blessed G. Cell loss in the locus coeruleus in senile dementia of Alzheimer type. *J Neurol Sci* 1981;49:419-28.
 33. Weibel ER. *Stereological Methods, Vol. 1: Practical Methods for Biological Morphometry*. Academic Press, London 1979.

NEUROPATHOLOGY OF THE NUCLEUS BASALIS MEYNERT COMPLEX, THE SUPRAOPTIC AND PARAVENTRICULAR NUCLEI, AND THE ORGANUM VASCULOSUM OF THE LAMINA TERMINALIS IN AGING AND ALZHEIMER'S DISEASE

7.1 Abstract

A review of the recent literature concerning neuropathologic determinants in Alzheimer's disease is presented. Data are given on neurofibrillary tangles, senile plaques, congophilic angiopathy, (granulo)vacuolar degeneration, lipofuscin accumulation and neuronophagia in the nucleus basalis Meynert complex, the supraoptic and paraventricular nuclei, and in the organum vasculosum of the lamina terminalis. The results will be discussed in relation to the issue of primary and/or secondary degeneration of the cholinergic system in Alzheimer's disease.

7.2 General introduction

The main neuropathologic features of Alzheimer's disease (AD) consist of granulovacuolar degeneration, the presence of Hirano bodies, neurofibrillary degeneration, senile plaques, congophilic angiopathy, and loss and shrinkage of neurons [94, 121].

7.2.1 Granulovacuolar degeneration

Granulovacuolar degeneration of Simchowicz [111] has been described in neurons of the pyramidal cell layer of the hippocampus [56, 94, 121]. This neuronal change consists of one or more vacuoles with a diameter of 3-5 μm in the cytoplasm. Each vacuole contains a granule, immunohistochemically positive for

tubulin, abnormally phosphorylated neurofilaments and the microtubule-associated protein tau [29]. Sometimes the cytoplasm is completely filled with and distended by several (up to 20) vacuoles, giving the neuron a swollen appearance. The number of neurons showing granulovacuolar degeneration (GVD) in AD varies between 20 and 50% of the pyramidal neurons [119], and correlates with the duration of dementia [12]. The localization is mainly restricted to the ventrolateral quadrant of the hippocampus [13, 135]. It needs to be stressed that GVD may be present also in nondemented subjects over the age of 65; in the ninth decade GVD can be demonstrated in 75% of the control cases [119]. However, the number of affected neurons does not exceed 9% of the pyramidal cells in the ventrolateral quadrant. Therefore, GVD is not pathognomonic for AD as it is present (to a limited extent) in normal aging too. In AD GVD has also been described in the nucleus basalis Meynert complex (NBMC) [60, 128] and, recently, in the cingulate and insular cortex [20]. Moreover, GVD has been reported in progressive supranuclear palsy [113], in amyotrophic lateral sclerosis, the Parkinsonism-dementia complex of Guam [52, 54], and in Down's syndrome [71]. These findings constitute important exceptions to the rule that only pyramidal neurons in the hippocampus are subjected to GVD and that GVD is limited to AD and aging. In this study semi-quantitative data on GVD in the NBMC in aging and AD are presented.

7.2.2 Hirano bodies

Hirano bodies were originally described in the Parkinsonism-dementia syndrome of Guam [53] and are mainly found adjacent to and within pyramidal neurons of the hippocampus. They are ovoid in shape, eosinophilic, and 10-30 μm long. They contain actin [38] and are immunohistochemically positive for microtubule-associated protein-2 and tau [95]. They occur both in normal aging and in Alzheimer's disease [42], as well as in several other neurological disorders [54, 100, 108, 122]. Hirano bodies can not be considered as pathognomonic for AD, and their

pathogenesis and relevance is poorly understood. In the present study semi-quantitative data on Hirano bodies in the NBMC in aging and AD are given.

7.2.3 Amyloid

Neurofibrillary degeneration, the dystrophic neurites and the core of senile plaques, and the congophilic angiopathy are all composed of a protein that has been designated as amyloid by its staining characteristics [30, 31, 97] and its X-ray diffraction [33], demonstrating protein arrangements in a twisted β -pleated sheet conformation [65]. The optical properties of amyloid as revealed by Congo-red-staining (yellowish-green birefringence under polarized light) depends on this β -pleated sheet conformation [43].

The biochemical constitution of extraneuronal amyloid in senile plaque cores and congophilic angiopathy has recently been elucidated. In both AD and Down's syndrome (trisomy 21) the β -protein or A β -protein has been shown to be the major component of the congophilic angiopathy [46] and the senile plaques [79, 110, 133]. This β -protein consists of a sequence of 42 amino acids and is cleaved by proteolysis from a larger β -protein precursor (BPP). The BPP consists of 695 amino acids and resembles a cell surface receptor [61]. The BPP-gene is located on chromosome 21 [48, 61, 101, 114] in the same region of two loci that are linked to the genetic defect in familial AD (FAD)[112]. However, recent linkage analyses have shown that loci for the FAD are localized some distance from the BPP-gene and thus are not linked to it [107, 124].

An increased dosage of the gene coding for the BPP in both AD and Down's syndrome (trisomy 21) was postulated as the pathogenic mechanism [28], but this hypothesis could not be confirmed [114, 124]. Moreover, (1) the absence of linkage between the FAD-gene and the BPP-gene [107, 124], (2) the ubiquity of BPP-mRNA in many organs in a variety of species, with the highest levels in brain tissue [11, 47], and (3) and the resemblance of BPP to a cell

surface receptor [61], all suggest a physiological rather than a pathological role in AD [93]. Instead, as β -pleated sheet fibrils can aggregate as amyloid [44] after partial proteolysis of several normal plasma and tissue proteins, such as prealbumin [32], it is more reasonable to suggest that the abnormal formation of β -protein arises from posttranslational modification from either the BPP or the proteases responsible for the conversion of BPP into the β -protein. For instance, due to alternative splicing the BPP-mRNA may contain an additional domain of 56 amino acids with a sequence homologous to serine protease inhibitors [66, 96, 115]. Moreover, the serine protease inhibitor α_1 -antichymotrypsin is tightly associated with the β -amyloid deposits in senile plaque cores and in the congophilic angiopathy [1]. These latter two unrelated protease inhibitors associated with the β -protein may contribute to the resistance of amyloid deposits to clearing by further proteolytic cleavage.

The intraneuronal neurofibrillary tangles (NFT) are intracellular, perikaryal accumulations of fibrous material, ultrastructurally composed of paired helical filaments (PHF) [64, 132]. From immunohistochemical studies it became clear that several proteins may participate in the composition of the PHF. However, it is still not certain which protein is actually involved in the PHF composition: neurofilament proteins [27], microtubule-associated protein 2 (MAP2) [68], microtubule-associated protein tau (tau) [134], ubiquitin [73, 86] or β -protein [50, 58]. In a recent study [49] the presence of β -protein-immunoreactivity in PHF could not be confirmed. Although β -protein was demonstrated in different types of neurons, including those with NFT, it was not present in the PHF itself [49]. Recently it has been shown, that the process of tangle formation is reflected by its changing immunoreactivity: accumulation of abnormally phosphorylated-tau proteins precedes the formation of intraneuronal NFT [14], and that the endstage is characterized by extraneuronal "ghost-tangles" that are only immunoreactive to ubiquitin [23].

In conclusion, the β -protein is the major component of amyloid fibrils of senile plaque cores, of congophilic angiopathy and perhaps of the PHF of the NFT. Additionally, the metabolism

of the BPP may be modified by altered proteolytic processing in AD, resulting in the deposition of the amyloid fibrils composed of β -protein.

7.2.4 Neurofibrillary degeneration

The neurofibrillary degeneration or tangle (NFT) formation was first described by Alzheimer [3, 4] in the cerebral cortex of a 51-year old woman with a dementing illness. NFT's are easily seen in formalin-fixed tissue sections using silver impregnation methods [39, 40], fluorescence methods as thioflavine-S [109] and congored [98], the congored polarization method [97] and several immunohistochemical stainings against their composing proteins. Apart from AD NFT could also be demonstrated in normal aging [117], Down's syndrome [71], the Parkinsonism-dementia complex of Guam [52] and many other neurological disorders [121]. Recently, NFT were demonstrated in the NBMC ipsilateral to a massive cerebral infarct in the territory of the middle cerebral artery. Tangles were absent or rare in the contralateral NBMC and in other brain areas, suggesting that NFT can occur as a retrograde reaction in basalis neurons secondary to an old infarction [62].

In AD NFT are abundantly present in the hippocampus, entorhinal cortex and amygdala [63, 118], numerous in the neocortex [75, 129], and to a lesser extent in subcortical structures as the NBMC [7, 99, 103, 106], the thalamus and hypothalamus [81], and brainstem structures like the substantia nigra and locus coeruleus [59, 74]. In the neocortex the NFT occur in clusters in lamina III and V [91]. In the entorhinal cortex NFT has been shown to cluster in layer II [57]. It is still not clear whether NFT reflect lost neurons or represent degenerated (but not yet lost) neurons [77].

In the present study quantitative data are presented on the numbers of NFT in the subdivisions of the NBMC, the SON and the PVN; the numbers of NFT are compared to the number of neurons lost in these structures [125, 126].

7.2.5 Senile plaques

Senile plaques (SP), first described by Blocq and Marinesco [17], are discrete, roughly spherical structures within the neuropil with a diameter ranging from 10 to 200 μm across. SP are subdivided into three stages of increasing degeneration [131]:

- the primitive plaque (few swollen neurites and few astrocytic processes, without an amyloid plaque core);
- mature or diffuse plaque (many swollen neurites and astrocytic processes, microglial cells, with a dense central amyloid core);
- burnt-out plaque (a dense central amyloid core, with many astrocytic and microglial cells).

SP can be detected in formalin-fixed tissue sections using silver impregnation methods [39, 40], fluorescence methods as thioflavine-S [109] and congored [98], and the congored polarization method [97]. The distended neurites of primitive and mature plaques show immunoreactivity against axons and axonal endings of cholinergic neurons [9], noradrenergic neurons [67], somatostatinergic [87], GABA-ergic neurons [127], neuropeptide-Y containing neurons [24], substance-P neurons [8] and galaninergic neurons [21].

Apart from AD SP have been demonstrated in normal aging [117], Down's syndrome and Pick's disease [131], the Parkinsonism-dementia complex of Guam [52], Creutzfeldt-Jacob disease [123] and other neurological disorders [121].

In AD SP are most abundantly present in the hippocampus, in the corticomedial nuclei of the amygdala [76] and in the association areas of the neocortex and less numerous in primary visual, auditory, somatosensory and motor areas [37, 91, 102]. The density of both SP and NFT in the cerebral cortex shows a significant correlation with the degree of dementia [16, 129].

In the neocortex a laminar [37, 91, 102] and columnar [10] distribution of SP has been demonstrated [10]. The site of the SP is often closely related to (degenerating) capillaries [15, 84, 85, 90, 92]. This observation together with the fact that

the β -protein was found to be the major component of both the SP-core and the congophilic angiopathy, strongly suggest a hematogenous origin of the amyloid in AD, although no real evidence is available of a dysfunction of the blood-brain barrier [2, 104].

In the NBMC the presence of SP has been demonstrated [7, 59, 89, 105, 106]. Although it is commonly accepted that the number of NFT in the NBMC exceeds that of SP, no quantitative data on SP of the subdivisions of the NBMC are yet available. The present study shows quantitative data on SP in the NBMC, the SON and PVN; the number of SP are compared to the number of neurons lost in these structures [125, 126].

7.2.6 Congophilic angiopathy

The congophilic angiopathy (CA) has been found in the great majority of AD patients [45, 84], affecting the small pial and intracortical arterioles, the leptomenigeal vessels and the intracortical capillaries [121]. In addition, CA has been demonstrated in the arterioles and arteries of the anterior perforated substance in the basal forebrain within the lateral part of the NBMC [7]. In the present study qualitative data are given on the presence of CA in the NBMC and the SON and PVN in the hypothalamus.

The major chemical component of CA is the β -protein [46], the same as for the amyloid core of SP [79, 110, 133]. This finding suggests a hematogeneous origin of the amyloid proteins due to possible damage of the blood-brain barrier in AD. This hypothesis is strengthened by the presence of serum proteins in the extravascular compartment [130], the presence of immunoglobulins and complement factors in SP [34] and elevated cerebrospinal fluid/serum ratios of albumin and IgG in AD [35, 36]. However, these findings have to be interpreted with caution, because 1) postmortem leakage of serum proteins can occur, 2) areas with ischaemic necrosis contributing to the CSF compartment cannot completely be excluded, 3) evidence of astrocytic production of complement factors C3 and Factor B has recently been found [72],

4) the distribution of CA is mainly restricted to the arterioles and the capillaries in the neocortex [121], whereas CA is hardly present in noncortical structures, and 5) the mRNA's of the β -protein precursor are found to be localized in the neurons [25, 69, 80]. The postulated dysfunction of the blood-brain barrier is studied in a brain structure devoid of an intact blood-brain barrier, the organum vasculosum of the lamina terminalis (OVLT). The OVLT is a highly vascular, unpaired structure located immediately dorsal to the optic chiasm. The capillary fenestrations in the OVLT provide specific sites for the transfer of proteins and solutes, irrespective of molecular size and lipid solubility. Due to the absence of an intact blood-brain barrier and its high vascularity, the OVLT must be considered as a suitable structure to investigate whether amyloid depositions in AD differ quantitatively from normal aging, and to verify whether the cerebral amyloid deposits originate from the blood via a damaged blood-brain barrier.

7.2.7 Neuron loss and shrinkage

At the microscopical level the neocortical atrophy observed in AD [22, 121] consists of both cell loss and cell shrinkage [88, 116]. Cell loss has also been noticed in subcortical structures, like the noradrenergic locus coeruleus [78, 120], the serotonergic raphe nuclei [26], the ventral tegmental area [41] and the NBMC [6, 103, 106, 125, 128]. The SON and PVN, however, showed stability in neuron numbers [55, 126]. In neuroscience research on cell loss, emphasis is now being put on:

1. obtaining total neuron numbers instead of neuron numbers per unit volume to avoid bias due to macroscopical volume loss;
2. measuring neuron sizes to detect possible neuron shrinkage.

As recent studies report minor reductions in total cell numbers combined with major reductions in cell size, these issues are of importance.

7.2.8 Aim of study

The present study shows:

1. quantitative data on NFT, SP and number of neurons showing lipofuscin accumulation in the NBMC, the SON and PVN;
2. semi-quantitative data on GVD and Hirano bodies in the NBMC, SON and PVN;
3. semi-quantitative data on CA in the NBMC, SON and PVN and in the OVLТ, and on the staining intensity of the lipofuscin;

7.3 Material and methods

7.3.1 Material

For detailed information on the neuropathological diagnosis of the cases studied and on the brain structures, the reader is referred to Chapter 3, "Material and Methods". Shortly, twelve cases of AD were selected, one case of Parkinson's disease (PD), and ten nondemented controls. The twelve AD cases could be subdivided in five early-onset (first symptoms of the disease manifested before 65 years of age) and seven late-onset AD cases. Brain regions of interest included the NBMC with the subdivisions Ch1+Ch2, Ch3, Ch4a1, Ch4am, Ch4i and Ch4p [82, 83], the SON and the PVN, and the OVLТ. Characteristics of the brain material used are summarized in Chapter 3, Table 3.1.

7.3.2 Methods

All 23 brains were fixed in toto in 4% formaldehyde. After embedding in paraffin serial sections with a thickness of 10 or 20 μm were cut using a Jung 2050 microtome. Sections were stained at regular intervals of 800 μm throughout the entire rostrocaudal extent of the NBMC, SON and PVN. The Klüver-Barrera-stained sections and the adjacent Nissl-stained sections were used for identification of the NBMC and its subdivisions

Ch1 to Ch4, and for the detection of granulovacuolar degeneration, respectively. The adjacent congored-stain was used in fluorescence microscopy for quantification of the NFT, SP and CA [97, 98]. Although congored exhibits unspecific binding to lipofuscin, red blood cells, and elastic fibers, especially within the lamina elastica interna of the arteriole walls [97], it was found in our laboratory [70] that the fluorescence congored technique [98] was qualitatively and quantitatively superior to the polarized congored technique [97], the silver impregnation methods [39, 40] and the thioflavine-S fluorescence technique [109]. Using the Zeiss combined fluorescence and brightfield light microscope, and applying different colour filters, the same section could be analyzed with different optical techniques, permitting direct comparison of fluorescence congored-staining, brightfield microscopic patterns, and autofluorescence patterns of lipofuscin, red blood cells and elastic fibers. The OVLT was analyzed with both fluorescence congored and thioflavine-S.

Quantitative analysis was carried out by taking 10 samples of 250x250 μm^2 at a x400 magnification in each SON and PVN, and in each subdivision of the NBMC. This approach resulted in a mean density (number/ mm^2) of all the neuropathological features observed:

1. the NFT, that were subdivided into the neuropil threads [18, 19], the intraneuronal neurofibrillary tangles and the extraneuronally localized ghost tangles;
2. the SP, that were subdivided into the primitive, mature or diffuse, and the burnt-out plaques [131];
3. the lipofuscin containing neurons.

The same samples were also semi-quantitatively analyzed for:

4. CA, that was subdivided into capillary and arterial CA. Scores ranged from absent (0), weakly present (1), to abundant CA (2).
5. the intensity of the lipofuscin with scores ranging from moderate (1) to strong intensity (2).

Statistical analyses were performed using the distribution-free, nonparametric Mann-Whitney U-test.

7.4 Results

Fluorescence congored-staining revealed differences in the amount of NFT, SP and CA for the subdivisions of the NBMC in AD. In age-matched controls NFT, SP and CA were almost completely absent. In both the SON and PVN small amounts of neuropil threads were present in AD, whereas no amyloid deposits were found in age-matched controls. The morphology for each of these degenerative changes (Figs. 7a-7f) appeared similar for all brain structures.

The NFT showed three forms:

- neuropil threads ranging in length from 20 to 200 μm (Fig. 7a) that were to be sprout out of the tangle (Fig. 7b);
- intraneuronal neurofibrillary degeneration;
- extraneuronal neurofibrillary degeneration or ghost-tangles ranging in size from 20-50 μm (Fig. 7c), with a globose shape, with wound fibers, reminiscent of a ball of string.

In AD the neuropil threads and ghost-tangles were most frequently observed in the NBMC, and virtually absent in the SON and PVN (Table 7.1).

The SP were distinguished into:

- primitive plaques;
- mature plaques with a central amyloid core (Fig. 7d);
- burnt-out plaques (Fig. 7e),

The primitive plaques were most frequently present, but numerically outnumbered by NFT (Tables 7.1 and 7.2). Enormous amounts of NFT could be demonstrated in the NBMC. Both the number of neuropil threads and ghost-tangles increased in rostrocaudal direction (from Ch1+Ch2 to Ch4p), and at the same time the ratio neuropil-threads/ghost-tangles decreased from 1.5 to 0.5. As in age-matched controls almost solely neuropil threads and hardly any ghost-tangles are found (ratio about 4:1), this finding may suggest that neurofibrillary degeneration starts with the formation of neuropil threads. This hypothesis is supported by the frequently observed phenomenon that one such neuropil thread is connected with the ghost-tangle.

A rostrocaudal increase (from Ch1+Ch2 to Ch4p) in SP could be

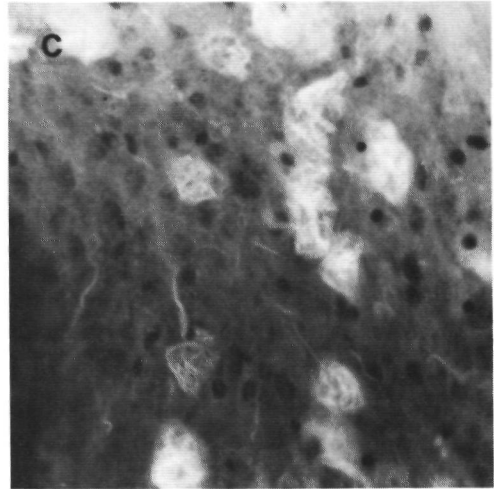
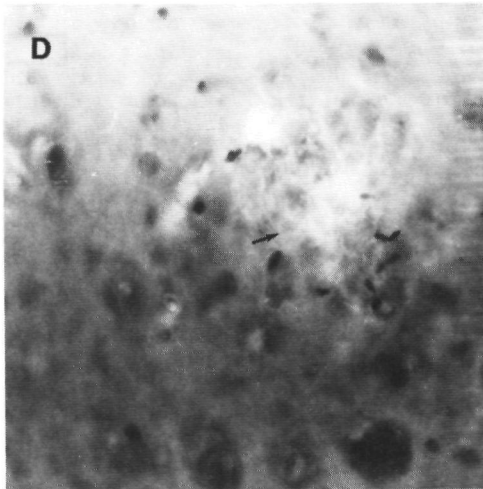
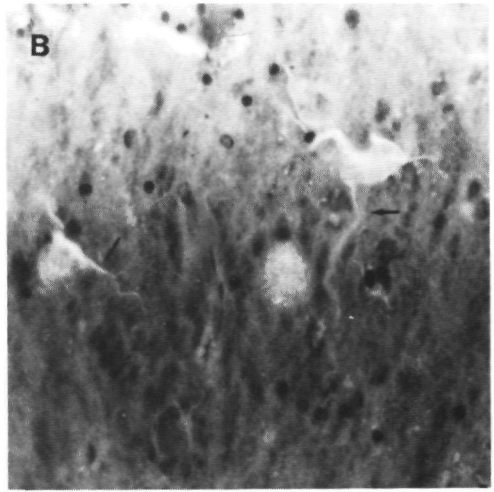
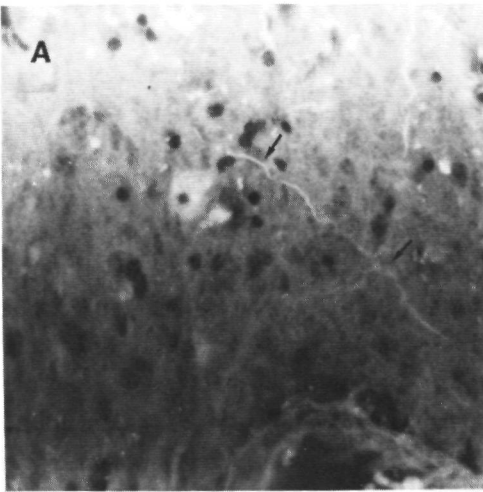


Fig. 7a long neuropil thread (see arrows) (x400)
b neuropil thread sprouting out of tangles (arrows) (x400)
c cluster of ghost tangles (x400)
d mature plaque with central amyloid core (arrow) (x400)

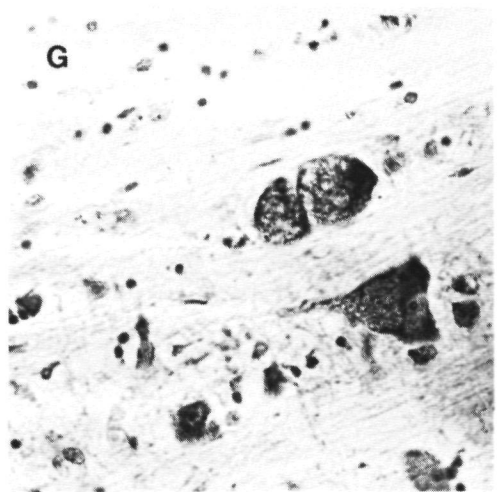
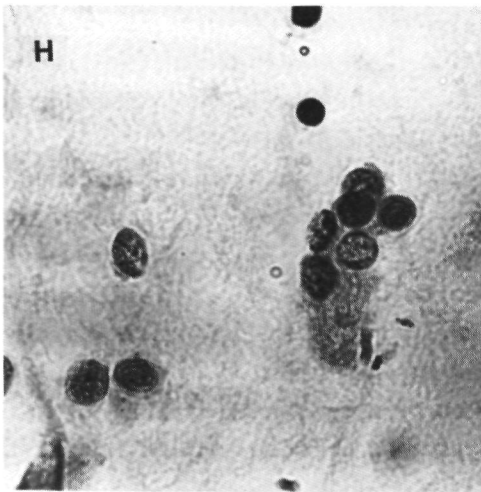
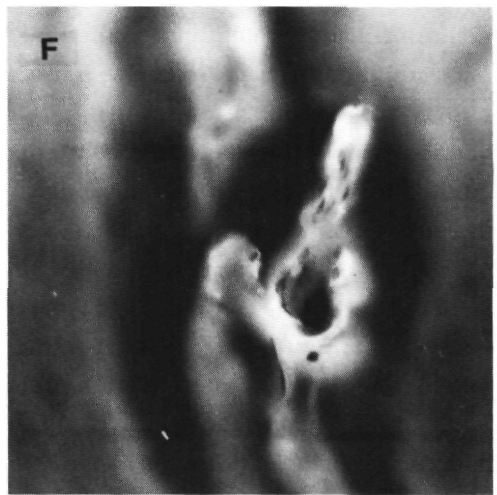
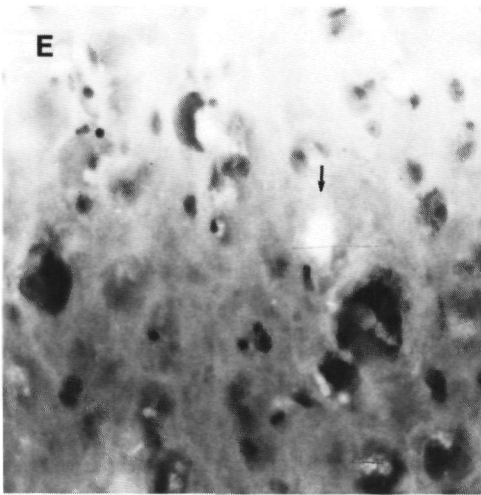


Fig. 7e burnt-out plaque (arrow) (x400)
f congophilic angiopathy (x1000)
g granulovacuolar degeneration (x400)
h neuronophagia (x1000)

pointed out too (Table 7.2), whereas the CA (Fig. 7f) was evenly distributed throughout the subdivisions of the NBMC in AD (Table 7.3). The increase of degenerative changes (NFT and SP) in rostrocaudal direction, is in agreement with cell counts in the NBMC, showing stability of cell number in the anteriorly located Ch1+Ch2 region and significant cell loss in the posteriorly located Ch4p [125].

No differences could be detected in the percentage of lipofuscin containing neurons nor in the intensity of lipofuscin-staining between age-matched controls and AD.

No differences between left and right hemispheres could be detected for either of the degenerative changes.

No Hirano bodies were found in the NBMC, the SON and PVN in age-matched controls and AD.

The general aspect of NBMC neurons in old age showed dissolution of the Nissl substance and vacuolization of the neurons did regularly occur, sometimes showing the aspect of typical granulovacuolar degeneration (GVD) (Fig. 7g). The latter was invariantly present in AD, especially in the Ch4 region of the NBMC. Occasionally, neurons showing GVD, contained also neurofibrillary degeneration with the congophilic threads twisting around the vacuoles as a loosely wound ball of string. The vacuolized enlarged neurons were sometimes surrounded by microglia: neuronophagia (Fig. 7h).

Concerning the OVLT no differences in CA between normal aging and AD were found in both the congored and the thioflavine-S-staining. Perivascular amyloid depositions were almost absent in both conditions (Table 7.4).

TABLE 7.1

Numbers of neurofibrillary tangles in different brain structures
in normal aging and Alzheimer's disease ^{A, B}

Structure	Neurofibrillary tangles							
	neuropil threads		intraneuronal tangles		ghost-tangles		total	
	L (n=8)	R (n=8)	L (n=8)	R (n=8)	L (n=8)	R (n=8)	L (n=8)	R (n=8)
Normal aging								
- Ch1+Ch2	1.2 ± 0.8	2.0 ± 1.0	0.0 ± 0.0	0.0 ± 0.0	0.2 ± 0.2	1.0 ± 0.5	1.4 ± 0.8	3.0 ± 1.3
- Ch3	2.4 ± 1.3	1.6 ± 0.7	0.0 ± 0.0	0.0 ± 0.0	0.2 ± 0.2	0.4 ± 0.3	2.6 ± 1.4	2.0 ± 0.9
- Ch4am	1.0 ± 0.7	1.4 ± 0.6	0.0 ± 0.0	0.0 ± 0.0	0.4 ± 0.3	0.4 ± 0.3	1.4 ± 0.9	1.8 ± 0.8
- Ch4al	1.4 ± 0.6	1.2 ± 0.6	0.0 ± 0.0	0.0 ± 0.0	0.4 ± 0.3	0.4 ± 0.3	1.8 ± 0.8	2.0 ± 0.8
- Ch4i	1.2 ± 0.7	2.8 ± 1.2	0.0 ± 0.0	0.0 ± 0.0	0.6 ± 0.3	0.4 ± 0.3	1.8 ± 0.9	3.2 ± 1.4
- Ch4p	4.0 ± 1.0	4.6 ± 1.1	0.0 ± 0.0	0.0 ± 0.0	0.4 ± 0.3	1.4 ± 0.6	4.4 ± 1.1	6.0 ± 1.6
- - (L R) - - -								
- SON (n=7;n=8)	0.0 ± 0.0	0.0 ± 0.0	0.0 ± 0.0	0.0 ± 0.0	0.0 ± 0.0	0.0 ± 0.0	0.0 ± 0.0	0.0 ± 0.0
- PVN (n=5;n=5)	0.0 ± 0.0	0.0 ± 0.0	0.0 ± 0.0	0.0 ± 0.0	0.0 ± 0.0	0.0 ± 0.0	0.0 ± 0.0	0.0 ± 0.0
Alzheimer's disease								
Structure	(n=7)	(n=10)	(n=7)	(n=10)	(n=7)	(n=10)	(n=7)	(n=10)
- Ch1+Ch2	30.6 ± 3.3 ²	29.7 ± 3.5 ³	7.6 ± 1.9 ²	3.4 ± 0.8 ²	23.6 ± 3.5 ²	20.6 ± 3.0 ³	61.7 ± 4.3 ²	53.8 ± 3.7 ³
- Ch3	35.7 ± 3.2 ²	30.6 ± 4.5 ³	2.1 ± 0.8 ¹	0.5 ± 0.3	15.8 ± 2.5 ²	14.7 ± 3.2 ³	53.6 ± 3.2 ²	45.8 ± 4.7 ³
- Ch4am	35.7 ± 4.9 ²	24.8 ± 4.6 ³	5.7 ± 1.2 ²	3.2 ± 1.1 ¹	37.4 ± 6.0 ²	25.8 ± 7.2 ³	78.8 ± 6.2 ²	53.8 ± 6.1 ³
- Ch4al	44.1 ± 4.9 ²	28.8 ± 4.8 ³	5.5 ± 2.3 ²	5.3 ± 1.5 ²	50.5 ± 10.3 ²	40.8 ± 9.4 ³	100.1 ± 10.5 ²	74.9 ± 9.0 ³
- Ch4i	38.9 ± 6.1 ²	27.5 ± 5.4 ³	5.3 ± 1.7 ²	5.3 ± 2.0 ¹	56.7 ± 12.1 ²	41.8 ± 7.3 ³	100.9 ± 11.0 ²	74.6 ± 6.1 ³
- Ch4p	40.9 ± 3.5 ²	33.3 ± 4.2 ³	7.3 ± 2.5 ²	6.6 ± 1.4 ³	65.6 ± 10.1 ²	67.2 ± 12.5 ³	113.8 ± 9.2 ²	107.1 ± 10.3 ³
- - (L R) - - -								
- SON (n=8;n=11)	0.1 ± 0.1	0.0 ± 0.0	0/0 ± 0.0	0.0 ± 0.0	0.0 ± 0.0	0.0 ± 0.0	0.1 ± 0.1	0.0 ± 0.0
- PVN (n=5;n=6)	0.4 ± 0.2	0.5 ± 0.3	0.0 ± 0.0	0.0 ± 0.0	0.0 ± 0.0	0.0 ± 0.0	0.4 ± 0.2	0.5 ± 0.3

L, left hemisphere; R, right hemisphere;

^A, the number of NFT is expressed as number/mm²;

^B, data are mean of the number, n, cases ± standard error of the mean (SEM);

¹, p<0.05; ², p<0.01; ³, p<0.001, according to Mann-Whitney U-test.

TABLE 7.2

Numbers of senile plaques in different brain structures
in Alzheimer's disease ^{a, b}

Structure	Senile plaques							
	primitive plaques		mature plaques		burnt-out plaques		total	
	L (n=7)	R (n=10)	L (n=7)	R (n=10)	L (n=7)	R (n=10)	L (n=7)	R (n=10)
- Ch1+Ch2	0.9 ± 0.5	0.8 ± 0.4	0.2 ± 0.2	0.0 ± 0.0	1.1 ± 1.1	0.2 ± 0.2	2.3 ± 1.5	1.0 ± 0.4
- Ch3	0.5 ± 0.5	0.8 ± 0.4	0.0 ± 0.0	0.0 ± 0.0	0.0 ± 0.0	0.0 ± 0.0	0.5 ± 0.5	0.8 ± 0.4
- Ch4am	1.4 ± 0.5	0.5 ± 0.2	0.0 ± 0.0	0.0 ± 0.0	0.7 ± 0.7	0.8 ± 0.6	2.1 ± 0.8	1.3 ± 0.6
- Ch4al	2.1 ± 0.8 ¹	1.1 ± 0.4	0.0 ± 0.0	0.0 ± 0.0	0.7 ± 0.5	1.6 ± 1.3	2.8 ± 0.8	2.7 ± 1.3
- Ch4i	1.4 ± 0.6	1.6 ± 0.6	0.0 ± 0.0	0.2 ± 0.2	0.2 ± 0.2	0.3 ± 0.2	1.6 ± 0.6	2.1 ± 0.6
- Ch4p	2.3 ± 0.6 ¹	1.6 ± 0.6	0.0 ± 0.0	0.8 ± 0.8	0.2 ± 0.2	0.5 ± 0.2	2.5 ± 0.6	2.9 ± 0.6
--- (L R) ---								
- SON (n=8;n=11)	0.0 ± 0.0	0.0 ± 0.0	0.0 ± 0.0	0.0 ± 0.0	0.0 ± 0.0	0.0 ± 0.0	0.0 ± 0.0	0.0 ± 0.0
- PVN (n=5;n=6)	0.0 ± 0.0	0.0 ± 0.0	0.0 ± 0.0	0.0 ± 0.0	0.0 ± 0.0	0.0 ± 0.0	0.0 ± 0.0	0.0 ± 0.0

Data on numbers of SP in different brain structures in normal aging are not shown, because no SP were sampled.

L, left hemisphere; R, right hemisphere; ^a, the number of SP is expressed as number/mm²; ^b, data are mean of the cases ± standard error of the mean (SEM); ¹, p<0.05; ², p<0.01; ³, p<0.001, according to Mann-Whitney U-test.

TABLE 7.3

Congophilic angiopathy and lipofuscin in different brain structures in normal aging and Alzheimer's disease ^{A, B}

Structure	Congophilic angiopathy				Lipofuscin			
	capillaries		arterioles		% of all neurons		lipofuscin intensity	
	L (n=8)	R (n=8)	L (n=8)	R (n=8)	L (n=8)	R (n=8)	L (n=8)	R (n=8)
Normal aging								
- Ch1+Ch2	0.0 ± 0.0	0.0 ± 0.0	0.0 ± 0.0	0.0 ± 0.0	82.5 ± 2.7	78.8 ± 3.0	1.3 ± 0.1	1.3 ± 0.1
- Ch3	0.0 ± 0.0	0.0 ± 0.0	0.0 ± 0.0	0.0 ± 0.0	67.3 ± 2.4	64.4 ± 2.7	1.0 ± 0.1	1.0 ± 0.1
- Ch4am	0.0 ± 0.0	0.0 ± 0.0	0.0 ± 0.0	0.0 ± 0.0	84.3 ± 1.6	84.4 ± 2.2	1.2 ± 0.1	1.2 ± 0.1
- Ch4al	0.0 ± 0.0	0.0 ± 0.0	0.0 ± 0.0	0.0 ± 0.0	81.2 ± 2.0	87.5 ± 1.8	1.2 ± 0.1	1.3 ± 0.1
- Ch4i	0.1 ± 0.1	0.1 ± 0.1	0.0 ± 0.0	0.0 ± 0.0	89.0 ± 2.9	89.3 ± 2.0	1.4 ± 0.1	1.4 ± 0.1
- Ch4p	0.2 ± 0.1	0.1 ± 0.1	0.1 ± 0.1	0.0 ± 0.0	86.5 ± 2.9	88.2 ± 2.3	1.3 ± 0.1	1.4 ± 0.1
- - (L R) - - -								
- SON (n=7;n=8)	0.0 ± 0.0	0.0 ± 0.0	0.0 ± 0.0	0.0 ± 0.0	79.8 ± 3.2	80.4 ± 3.1	1.0 ± 0.1	1.0 ± 0.1
- PVN (n=5;n=5)	0.0 ± 0.0	0.0 ± 0.0	0.0 ± 0.0	0.0 ± 0.0	75.3 ± 2.1	78.6 ± 3.0	1.0 ± 0.1	1.0 ± 0.1
Alzheimer's disease								
	(n=7)	(n=10)	(n=7)	(n=10)	(n=7)	(n=10)	(n=7)	(n=10)
- Ch1+Ch2	1.5 ± 0.1 ²	1.4 ± 0.1 ³	0.7 ± 0.1 ²	1.0 ± 0.1 ³	81.3 ± 3.3	84.4 ± 3.6	1.3 ± 0.2	1.3 ± 0.1
- Ch3	1.4 ± 0.1 ²	1.1 ± 0.1 ³	1.1 ± 0.1 ²	0.3 ± 0.1 ¹	68.9 ± 2.8	75.0 ± 2.7	1.0 ± 0.1	1.0 ± 0.1
- Ch4am	1.5 ± 0.1 ²	1.1 ± 0.1 ³	0.7 ± 0.1 ²	0.9 ± 0.1 ³	82.0 ± 2.2	89.2 ± 2.3	1.2 ± 0.1	1.2 ± 0.1
- Ch4al	1.6 ± 0.1 ²	1.3 ± 0.1 ³	0.8 ± 0.1 ²	0.9 ± 0.1 ³	74.0 ± 3.1	85.9 ± 2.6	1.0 ± 0.1	1.2 ± 0.1
- Ch4i	1.3 ± 0.1 ²	1.2 ± 0.1 ³	1.1 ± 0.1 ²	1.4 ± 0.2 ³	83.0 ± 3.1	84.7 ± 2.8	1.2 ± 0.1	1.2 ± 0.1
- Ch4p	1.5 ± 0.1 ²	1.4 ± 0.1 ³	0.8 ± 0.1 ²	0.9 ± 0.2 ³	82.4 ± 2.3	78.3 ± 2.5	1.2 ± 0.1	1.2 ± 0.1
- - (L R) - - -								
- SON (n=8;n=11)	0.0 ± 0.0	0.0 ± 0.0	0.0 ± 0.0	0.0 ± 0.0	74.0 ± 3.1	79.8 ± 2.6	1.0 ± 0.1	1.0 ± 0.1
- PVN (n=5;n=6)	0.0 ± 0.0	0.0 ± 0.0	0.0 ± 0.0	0.0 ± 0.0	78.2 ± 2.5	82.5 ± 1.9	1.0 ± 0.1	1.0 ± 0.1

L, left hemisphere; R, right hemisphere; ^A, semi-quantitative data for CA: (0) absent, (1) weakly, (2) strongly present, and for lipofuscin intensity: (1) moderate, (2) strong intensity; ^B, data are mean of n cases ± (SEM);

¹, p<0.05; ², p<0.01; ³, p<0.001, according to Mann-Whitney U-test.

TABLE 7.4

Congophilic angiopathy in the organum vasculosum of the lamina terminalis in age-matched controls and Alzheimer's disease ^{^,B}

	congored	thioflavine-S
Normal aging (n=10)	0.1 ± 0.0	0.0 ± 0.0
Alzheimer's disease (n=11)	0.2 ± 0.0	0.1 ± 0.1

[^], semi-quantitative data on CA in the OVLT: (0) absent, (1) weakly, (2) strongly present;

^B, data are mean of the number, n, cases ± standard error of the mean (SEM).

7.5 Discussion

Our results on NFT, SP and CA in AD, confirm previous studies [7, 59, 60, 99, 106]. The presence of numerous NFT and few SP is also in agreement with these reports. However, the finding of many neuropil threads in the NBMC in AD and its presence already in normal aging, as well as the proposed pathogenic relationship to ghost-tangles, has not yet been reported in literature. This may be due to the use of fluorescence [98] instead of the common polarized light technique of the congored-staining, because neuropil threads are not birefringent in polarized light microscopy [Vogels, unpublished observations]. The length of the neuropil threads (20-200 µm) is suggestive for an axonal rather than for a dendritic localization. Their presence in normal aging, outnumbering the few ghost-tangles, suggests the representation of the first stage of neurofibrillary tangle degeneration. This concept of axonal retrograde degeneration of the NBMC is in accordance with the hypothesis that NFT are largely confined to subcortical nuclei projecting to the severely affected neocortex in AD [91]. It also corresponds to the secondary cell shrinkage in the NBMC [125].

The results on the small number of SP are conflicting. On

the one hand they are in agreement with a recent study, using immunohistochemically antibodies to the β -protein and revealing almost no plaques in the NBMC [89], on the other hand, two studies report SP in similar amounts as NFT [7, 60]. The discrepancy in SP number may be explained by the different staining methods. From our results no relationship between the different types of SP can be detected [131].

The presence and amounts of CA in the NBMC confirms previous studies [7, 59]. It can not be ruled out that the CA increases the diffusion barrier of the vessel walls, and influences the degeneration of the neurons of the NBMC, since neurons as large as those in the NBMC may be especially vulnerable to decreased oxygen and glucose supply. However, the same may be true for the neocortex where the cholinergic axons terminate. Due to diffusion barriers a decrease in the supply of nerve growth factor in the neocortex may result in retrograde degeneration of the NBMC neurons [5, 51].

The virtual absence of CA in the OVLT, a region devoid of an intact blood-brain barrier, in both normal aging and AD, suggests a nonhaematogeneous origin of the CA-amyloid. Consequently, due to the insolubility of the amyloid, the precursor of β -protein must be produced on the spot and the metabolism of β -protein precursor may be modified by altered proteolytic processing (e.g. the production of the serine protease inhibitor α_1 -antichymotrypsin in the pericytes [1]) resulting in the deposition of the β -protein amyloid fibrils.

The presence of granulovacuolar degeneration (GVD) has already been reported for the NBMC [60, 128]. However, the ubiquity of GVD in NBMC neurons is prominent, and its possible relation to the formation of the NFT may reflect a certain stage of degeneration of the NBMC-neurons.

7.6 References

1. Abraham CR, Selkoe DJ and Potter H. Immunochemical identification of the serine protease inhibitor α_1 -antichymotrypsin in the brain amyloid

- deposits of Alzheimer's disease Cell 1988;52:487-501.
2. Alafuzoff I, Adolfsson I, Grundke-Iqbal I and Winblad B. Blood-brain barrier in Alzheimer dementia and in non-demented elderly. Acta Neuropathol (Berl) 1987;73:160-6.
 3. Alzheimer A. Uber eine eigenartige Erkrankung der Hirnrinde. Allgemeine Zeitschrift fur Psychiatrie 1907;64:146-8.
 4. Alzheimer A. Uber eine eigenartige Erkrankung der Hirnrinde. Zentralblatt fur die gesamte Neurologie und Psychiatrie 1907;18:177-9.
 5. Appel SH A unifying hypothesis for the cause of amyotrophic lateral sclerosis, Parkinsonism, and Alzheimer's Disease. Ann Neurol 1981;10: 499-505.
 6. Arendt T, Bigl V, Arendt A and Tennstedt A. Loss of neurons in nucleus basalis of Meynert in Alzheimer's disease, paralysis agitans and Korsakoff's disease. Acta Neuropathol 1983;63:101-8.
 7. Arendt T, Taubert G, Bigl V and Arendt A. Amyloid deposition in the nucleus basalis of Meynert complex: a topographic marker for degenerating cell clusters in Alzheimer's disease. Acta Neuropathol (Berl) 1988;75: 226-32.
 8. Armstrong DM and Terry RD. Substance P immunoreactivity in within senile plaques. Neurosci Lett 1985;58:139-44.
 9. Armstrong DM, Bruce G, Hersh LB and Terry RD. Choline acetyltransferase immunoreactivity in neuritic plaques of Alzheimer brain. Neurosci Lett 1986;71:229-34.
 10. Armstrong RA, Myers D and Smith CUM. Further studies on the patterns of senile plaques in senile dementia of the Alzheimer type (SDAT) with a hypothesis on the colonization of the cortex. Neurosci Res Comm 1989;4: 17-24.
 11. Bahmanyar S, Higgins GA, Goldgaber D, Lewis DA, Morrison JH, Wilson MC, Shankar SK and Gajdusek DC. Localization of amyloid β -protein mRNA in brains from patients with Alzheimer's disease. Science 1987;237:77-80.
 12. Ball MJ and Vis CL. Relationship of granulovacuolar degeneration in hippocampal neurones to aging and to dementia in normal-pressure hydrocephalics. J Gerontol 1978;33:815-24.
 13. Ball MJ. Topographic distribution of neurofibrillary tangles and granulovacuolar degeneration in hippocampal cortex of aging and demented patients: a quantitative study. Acta Neuropathol (Berl) 1978;42:73-80.
 14. Bancher C, Brunner C, Lassmann H, Budka H, Jellinger K, Wiche G, Seitelberger F, Grundke-Iqbal I, Iqbal K and Wisniewski HM. Accumulation of abnormally phosphorylated-Tau precedes the formation of neurofibrillary tangles in Alzheimer's disease. Brain Res 1989;477:90-9
 15. Bell MA and Scarrow M. Staining for microvascular alkaline phosphatase in thick celloidin sections of nervous tissue morphometric and pathological applications. Microvasc Res 1984;27:189-203.
 16. Blessed G, Tomlinson BE and Roth M. The association between quantitative measures of dementia and of senile change in the gray matter of elderly subjects. Br J Psychiatr 1968;114:797-811.
 17. Blocq P and Marinesco G. Sur les lesions et la pathogénie de l'épilepsie dite essentielle. Semaine Médicale 1892;12:445-6.
 18. Braak H, Braak E, Grundke-Iqbal I and Iqbal K. Occurrence of neuropil threads in the senile human brain and in Alzheimer's disease: a third location of paired helical filaments outside of neurofibrillary tangles and neuritic plaques. Neurosci Lett 1986;65:351-5.
 19. Braak H and Braak E. Neuropil threads occur in dendrites of tangle-bearing nerve cells. Neuropathol Appl Neurobiol 1988;14:39-44.
 20. Broere CAJ, Vogels OJM and Renkawek K. Granulovacuolar degeneration in

- the neocortex in Alzheimer's disease. Submitted 1989.
21. Broere CAJ, Vogels OJM and Renkawek K. Galanin-like immunoreactivity in the neocortex in Alzheimer's disease. Submitted 1989.
 22. Broere CAJ, Vogels OJM, Renkawek K and Keyser A. Macroscopical neocortical atrophy in Alzheimer's disease is selectively due to loss of neocortical surface. Submitted 1989.
 23. Brunner C, Bancher C, Lassmann H, Budka H, Grundke-Iqbal I, Iqbal K and Wisniewski HM. An immunocytochemical study on the maturation of neurofibrillary tangles in Alzheimer's disease. *Clin Neuropathol* 1988;7:150.
 24. Chan-Palay V, Lang W, Haesler U, Kohler C and Yasargil G. Distribution of altered hippocampal neurons and axons immunoreactive with antisera against Neuropeptide Y in Alzheimer type dementia. *J Comp Neurol* 1986;248:376-94.
 25. Cohen ML, Golde TE, Usiak MF, Younkin LH and Younkin SG. In situ hybridization of nucleus basalis neurons shows increased β -amyloid mRNA in Alzheimer disease. *Proc Natl Acad Sci USA* 1988;85:1227-31.
 26. Curcio CA and Kemper T. Nucleus raphe dorsalis in dementia of Alzheimer type: neurofibrillary changes and neuronal packing density. *J Neuropathol Exp Neurol* 1984;43:359-68.
 27. Dahl D, Nguyen BT and Bignami A. Ultrastructural localization of neurofilament proteins in aluminum-induced neurofibrillary tangles and rat cerebellum by immunoperoxidase labeling. *Dev Neurosci* 1982;5:54-63.
 28. Delabar J-M, Goldgaber D, Lamour Y, Nicole A, Huret J-L, DeGrouchy J, Brown P, Gajdusek DC and Sinet PM. β -Amyloid gene duplication in Alzheimer's disease and karyotypically normal Down's syndrome. *Science* 1987;235:1390-2.
 29. Dickson DW, Ksiezak-Reding H, Davies P and Yen SH. A monoclonal antibody that recognizes a phosphorylated epitope in Alzheimer neurofibrillary tangles, neurofilaments and tau proteins immunostains granulovacuolar degeneration. *Acta Neuropathol (Berl)* 1987;73:254-8.
 30. Divry P. Etude histo-chimique des plaques séniles. *J Belge Neurol Psychiatr* 1927;27:643-57.
 31. Divry P. De la nature de l'altération fibrillaire d'Alzheimer. *J Belge Neurol Psychiatr* 1934;34:147-201.
 32. Dwulet FE and Benson MD. Characterization of a transthyretin (prealbumin) variant associated with familial amyloidotic polyneuropathy type II (Indiana/Swiss). *J Clin Invest* 1986;78:880-6.
 33. Eanes ED and Glenner GG. X-ray diffraction studies of amyloid filaments. *J Histochem Cytochem* 1968;16:673-7.
 34. Eikelenboom P and Stam FC. Immunoglobulins and complement factors in senile plaques. *Acta Neuropathol* 1982;57:239-42.
 35. Elovaara I, Icen A, Palo J and Erkinjuntti T. CSF in Alzheimer's disease. Studies on blood-brain barrier function and intrathecal protein synthesis. *J Neurol Sci* 1985;70:73-80.
 36. Elovaara I, Palo J, Erkinjuntti T and Sulkava R. Serum and cerebrospinal fluid proteins and the blood-brain barrier in Alzheimer's disease and multi-infarct dementia. *Eur Neurol* 1987;26:229-34.
 37. Esiri MM, Pearson RCA and Powell TPS. The cortex of the primary auditory area in Alzheimer's disease. *Brain Res* 1986;366:385-7.
 38. Galloway PG, Perry G and Gambetti P. Hirano body filaments contain actin and actin-associated proteins. *J Neuropathol Exp Neurol* 1987;46:185-99.
 39. Gallyas F. Silver staining of Alzheimer's neurofibrillary changes by means of physical development. *Acta Morphol Acad Sci Hung* 1971;19:1-8.
 40. Gallyas F and Wolff JR. Metal-catalyzed oxidation renders silver intensification selective. *J Histochem Cytochem* 1986;12:1667-72.

41. German DC, White CL and Sparkman DR. Alzheimer's disease: neurofibrillary tangles in nuclei that project to the cerebral cortex. *Neurosci* 1987;21:305-12.
42. Gibson P and Tomlinson BE. The numbers of Hirano bodies in the hippocampus of normal and demented subjects with Alzheimer's disease. *J Neurol Sci* 1977;33:199-206.
43. Glenner GG, Eanes ED and Page DL. The relation of the properties of Congo red stained amyloid fibrils to the β -conformation. *J Histochem Cytochem* 1972;20:821-6.
44. Glenner GG, Eanes ED, Bladen HA, Linke RP and Termine JD. Beta-pleated sheet fibrils: a comparison of native amyloid with synthetic protein fibrils. *J Histochem Cytochem* 1974;22:1141-58.
45. Glenner GG, Henry JH and Fujihara S. Congophilic angiopathy in the pathogenesis of Alzheimer's degeneration. *Ann Pathol* 1981;1:120-9.
46. Glenner GG and Wong CW. Alzheimer's disease: initial report of the purification and characterization of a novel cerebrovascular amyloid protein. *Biochem Biophys Res Commun* 1984;122:885-90.
47. Goedert M. Neuronal localization of amyloid beta protein precursor mRNA in normal human brain and in Alzheimer's disease. *EMBO J* 1987;6:3627-32.
48. Goldgaber D, Lerman MJ, McBride OW, Saffiotti V and Gajdusek DC. Characterization and chromosomal localization of a cDNA encoding brain amyloid of Alzheimer's disease. *Science* 1987;235:877-80.
49. Grundke-Iqbal I, Iqbal K, George L, Tung Y-C, Kim KS and Wisniewski HM. Amyloid protein and neurofibrillary tangles coexist in the same neuron in Alzheimer disease. *Proc Natl Acad Sci USA* 1989;86:2853-7.
50. Guiry DC, Miyazaki M, Multhaup G, Fischer P, Garruto RM, Beyreuther K, Masters CL, Simms G, Gibbs CJ and Gajdusek DC. Amyloid of neurofibrillary tangles of Guamanian parkinsonism-dementia and Alzheimer disease share identical amino acid sequence. *Proc Natl Acad Sci USA* 1987;84:2073-7.
51. Hefti F. Is Alzheimer's Disease caused by lack of nerve growth factor? *Ann Neurol* 1983;13:109-10.
52. Hirano A, Malamud N and Kurland LT. Parkinson-dementia complex, an endemic disease on the Island of Guam. *Brain* 1961;84:662-79.
53. Hirano A, Malamud N, Elizan TS and Kurland LT. Amyotrophic lateral sclerosis and Parkinsonism-dementia complex on Guam. *Arch Neurol* 1966;15:35-51.
54. Hirano A, Tuazon R and Zimmerman HM. Neurofibrillary changes, granulovacuolar bodies and argentophilic globules observed in tuberous sclerosis. *Acta Neuropathol* 1968;11:257-61.
55. Hofman MA, Fliers E, Goudsmit E and Swaab DF. Morphometric analysis of the suprachiasmatic and paraventricular nuclei in the human brain: sex differences and age-dependent changes. *J Anat* 1988;160:127-43.
56. Hooper MW and Vogel FS. The limbic system in Alzheimer's disease: a neuropathologic investigation. *Am J Pathol* 1976;85:1-20.
57. Hyman BT, Van Hoesen GW, Damasio AR and Barnes CL. Cell specific pathology isolates the hippocampal formation. *Science* 1984;225:1168-70.
58. Hyman BT, Van Hoesen GW, Beyreuther K and Masters CL. A4 amyloid protein immunoreactivity is present in Alzheimer's disease neurofibrillary tangles. *Neurosci Lett* 1989;101:352-5.
59. Ishii T. Distribution of Alzheimer's neurofibrillary changes in the brain stem and hypothalamus of senile dementia. *Acta Neuropathol* 1966;6:181-7.
60. Jacobs RW, Farivar N and Butcher LL. Plaque-like lesions in the basal forebrain in Alzheimer's disease. *Neurosci Lett* 1985;56:347-51.
61. Kang J, Lemaire HG, Unterback A, Salbaum JM, Masters CL, Grezeschik KH,

- Multhaup G, Beyreuther K and Muller-Hill B. The precursor of Alzheimer disease amyloid A4 protein resembles a cell-surface receptor. *Nature* 1987;325:733-6.
62. Kato T, Hirano A, Katagiri T, Sasaki H and Yamada S. Neurofibrillary tangle formation in the nucleus basalis of Meynert ipsilateral to a massive cerebral infarct. *Ann Neurol* 1988;23:620-3.
 63. Kemper T. Senile dementia: a focal disease in the temporal lobe. In: Nandy K, ed. *Senile dementia: a biomedical approach*. Elsevier, New York, 1978;1105-31.
 64. Kidd M. Alzheimer's disease. An electron microscopic study. *Brain* 1964;87:307-20.
 65. Kirschner DA, Abraham C and Selkoe DJ. X-ray diffraction from intraneuronal paired helical filaments and extraneuronal amyloid fibers in Alzheimer's disease indicates cross- β -conformation. *Proc Natl Acad Sci USA* 1986;83:503-7.
 66. Kitaguchi N, Takahashi Y, Tokushima Y, Shiojiri S and Ito H. Novel precursor of Alzheimer's disease amyloid protein shows protease inhibitory activity. *Nature* 1988;331:530-32.
 67. Kitt CA, Struble RG, Cork LC, Mobley WC, Walker L, Joh T and Price DL. Catecholaminergic neurites in senile plaques in prefrontal cortex of aged non human primates. *Neurosci* 1985;16:691-9.
 68. Kosik K, Duffy LK, Dowling MM, Abraham C, McCluskey A and Selkoe DJ. Microtubule-associated protein 2. Monoclonal antibodies demonstrate the selective incorporation of certain epitopes into Alzheimer neurofibrillary tangles. *Proc Natl Acad Sci USA* 1984;81:7941-5.
 69. Lewis DA, Higgins GA, Young WG, Goldgaber D, Gajdusek DC, Wilson MC and Morrison JH. Distribution of precursor amyloid β -protein messenger RNA in human cerebral cortex: relationship to neurofibrillary tangles and neuritic plaques. *Proc Natl Acad Sci USA* 1988;85:1691-5.
 70. Lubbers LJ. Histotechnische mogelijkheden voor het aantonen van neurofibrillaire tangles en seniele plaques bij de ziekte van Alzheimer. *Afstudeerscriptie OLAN, Nijmegen*, 1988.
 71. Malamud N. Neuropathology of organic brain syndromes associated with aging. In: Gaitz FM, ed. *Advance in behavioral biology. Vol 3. Aging and the brain*. New York. Plenum Press. 1972:63-87.
 72. Mallat M and Levi-Strauss M. Astrocytic production of complements: C3 and Factor B. *J Neuroimmunol* 1977;16:114-5.
 73. Manetto V, Perry G, Tabaton M, Mulvihill P, Fried VA, Smith HT, Gambetti P and Autilio-Gambetti L. Ubiquitin is associated with abnormal cytoplasmic filaments characteristic of neurodegenerative diseases. *Proc Natl Acad Sci USA* 1988;85:4501-5.
 74. Mann DMA, Yates PO and Marcyniuk B. Alzheimer's presenile dementia, senile dementia of Alzheimer type and Down's syndrome in middle age form an age related continuum of pathological changes. *Neuropathol Appl Neurobiol* 1984;10:185-207.
 75. Mann DMA, Yates PO and Marcyniuk B. Some morphometric observations on the cerebral cortex and hippocampus in presenile Alzheimer's disease, senile dementia of Alzheimer type and Down's syndrome in middle age. *J Neurol Sci* 1985;69:139-59.
 76. Mann DMA, Tucker CM and Yates PO. Alzheimer's disease: an olfactory connection? *Mech Ageing Dev* 1988;42:1-15.
 77. Mann DMA. Neuropathological and neurochemical aspects of Alzheimer's disease. In: Iversen LL, Iversen SD, Snyder SH, eds. *Handbook of Psychopharmacology. Vol 20. Psychopharmacology of the aging nervous system*. Plenum Press. New York. 1988:1-67.

78. Marcyniuk B, Mann DMA and Yates PO. The topography of cell loss from locus caeruleus in Alzheimer's disease. *J Neurol Sci* 1986;76:335-45.
79. Masters CL, Simms G, Weinman NA, Multhaup G, McDonald BL and Beyreuther K. Amyloid plaque core protein in Alzheimer's disease and Down's syndrome. *Proc Natl Acad Sci USA* 1985;82:4245-9.
80. Masters CL, Multhaup G, Simms G, Pottgiesser J, Martins RN and Beyreuther K. Neuronal origin of a cerebral amyloid: neurofibrillary tangles of Alzheimer's disease contain the same protein as the amyloid of plaque cores and blood vessels. *EMBO J* 1985;4:2757-63.
81. McDuff T and Sumi SM. Subcortical degeneration in Alzheimer's disease. *Neurology* 1985;35:123-6.
82. Mesulam M-M, Mufson EJ, Levey AI and Wainer BH. Cholinergic innervation of cortex by the basal forebrain: cytochemistry and cortical connections of the septal area, diagonal band nuclei, nucleus basalis (substantia innominata) and hypothalamus in the rhesus monkey. *J Comp Neurol* 1983;214:170-97.
83. Mesulam M-M and Geula C. Nucleus basalis (Ch4) and cortical cholinergic innervation in the human brain: observations based on the distribution of Acetylcholinesterase and Choline Acetyltransferase. *J Comp Neurol* 1988;275:216-40.
84. Miyakawa T, Shimoji A, Kuramoto R and Higuchi Y. The relationship between senile plaques and cerebral blood vessels in Alzheimer's disease and senile dementia. *Virchows Arch B* 1982;40:121-9.
85. Miyakawa T, Watanabe K and Katsuragi S. Ultrastructure of amyloid fibrils in Alzheimer's disease and Down's syndrome. *Virchows Arch B* 1986;52:101-6.
86. Mori H, Kondo J and Ihara Y. Ubiquitin is a component of paired helical filaments in Alzheimer's disease. *Science* 1987;235:1641-4.
87. Morrison JH, Rogers J, Scherr S, Benoit R and Bloom SE. Somatostatin immunoreactivity in senile plaques of Alzheimer's disease. *Nature* 1985;314:90-4.
88. Mountjoy CQ, Roth M, Evans NJR and Evans HM. Cortical neuronal counts in normal elderly controls and demented patients. *Neurobiol Aging* 1983;4:1-11.
89. Ogomori K, Kitamoto T, Tateishi J, Sato Y, Suetsugu M and Abe M. β Protein amyloid is widely distributed in the central nervous system of patients with Alzheimer's disease. *Am J Pathol* 1989;134:243-51.
90. Oppenheim G. Uber "drusige Nekrosen" in der Großhirnrinde. *Neurol Zbl* 1909;28:410-3.
91. Pearson RCA, Esiri MM, Horne RW, Wilcock GK and Powell TPS. Anatomical correlates of the distribution of the pathological changes in the neocortex in Alzheimer disease. *Proc Natl Acad Sci USA* 1985;82:4531-4.
92. Peers MC, Lenders MB, Defossez A, Delacourte A and Mazzuca M. Cortical angiopathy in Alzheimer's disease: the formation of dystrophic perivascular neurites is related to the exudation of amyloid fibrils from the pathological vessels. *Virchows Arch A* 1988;414:15-20.
93. Pericak-Vance MA, Yamaoka LH, Haynes CS, et al. Genetic linkage studies in Alzheimer's disease families. *Exp Neurol* 1988;102:271-9.
94. Perl DP and Pendlebury WW. Neuropathology of dementia. *Neurol Clin* 1986;4:355-68.
95. Peterson C, Kress V, Vallee R and Goldman JE. High molecular weight microtubule-associated proteins bind to actin lattices (Hirano bodies). *Acta Neuropathol (Berl)* 1988;77:168-74.
96. Ponte P, Gonzalez-DeWhitt P, Schilling J, Miller J, Hsu D, Greenberg B, Davis K, Wallace W, Lieberburg I, Fuller F and Cordell B. A new A4

- amyloid mRNA contains a domain homologous to serine protease inhibitors. *Nature* 331:525-7.
97. Puchtler H, Sweat F and Levine M. On the binding of Congo red by amyloid. *J Histochem Cytochem* 1962;10:355-64.
 98. Puchtler H and Sweat F. Congo red as a stain for fluorescence microscopy of amyloid. *J Histochem Cytochem* 1965;13:693-4.
 99. Rasool CG, Svendsen CN and Selkoe DJ. Neurofibrillary degeneration of cholinergic and noncholinergic neurons of the basal forebrain in Alzheimer's disease. *Ann Neurol* 1986;20:482-8.
 100. Rewcastle NB and Ball MJ. Electron microscopic structure of the "inclusion bodies" in Pick's disease. *Neurology* 1968;18:1205-13.
 101. Robakis NK, Ramakrishna N, Wolfe G and Wisniewski HM. Molecular cloning and characterization of a cDNA encoding the cerebrovascular and the neuritic plaque amyloid peptides. *Proc Natl Acad Sci USA* 1987;84:4190-4.
 102. Rogers JD and Morrison JM. Quantitative morphology and regional and laminar distribution of senile plaques in Alzheimer's disease. *J Neurosci* 1985;5:2801-8.
 103. Rogers JD, Brogan D and Mirra SS. The nucleus basalis of Meynert in neurological disease: a quantitative morphological study. *Ann Neurol* 1985;17:163-70.
 104. Rozemuller JM, Elkelenboom P, Kamphorst W and Stam FC. Lack of evidence for dysfunction of the blood-barrier in Alzheimer's disease: an immunohistochemical study. *Neurobiol Aging* 1988;9:383-91.
 105. Rudelli RD, Ambler MW and Wisniewski HM. Morphology and distribution of Alzheimer neuritic (senile) and amyloid plaques in striatum and diencephalon. *Acta Neuropathol (Berl)* 1984;64:273-81.
 106. Saper CB, German DC and White CL. Neuronal pathology in nucleus basalis and associated cell groups in senile dementia of Alzheimer type: possible role in cell loss. *Neurology* 1985;35:1089-95.
 107. Schellenberg GD, Bird TD, Wijsman EM, Moore DK, Boehnke M, Bryant EM, Lampe TH, Nochlin D, Sumi SM, Deep SS, Beyreuther K and Martin GM. Absence of linkage of chromosome 21q21 markers to familial Alzheimer's disease. *Science* 1988;241:1507-10.
 108. Schochet SS and McCormick WF. Ultrastructure of Hirano bodies. *Acta Neuropathol* 1972;21:50-60.
 109. Schwartz Ph. Amyloid degeneration and tuberculosis in the aged. *Gerontologica* 1972;18:321-62.
 110. Selkoe DJ, Abraham CR, Podlisny MB and Duffy LK. Isolation of low-molecular weight proteins from amyloid plaque fibers in Alzheimer's disease. *J Neurochem* 1986;46:1820-34.
 111. Simchowicz T. Histologische Studien über die senile Demenz. Histologische und histopathologische Arbeiten über die Grosshirnrinde. 1911;4: 267-444.
 112. St. George-Hyslop PH, Tanzi RE, Polinsky RJ, Haines JL, Nee L, Watkins PC, Myers RH, Feldman RG, Pollen D, Drachman D, Growdon J, Bruni A, Fonsin J-F, Salmon D, Frommelt P, Amaducci L, Sorbi S, Piacentini S, Stewart GD, Hobbs WJ, Conneally WJ and Gusella JF. The genetic defect causing familial Alzheimer's disease maps on chromosome 21. *Science* 1987;235:885-90.
 113. Steele JC, Richardson JC and Olszewski J. Progressive supranuclear palsy. *Arch Neurol* 1964;10:333-59.
 114. Tanzi RE, Gusella JF, Watkins PC, Bruns GAP, St. George-Hyslop P, Van Keuren ML, Patterson D, Pagan S, Kurnit DM and Neve RL. Amyloid β -protein gene; cDNA, mRNA distributions, and genetic linkage near the Alzheimer locus. *Science* 1987;235:880-4.

115. Tanzi RE, McClatchey AI, Lambertı ED, Villa-Komaroff L, Gusella JF and Neve RL. Protease inhibitor domain encoded by an amyloid protein precursor mRNA associated with Alzheimer's disease. *Nature* 1988;331: 528-30.
116. Terry RD, Peck A, DeTeresa R and Schechter R. Some morphometric aspects of the brain in senile dementia of the Alzheimer type. *Ann Neurol* 1981;10:184-92.
117. Tomlinson BE, Blessed G and Roth M. Observations on the brains of non-demented old people. *J Neurol Sci* 1968;7:331-56.
118. Tomlinson BE, Blessed G and Roth M. Observations on the brains of demented old people. *J Neurol Sci* 1970;11:207-42.
119. Tomlinson BE and Kitchener D. Granulovacuolar degeneration of hippocampal pyramidal cells. *J Pathol* 1972;106:165-85.
120. Tomlinson BE, Irving D and Blessed G. Cell loss in the locus coeruleus in senile dementia of Alzheimer type. *J Neurol Sci* 1981;49:419-28.
121. Tomlinson BE and Corsellis JAN. Aging and the dementias. In: Greenfield JG, Adams JH, Corsellis JAN, Duchen LW, eds. *Greenfield's Neuropathology*. 4th ed. London: John Wiley & Sons, Inc. 1984:951-1025.
122. Tomonaga M. Ultrastructure of Hirano bodies. *Acta Neuropathol* 1974;28: 365-6.
123. Traub RD, Gajdusek DC and Gibbs CJ. Transmissible virus dementia: The relation of transmissible spongiform encephalopathy to Creutzfeldt-Jakob disease. In: Kinsbourne M, Smith L, eds. *Aging and Dementia*. Spectrum Flushing. New York. 1977;91-146.
124. Van Broeckhoven C, Genthe AM, Vandenbergh A, Horsthemke B, Backhovens H, Raeymaekers P, Van Hul W, Wehnert A, Gheuens J, Cras P, Bruylant M, Martin JJ, Salbaum M, Multhaup G, Masters CL, Beyreuther K, Gurling HMD, Mullan MJ, Holland A, Barton A, Irving N, Williamson R, Richards SJ and Hardy JA. Failure of familial Alzheimer's disease to segregate with the A4-amyloid gene in several European families. *Nature* 1987;329:153-5.
125. Vogels OJM, Broere CAJ, Ter Laak HJ, Ten Donkelaar HJ, Nieuwenhuys R and Schulte BPM. Cell loss and shrinkage in the nucleus basalis Meynert complex in Alzheimer's disease. *Neurobiol Aging* 1990;11: in press.
126. Vogels OJM, Broere CAJ and Nieuwenhuys R. Neuronal hypertrophy in the human supraoptic and paraventricular nucleus in aging and Alzheimer's disease. *Neurosci Lett* 1990: in press.
127. Walker LC, Kitt CA, Struble RG, Schmechel DE, Oertel WH, Cork LC and Price DL. GAD like immunoreactive neurites in senile plaques. *Neurosci Lett* 1985;59:165-9.
128. Whitehouse PJ, Price DL, Struble RG, Clark AW, Coyle JT and DeLong MR. Alzheimer's Disease and Senile Dementia: loss of neurons in the basal forebrain. *Science* 1982;215:1237-9.
129. Wilcock GK and Esiri MM. Plaques, tangles and dementia: a quantitative study. *J Neurol Sci* 1982;56:343-56.
130. Wilmes F and Hossman KA. A specific immunofluorescence technique for the demonstration of vasogenic edema in paraffin embedded material. *Acta Neuropathol* 1979;45:47-51.
131. Wisniewski HM and Terry RD. Re-examination of the pathogenesis of the senile plaque. In: Zimmerman HM, ed. *Progress in Neuropathology*. New York, London. Grune & Stratton. 1973;1-26.
132. Wisniewski HM and Soiffer D. Neurofibrillary pathology: current status and research perspectives. *Mech Aging Dev* 1979;9:119-142.
133. Wong CW, Quaranta V and Glenner GG. Neuritic plaques and cerebrovascular amyloid in Alzheimer disease are antigenically related. *Proc Natl Acad Sci USA* 1985;82:8729-32.

134. Wood JG, Mirra SS, Pollock NJ and Binder LI. Neurofibrillary tangles of Alzheimer disease share antigenic determinants with the axonal microtubule-associated protein tau. Proc Natl Acad Sci USA 1986;83:4040-3.
135. Woodard JS. Clinico-pathologic significance of granulovacuolar degeneration in Alzheimer's disease. J Neuropathol Exp Neurol 1970;21:85-91.

GALANIN-LIKE IMMUNOREACTIVITY WITHIN CH2 NEURONS IN THE VERTICAL LIMB NUCLEUS OF THE DIAGONAL BAND OF BROCA IN AGING AND ALZHEIMER'S DISEASE

O.J.M. Vogels, K. Renkawek· C.A.J. Broere,
H.J. ter Laak and F. van Workum.

Acta Neuropathologica 1989;78:90-5

8.1 Abstract

The neuropeptide galanin is known to inhibit the evoked release of acetylcholine in ventral hippocampus of the rat. Co-localization of this peptide with choline acetyltransferase in neurons of the cholinergic septal nuclei has been demonstrated in rat and nonhuman primate. The severe deficiency of the cholinergic hippocampal projection system arising mainly from the vertical limb nucleus of the diagonal band of Broca also referred to as Ch2 region, is a constant finding in Alzheimer's disease, a disorder which is neuropathologically characterized by the appearance of senile plaques, neurofibrillary tangles and congophilic angiopathy in neo- and archicortical structures. In the present study for the first time galanin immunoreactivity in the human Ch2 region is morphologically investigated and related to the severity of hippocampal plaques and neurofibrillary tangles in Alzheimer's disease. An inverse relationship between decreasing galanin immunoreactivity in the Ch2 region and increasing amounts of senile plaques and neurofibrillary tangles in the hippocampus can be indicated. Considering the cholinergic deficiency in Alzheimer's disease as a secondary phenomenon to primary cortical and hippocampal lesions, and realizing the inhibitory effect of galanin upon acetylcholine release in

hippocampus, this preliminary study suggests, that a decreased galanin immunoreactivity in Ch2 in Alzheimer's disease reflects a possible negative feedback mechanism to a degenerating cholinergic projection system.

8.2 Introduction

Galanin is a 29-amino acid peptide, isolated from the porcine intestine [27]. Galanin-like immunoreactivity (GA-LI) was found to be widely distributed in the animal central nervous system of different species [13,15,22,25,29], including human [5,11]. This neuropeptide may be of special interest because the presence of choline acetyltransferase like immunoreactivity (ChAT-LI) and GA-LI has been shown in the same basal forebrain neurons in rat [12] and monkey [13,29].

Co-localization of ChAT-LI and GA-LI in a large population of cholinergic neurons in the rat vertical limb nucleus of the diagonal band of Broca has been demonstrated [12] as well as GA-LI emerging as faintly labeled puncta within the rat hippocampus [14].

The existence of a GA-like neuropeptide in putative cholinergic somata in the septum-basal forebrain was found to be much more pronounced in the owl monkey than in the rat, and within the hippocampus and dentate gyrus an extensive network of GA-immunoreactive (GA-IR) fibers could be demonstrated, closely resembling the distribution of putative cholinergic fibers [13]. This more extensive distribution of GA-like peptide in the cholinergic system of the monkey as compared to the rat may reflect an increased importance of this peptide in co-transmission processes in higher animals, and raises the possibility of a modulatory role for GA-like peptide(s) on functions associated with the hippocampus such as memory and learning. Recently it was demonstrated that one of the effects of galanin involves inhibition of the evoked release of acetylcholine in the rat ventral hippocampus [7].

The cholinergic nature of the projection from the vertical

limb nucleus of the diagonal band of Broca, better referred to as the Ch2 region [17], to the hippocampal formation is now well established in rat [2,23,30] and monkey [10,16].

Degeneration of the cholinergic system is the most consistently found abnormality in Alzheimer's disease (AD), that is characterized by memory impairment and intellectual decline [3,6]. Moreover, in AD the degree of dementia correlates with both the number of senile plaques and neurofibrillary tangles in neocortex and hippocampus [4] as well as with the deficiency of the acetylcholine synthesizing enzyme ChAT [19].

Therefore it is relevant to analyze to what degree GA-LI is present in the cholinergic system in normal brain and also whether or not GA-LI-content is changed in AD, senile dementia of the Alzheimer type (SDAT) and other dementing disorders.

Very recently GA-LI has been described in the cholinergic nucleus basalis of Meynert [5] also known as the Ch4 region, which has cholinergic projections to neocortex and amygdala [17]. It was claimed that GA-LI increases in AD and in Parkinson's disease accompanied with dementia.

The present preliminary study describes the existence and changes of GA-LI in the Ch2 region (vertical limb nucleus of the diagonal band of Broca, which has cholinergic projections to the hippocampus) of two human control brains, two Alzheimer's diseased brains and one senile atrophy brain.

8.3 Material and methods

Two brains from clinically diagnosed Alzheimer's disease patients (case 1 and 2) were selected. The neuropathological diagnosis was performed on paraffin embedded sections stained for Nissl, Bodian, Yamamoto Bielschowsky, and fluorescence congored [20,21] and thioflavine-S. These two Alzheimer cases differed in duration and severity of illness: case 1 had a duration-time of 8 years and showed clinically advanced aphaso-apraxy-agnostic symptoms; case 2 lasted for 4 years with less severe dysfunctioning.

In case 1 neurofibrillary tangles (NFT) were abundantly present in neocortex and hippocampus, especially in the subiculum area; the latter region was also interspersed with neuritic plaques as was the whole neocortex. Case 2 showed less NFT in the hippocampus and there was a predominance of small immature plaques in moderate numbers only. One case of familial frontal lobe dementia clinically imposing as Pick's disease (case 3) could not be neuropathologically confirmed as such, but was diagnosed as senile atrophy (SA): general atrophy of the hippocampus and whole neocortex was present especially in frontal and temporal lobes, showing severe loss of neurons; however, senile plaques and NFT were absent. Autopsy revealed no clues for extracranial causes of dementia. The two control cases (case 4 and 5) showed clinically and neuropathologically no evidence of neurological or psychiatric symptoms (Table 8.1).

Tissue blocks containing the vertical limb nucleus of the diagonal band of Broca (Ch2 region) were obtained and fixed 24 h in formaldehyde sublimate (case 2,3 and 4) or formaldehyde (case 1 and 5). After dehydration the slices were embedded in ralwax and sections with a thickness of 8 microns were cut using a Jung 2050 microtome. The sections were incubated with GA antiserum (Cambridge Research Biochemicals, Cambridge, UK) in a dilution of 1:500 for 48 h at room temperature. Staining was performed using the avidin-biotin-peroxidase complex technique (ABC)[9] according to the manufacture instructions (Vector). Immunoreactivity was demonstrated by 0.05% DAB - 0.01% H₂O₂ to which 0.01 M imidazole was added [26]. Sections were counterstained with haematoxylin. With regard to the specificity of the GA antiserum, control experiments were carried out by using a non-immune serum, and by preadsorbing GA antiserum with an excess of purified GA-peptide (Cambridge Research Biochemicals).

Sections were investigated at a 200x, 400x and 1000x magnification. In each case GA-LI was evaluated on ten randomly chosen testfields of 250x250 μm^2 . Three quantitative and three qualitative criteria were used for this purpose:

- mean total neuron number per mm^2 ; all neurons regardless of size and staining properties were counted at a 400x magnifica-

TABLE 8.1
brain material

case number	1	2	3	4	5
sex	F	M	M	F	M
age (y)	85	64	73	41	46
duration illness (y)	8	4	8.5		
postmortem delay (h)	4	3	3	24	9
fixation	Fa	FaS	FaS	FaS	Fa
clinical diagnosis	AD	AD	Pick	N	N
neuropathological diagnosis	AD	AD	SA	N	N
SP and NFT neocortex	++++	+	-	-	-
SP and NFT hippocampus	++++	++	-	-	-

Characteristics of brain material: gender, age, duration time of illness, postmortem delay, fixation, clinical and neuropathological diagnosis, and the amount of neocortical and hippocampal senile plaques and neurofibrillary tangles. F, female; M, male; y, year; h, hour; Fa, formaldehyde; FaS, formaldehyde sublimate; AD, Alzheimer's disease; SA, senile atrophy; N, normal; SP, senile plaque; NFT, neurofibrillary tangle; +++, numerous; ++, moderate; +, few; -, occasional or absent.

tion;

- mean GA-IR neuron number per mm² at 400x magnification;
- percentage GA-IR neuron number of total neuron number;
- estimation of amount of GA-IR granules per GA-IR neuron;
- estimation of staining intensity of GA-IR granules;
- description of neuron processes.

Data concerning the percentage GA-IR neuron number of total neuron number were statistically analyzed using the 2-sided Wilcoxon test.

8.4 Results

Using the quantitative and qualitative criteria described above, the following results were obtained: Table 8.2.

The control brains (case 4 and 5) exhibited extensive GA-LI in the cytoplasm of over 80% of all large and small Ch2 neurons (Figs. 1a and 1b). An almost uniform distribution of many small, intensively stained granules was present throughout the entire cytoplasm (Fig. 8.2a). However, at the very periphery of the cytoplasm an increased density of granules gave the impression of GA-LI on the outside surface of the soma as well. Some fusiform neurons showed a very dense, evenly intensive immunoreactivity, resembling the GA-1 type interneurons as described by Chan-Palay [5]. GA-IR neuronal processes were traced along a small distance, but were sometimes prominently present (Fig. 8.1a). In contrast to the control brains, the AD-cases showed less GA-LI (Fig. 8.1c). GA-LI was most decreased in the advanced AD-case (case 1), in which only 53% of all Ch2 neurons exhibited GA-LI with low amounts of weakly stained granules per neuron. Applying the 2-sided Wilcoxon test, this decrease in percentage GA-IR neurons in case 1 proved to be significant at the 0.01 level compared to both control cases 4 and 5, and at the 0.05 level compared to cases 2 and 3. All other comparisons between the cases 2-5 demonstrated no significant differences. Especially the non-GA-IR neurons appeared to be shrunken and showed hardly any visible processes. Only the larger neurons showed low amounts of weakly stained granules mainly located at the periphery of the cytoplasm, and sometimes GA-IR dots over the soma surface could be pointed out (Fig. 8.2b).

In the AD-case with less pronounced neuropathological cortical changes (case 2) the number of GA-IR neurons (78%) equaled that of the control brains, however the amount of GA-IR granules per neuron was clearly less in comparison with the control brains, but still more prominent than in the advanced AD-case (Fig. 8.2c). The difference in clinical severity between the two AD-cases, is also reflected in the numbers of senile plaques and neurofibrillary tangles in neocortex and hippocampus (Table 8.1.) Neuronal processes were hardly visible in both AD-cases. The fusiform GA-1 type interneurons were still present, but less easily detectable because of decrease in number as well as in staining intensity.

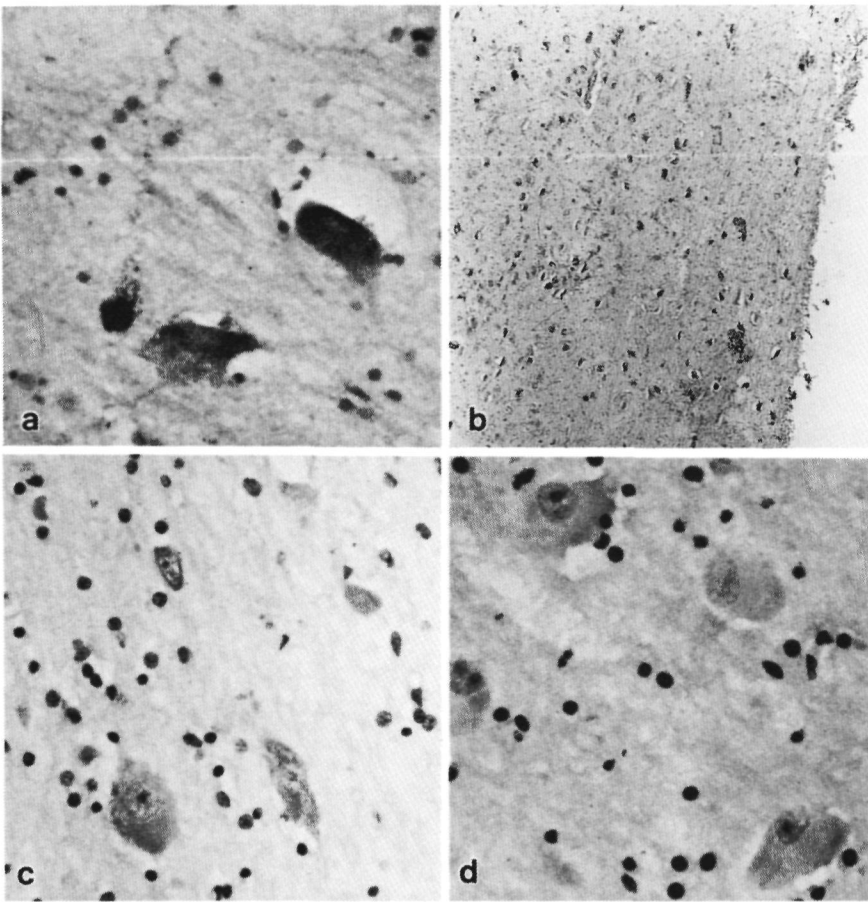


Fig. 8.1a+b Extensive galanin-like immunoreactivity (GA-LI) in the vertical limb nucleus of the diagonal band of Broca in normal aging (top left and right).
 c Strongly decreased GA-LI in advanced form of Alzheimer's disease (bottom left).
 d Absence of GA-LI in control case with excess of galanin peptide in antiserum (bottom right).
 Magnification: a,c,d 280x; b 28x

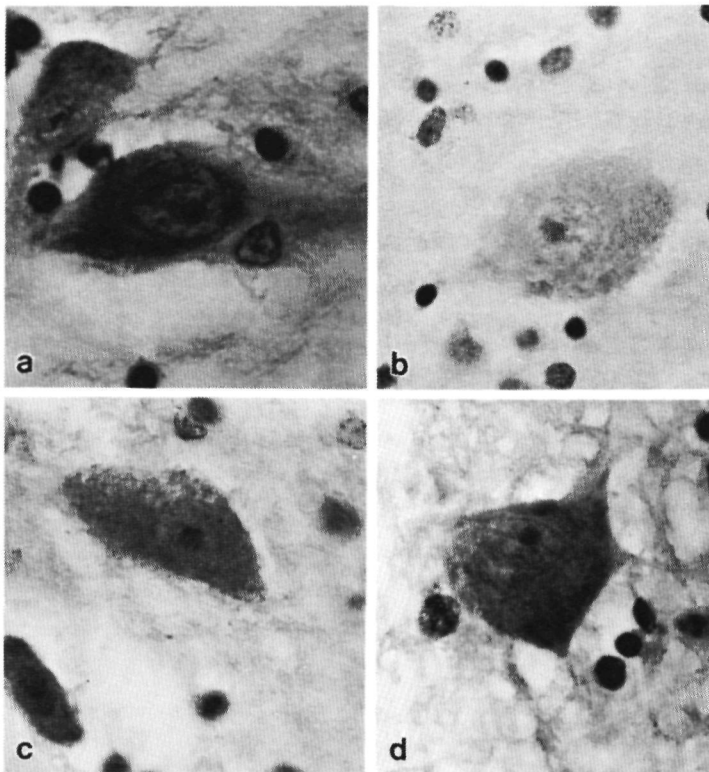


Fig. 8.2a Galanin-like immunoreactivity (GA-LI) in the vertical limb nucleus of the diagonal band of Broca: extensive in normal aging (top left).
b Strongly decreased GA-LI in advanced form of AD (top right).
c Decreased GA-LI in mild form of AD (bottom left).
d Extensive GA-LI in senile atrophy (bottom right).
Magnification: 600x

TABLE 8.2
Quantitative and qualitative results

case number	1	2	3	4	5
	severe	mild			
neuropathological diagnosis	AD	AD	SA	N	N
mean neuron number/mm ²	98	102	107	112	104
mean GA-IR number/mm ²	53	80*	83*	91**	85**
% GA-IR neurons	54	78	78	81	82
GA-IR granules/neuron	+	++	+++	+++	+++
intensity GA granules	+	+/**	++/**	+++	++/**
neuron processes: - amount	seldom	few	few	some	some
- length	short	short +long	short +long	short +long	short +long

AD, Alzheimer's disease; SA, senile atrophy; N, normal brain; GA-IR, galanin-like immunoreactive; +, low; ++, moderate; +++, high; *, p<0.05 and **, p<0.01 in 2-sided Wilcoxon test as compared to case 1.

Surprisingly, case 3, that could be readily diagnosed according to neuropathological criteria as senile atrophy without senile plaques or neurofibrillary tangles, showed GA-LI as extensively as compared to the control cases: almost 80% of all Ch2 neurons were GA-positive showing numerous intensively stained granules throughout the entire cytoplasm with an increase in density at the periphery of the cell. GA-IR processes were comparable to control brains (Fig. 8.2d).

Another interesting finding is the stability of mean neuron number/mm² in Ch2 region for all 5 cases.

Regarding to the specificity of the GA-antiserum, control experiments both with a non-immune serum as well as with an antiserum preadsorbed with an excess of GA-antigen showed completely no immune reaction (Fig. 8.1d).

These results demonstrate the presence of GA-LI in the Ch2 region of the human brain. The large putative cholinergic neurons show both cytoplasmatic GA-IR granules as well as

extracellular GA-IR dots along the cellular surface. This latter strongly suggests the possibility of GA-IR axon endings terminating upon the neuronal somata. Smaller fusiform neurons showed very dense, evenly intensive GA-LI. In Alzheimer's disease the GA-LI decreases: the number of GA-IR neurons diminishes significantly and/or the staining intensity decreases as does the amount of GA-IR granules per neuron, showing an inverse relationship to the numbers of NFT and SP in hippocampus. The senile atrophy brain showed GA-LI comparable to the control brains.

8.5 Discussion

The study presented here demonstrates the presence of GA-LI in the Ch2 region (vertical limb nucleus of the diagonal band of Broca) in two human control brains, two Alzheimer's diseased brains and one senile atrophy brain.

In the control brains GA-LI was present in most of the small and large putative cholinergic Ch2 neurons showing GA-IR granules in the cytoplasm and extracellular GA-IR dots along the outer cell membrane. The latter could probably be interpreted as GA-IR axon endings terminating upon neuronal somata.

In AD a prominent decrease in both intra- and extracellular GA-LI could be demonstrated, however, this decrease was absent in the senile atrophy brain that was clinically characterized by dementia, but neuropathologically showed no features of Alzheimer's or Pick's disease.

The Ch2 region is well known to have cholinergic projections to the hippocampus [2,10,16,23,30], a limbic structure that is functionally involved in memory and learning processes. AD is clinically characterized by memory impairment and intellectual decline [6]. In AD the degree of dementia correlates with both the numbers of senile plaques and neurofibrillary tangles in the neocortex and hippocampus [4] as well as with the deficiency of the acetylcholine synthesizing enzyme ChAT [19]. This cholinergic deficiency is most pronounced in the hippocampus [8,24].

Co-localization of ChAT- and GA-LI has been described in the

Ch2 region of the rat [13,15] and nonhuman primate [13,29]. This co-localization was more pronounced in the higher species. Recently it was demonstrated that one of the functions of galanin involves inhibition of the evoked release of acetylcholine in the rat ventral hippocampus in vivo and in vitro [7]; galanin therefore acts as an inhibitory modulator of cholinergic transmission in the hippocampus.

The cholinergic basal forebrain system can be subdivided into four regions (Ch1, Ch2, Ch3 and Ch4) with different projection patterns and different amounts of cholinergic neurons [17]. The major cholinergic regions are Ch2, that projects to the hippocampus, and Ch4 also known as the nucleus basalis of Meynert, that projects to the neocortex and amygdala.

Degeneration of the cholinergic system in AD is probably due to axonal damage as a result of cortical and hippocampal lesions as SP and NFT. Recent morphometric studies support this view of secondary degeneration: many of the magnocellular cholinergic neurons are not completely lost, but persist in a shrunken state [1,18,28]. Moreover, in AD a differential involvement of the Ch2 and Ch4 region can be indicated: in Ch4 secondary cell shrinkage occurs as well as primary cell loss to an extent of 20% of all cells regardless of size properties; in Ch2 no cell loss could be observed, instead a shift from large neurons into shrunken ones was prominently present [28].

In the present study no cell loss in the Ch2 region was present either for all five cases (Table 8.2) and this finding strongly supports the hypothesis of secondary degeneration of the Ch2 system due to hippocampal lesions.

Our results suggest an inverse relationship between decreased GA-LI in Ch2 in AD and increased numbers of neuropathological lesions in the hippocampus; the more severe these lesions, the lesser the GA-LI in Ch2 (Table 8.2). Because it has been shown that galanin inhibits the evoked release of acetylcholine in the hippocampus [7], a decreased GA-LI in Ch2 in AD suggests the possibility of a negative feed-back mechanism to a degenerating cholinergic system.

Interestingly, our results indicating a GA-LI decrease in Ch2

in AD, are inconsistent with the recently reported increase in GA-LI in Ch4 in AD and Parkinson's disease accompanied with dementia [5]. These contradictory results may be due to the differential involvement of Ch2 (only secondary) and Ch4 (both primary and secondary degeneration) in AD [28]. Differences in fixation and immunohistochemical procedures can be an additional reason.

However, three variables could have influenced our results: age, postmortem delay and differences in fixation (Table 8.1). Concerning age and postmortem delay, the GA-LI in cases 3, 4, and 5 (no presence of hippocampal SP and NFT) were comparable although ranging in age from 41 to 73 years and in postmortem delay from 3 to 24 hours (no significant differences could be demonstrated applying the 2-sided Wilcoxon test). Difference in fixation procedure slightly favoured the formaldehyde sublimate fixation, although this impression demands further clarification based on objective grounds. Although many immunopositive and immunonegative neurons are located within surrounding holes, this does not suggest neuron shrinkage and as a consequence possible nonspecific staining, but has to be considered as tissue shrinkage due to fixation artefacts.

In conclusion, our preliminary results demonstrate a decreased GA-LI in Ch2 in Alzheimer's disease patients, but probably not in patients with dementia of other origin. This decrease in GA-LI is inversely related to the numbers of SP and NFT in hippocampus in AD. This is in agreement with the functional effect of galanin, inhibition of acetylcholine release in the hippocampus.

8.6 References

1. Allen SJ, Dawbarn D and Wilcock GK. Morphometric immunochemical analysis of neurons in the nucleus basalis of Meynert in Alzheimer's Disease. *Brain Res* 1988;454:275-81.
2. Amaral DG and Kurz J. An analysis of the origins of the cholinergic and noncholinergic septal projections to the hippocampal formation of the rat. *J Comp Neurol* 1985;240:37-59.
3. Bartus RT, Dean III RL, Beer B and Lipka AS. The cholinergic hypothesis of geriatric memory dysfunction. *Science* 1982;217:408-17.
4. Blessed G, Tomlinson BE and Roth M. The association between quantitative

- measures of dementia and of senile change in the gray matter of elderly subjects. *Br J Psychiatr* 1968;114:797-811.
5. Chan-Palay V. Galanin hyperinnervates surviving neurons of the human basal nucleus of Meynert in dementias of Alzheimer's and Parkinson's Disease: a hypothesis for the role of Galanin in accentuating cholinergic dysfunction in dementia. *J Comp Neurol* 1988;273:543-57.
 6. Collerton D. Cholinergic function and intellectual decline in Alzheimer's Disease. *Neurosci* 1986;19:1-28.
 7. Fisone G, Wu CF, Consolo S, Nordström Ö, Brynne N, Bartfai T, Melander T and Hökfelt T. Galanin inhibits acetylcholine release in the ventral hippocampus of the rat: histochemical, autoradiographic, in vivo and in vitro studies. *Proc Natl Acad Sci USA* 1987;84:7339-43.
 8. Henke H and Lang W. Cholinergic enzymes in neocortex, hippocampus and basal forebrain of non-neurological and senile dementia of Alzheimer-type patients. *Brain Res* 1983;267:281-91.
 9. Hsu S-M, Raine L and Fanger H. Use of Avidin-Biotin-Peroxidase Complex (ABC) in immunoperoxidase techniques: a comparison between ABC and unlabeled antibody (PAP) procedures. *J Histochem Cytochem* 1981;29:577-80.
 10. Kitt CA, Mitchell SJ, DeLong MR, Wainer BH and Price DL. Fiber pathways of basal forebrain cholinergic neurons in monkeys. *Brain Res* 1987;406:192-206.
 11. Marti E, Gibson SJ, Polak JM, Facer P, Springall DR, Van Aswegen G, Aitchison M and Koltzenburg M. Ontogeny of peptide- and amine-containing neurons in motor, sensory, and autonomic regions of rat and human spinal cord, dorsal root ganglia, and rat skin. *J Comp Neurol* 1987;266:332-59.
 12. Melander T, Staines WA, Hökfelt T, Rokaeus A, Eckenstein F, Salvaterra PM and Wainer BH. Galanin-like immunoreactivity in cholinergic neurons of the septum-basal forebrain complex projecting to the hippocampus of the rat. *Brain Res* 1985;360:130-8.
 13. Melander T and Staines WA. A galanin-peptide coexists in putative cholinergic somata of the septum-basal forebrain complex and in acetylcholinesterase-containing fibers and varicosities within the hippocampus in the owl monkey (*aotus trivirgatus*). *Neurosci Lett* 1986;68:17-22.
 14. Melander T, Staines WA and Rokaeus Å. Galanin-like immunoreactivity in hippocampal afferents in the rat, with special reference to cholinergic and noradrenergic inputs. *Neurosci* 1986;19:223-40.
 15. Melander T, Hökfelt T and Rokaeus Å. Distribution of galanin-like immunoreactivity in the rat central nervous system. *J Comp Neurol* 1986;1248:475-17.
 16. Mesulam M-M, Mufson EJ, Levey AI and Wainer BH. Cholinergic innervation of cortex by the basal forebrain: cytochemistry and cortical connections of the septal area, diagonal band nuclei, nucleus basalis (substantia innominata), and hypothalamus in the Rhesus monkey. *J Comp Neurol* 1983;214:170-97.
 17. Mesulam M-M, Mufson EJ, Wainer BH and Levey AI. Central cholinergic pathways in the rat: an overview based on an alternative nomenclature (Ch1-Ch6). *Neurosci* 1983;10:1185-201.
 18. Pearson RCA, Sofroniew MV, Cuellar AC, Powell TPS, Eckenstein F, Esiri MM and Wilcock GK. Persistence of cholinergic neurons in the basal nucleus in a brain with senile dementia of the Alzheimer's type demonstrated by immunohistochemical staining for choline acetyltransferase. *Brain Res* 1983;289:375-9.
 19. Perry EK, Tomlinson BE, Blessed G, Bergmann K, Gibson PH and Perry RH. Correlation of cholinergic abnormalities with senile plaques and mental

- test scores in senile dementia. *Brit Med J* 1978;2:1457-9.
20. Puchtler H, Sweat F and Levine M. On the binding of Congo red by amyloid. *J Histochem Cytochem* 1962;10:355-64.
 21. Puchtler H and Sweat F. Congo red as a stain for fluorescence microscopy of amyloid. *J Histochem Cytochem* 1965;13:693-4.
 22. Rokaeus Å, Melander T, Hokfelt T, Lundberg JM, Tatemoto K, Carlquist M and Mutt V. A galanin like peptide in the central nervous system and intestine of the rat. *Neurosci Lett* 1984;47:161-6
 23. Rye DB, Warner BH, Mesulam M-M, Mufson EJ and Saper CB. Cortical projections arising from the basal forebrain: a study of cholinergic and noncholinergic components employing combined retrograde tracing and immunohistochemical localization of choline acetyltransferase. *Neurosci* 1984;13:627-43.
 24. Rylett RJ, Ball MJ and Colhoun EH. Evidence for high-affinity choline transport in synaptosomes prepared from hippocampus and neocortex of patients with Alzheimer's Disease. *Brain Res* 1983;289:169-75.
 25. Skofitsch G and Jacobowitz DM. Immunohistochemical mapping of galanin-like neurons in the rat central nervous system. *Peptides* 1985;6:509-46
 26. Straus W. Imidazole increases the sensitivity of the cytochemical reaction for peroxidase with diaminobenzidine at a neutral pH. *J Histochem Cytochem* 1982;30:491-3.
 27. Tatemoto K, Rokaeus Å, Jornvall H, McDonald TJ and Mutt V. Galanin - a novel biologically active peptide from porcine intestine. *FEBS Lett* 1983;164:124-8.
 28. Vogels OJM, ter Laak HJ, Broere CAJ, ten Donkelaar HJ, Nieuwenhuys R and Schulte BPM. Cell loss and shrinkage in the nucleus basalis Meynert complex in Alzheimer's Disease. *Neurobiol Aging* 1990: in press.
 29. Walker LC, Koliatsos VE, Kitt CA, Richardson RT and Price DL. Galanin-containing somata in the primate nucleus basalis/diagonal band complex. *Neurosci Abstr* 1987;273:13.
 30. Woolf NJ and Butcher LL. Cholinergic systems in the rat brain: I. Projections to the limbic telencephalon. *Brain Res Bull* 1984;13:751-84.

CORRELATIONS OF NEURON COUNTS IN BOTH THE NUCLEUS BASALIS OF MEYNERT COMPLEX AND HYPOTHALAMUS WITH NEUROPATHOLOGICAL DETERMINANTS IN CORTICAL AND SUBCORTICAL STRUCTURES IN ALZHEIMER'S DISEASE

9.1 Introduction

A variety of neurological conditions, known as "system degenerations", involve the selective loss of specific populations of neurons, frequently at widely separated loci within the nervous system. The populations of neurons destroyed by a particular disease are often functionally related. For example, in amyotrophic lateral sclerosis both upper and lower motor neurons are lost, in primary autonomic failure of the Shy-Drager type both pre-ganglionic and post-ganglionic autonomic neurons degenerate, and in olivo-ponto-cerebellar atrophy the main pattern of cerebellar connectivity is affected [review: 25]. In AD, the limbic and paralimbic regions are most severely affected [21].

It is now generally accepted, that the functional state of neurons depends on both the processes of axonal and transneuronal transport for intra- and intercellular communication, and on trophic support. In "neurological system degenerations", like AD, the processes of axonal and transneuronal transport may subserve the transmission from neuron to neuron of a toxic (e.g., aluminum [30]) or infectious agent (e.g., herpes simplex virus [4]), or alternatively that these diseases may result from the failure of normal transport of a trophic agent [1] (e.g. nerve growth factor [10]).

In AD the association areas of the cerebral cortex and the amygdala and hippocampus as well are severely affected by SP and NFT [8, 21, 24]. The reasons for this apparent vulnerability to

SP and NFT formation are not clear though the anatomical linkage of these regions to the outside world via the olfactory pathways (the corticomedial nuclei of the amygdala and the entorhinal cortex of the hippocampus are primary reception areas for olfactory information) suggests that any putative agent responsible for SP and NFT formation might gain access to the brain via the olfactory pathways [17, 20]. Moreover, the hippocampus is strongly interconnected with the temporal and posterior parietal higher order association cortical areas [review: 9]. Subcortical cell groups that contain large numbers of NFT, such as the cholinergic NBMC, the serotonergic raphe nuclei and the noradrenergic locus coeruleus, all have extensive neocortical projections, particularly to the limbic and paralimbic cortex [18, 19, 27].

Several studies describe significant correlations between cortical plaque counts and neuronal cell loss in (different subdivisions of) the NBMC [2, 3, 16], substantiating the hypothesis of a cholinergic pathogenesis of neuritic plaques in AD. However, others report no correlation between neuronal cell loss in the NBMC and plaque counts in various corresponding projection regions as the hippocampus, frontal and parietal cortex, and the parahippocampal gyrus [11, 12].

In this chapter two issues are addressed: 1), anatomical correlates of the distribution of the pathological changes in cortical and subcortical structures are determined in order to test the validity "the olfactory pathway hypothesis" for AD [21]; 2), correlates between the locus coeruleus and its projection areas in the hypothalamus (the SON and PVN) are determined, in order to trace a possible relationship between decreasing neuron numbers in the locus coeruleus [27] and neuronal hypertrophy in the hypothalamus [29].

9.2 Material and methods

The subdivisions of the NBMC according to the nomenclature of Mesulam (Ch1+Ch2, Ch3, Ch4a1, Ch4am, Ch4i and Ch4p) [18] and

their subsequent major projection areas are correlated [18]:

- Ch1+Ch2 with the hippocampus proper (HIP) and the entorhinal cortex (ERC);
- Ch3 with the anterior olfactory nucleus of the olfactory bulb (AON);
- Ch4a1 with area 11 according to Brodmann [5];
- Ch4am with areas 7 and 23;
- Ch4i with area 8;
- Ch4p with areas 20 and 22, and the hippocampus proper.
- The locus coeruleus (LC) with the SON and PVN in the hypothalamus [15].

Only structures from the same hemispheres were correlated with each other. Unfortunately, no correlates were determined between the AON and the hippocampus and/or amygdala due to lack of data in identical hemispheres.

Neuron counts in the subdivisions of the NBMC, and in the hippocampus, the AON, the LC, SON and PVN were carried out on sections stained for cresyl violet. Only numbers of magnocellular neurons ($>37.5 \mu\text{m}$) in the NBMC, the SON and PVN were subjected to the correlation analysis, because these numbers show the greatest reduction (NBMC) [28] or increase (SON and PVN) in AD [29]. SP, NFT and CA were quantitated on sections stained for congored fluorescence [23]. The data on structures other than the NBMC, the SON and PVN were provided by colleagues [6, 9, 26, 27]. Statistical analysis was performed using the Pearson's correlation test.

9.3 Results

The total neuron number of the hippocampus correlates significantly ($p < 0.05$) with the number of magnocellular Ch4p neurons of the NBMC ($r = 0.81$; $p = 0.020$). A tendency ($p < 0.10$) of a correlation ($r = 0.60$; $p = 0.051$) of numbers of magnocellular Ch3 neurons with total neuron numbers in the AON is found. No other correlates are found between neuron numbers of NBMC subdivisions and neuron numbers of their respective target structures.

TABLE 9.1

Pearson correlations of magnocellular neuron numbers
of the NBMC, the SON and PVN with neuropathological determinants
in cortical and subcortical structures

origin	target	n ₁	n ₂	N ₁ -N ₂	N ₁ -SP	N ₁ -NFT	N ₁ -CA
				r	r	r	r
Ch1+Ch2	HIP	4	4	0.49(-)	-0.65(^)	-0.53(-)	n.a
Ch1+Ch2	ERC	4	4	n.a	-0.78(**)	-0.63(^)	n.a
Ch3	AON	6	5	0.60(^)	n.a	n.a	n.a
Ch4a1	area 11	6	4	n.a	-0.69(**)	-0.34(-)	-0.52(-)
Ch4am	area 7	6	6	n.a	-0.77(***)	-0.42(-)	-0.51(^)
Ch4am	area 23	6	6	n.a	-0.71(***)	-0.06(-)	-0.55(^)
Ch4i	area 8	6	3	n.a	-0.61(^)	-0.02(-)	-0.58(^)
Ch4p	area 20	2	5	n.a	-0.93(***)	-0.29(-)	-0.50(-)
Ch4p	area 22	5	5	n.a	-0.70(**)	-0.22(-)	-0.41(-)
Ch4p	HIP	4	4	0.81(**)	-0.70(^)	-0.87(***)	n.a
LC	SON	9	7	-0.66(***)	0.29(-)	0.49(^)	n.a
LC	PVN	4	5	-0.30(-)	0.59(^)	0.51(-)	n.a

n.a, not available; n₁, number of normal aging hemispheres; n₂, number of AD hemispheres; N₁, number of magnocellular neurons (>37.5 μm) in NBMC, SON and PVN; N₂, neuron number in target structure; r, Pearson's correlation; SP, senile plaques; NFT, neurofibrillary tangle; CA, congophilic angiopathy; HIP, hippocampus; ERC, entorhinal cortex; AON, anterior olfactory nucleus; SON, supraoptic nucleus; PVN, paraventricular nucleus; LC, locus coeruleus; levels of significance are given in parentheses. -, p>0.10; ^, 0.05<p<0.10; **, 0.01<p<0.05; ***, p<0.01.

The neuron numbers of Ch1+Ch2, Ch4a1, Ch4am, Ch4am, Ch4p, and Ch4p appear to correlate significantly with SP-densities of, respectively, the entorhinal cortex ($r=-0.78$; $p=0.020$), area 11 ($r=-0.69$; $p=0.030$), area 7 ($r=-0.77$; $p=0.003$), area 23 ($r=-0.71$; $p=0.009$), area 20 ($r=-0.93$; $p=0.003$) and area 22 ($r=-0.70$; $p=0.020$). A tendency ($p<0.10$) of a correlation of neuron numbers of Ch1+Ch2, Ch4i and Ch4p with SP-densities of, respectively, the hippocampus ($r=-0.65$; $p=0.080$), area 8 ($r=-0.61$; $p=0.080$) and the hippocampus ($r=-0.70$; $p=0.052$) is found.

The Ch4p neuron number correlates significantly with the NFT-density in the hippocampus ($r=-0.87$; $p=0.005$), whereas a tendency of a correlation of Ch1+Ch2 neuron number with NFT-density of the entorhinal cortex is found ($r=-0.63$; $p=0.090$). No correlates are found between neuron numbers of other NBMC subdivisions and NFT-densities in their respective target structures.

No significant correlates between neuron numbers of the NBMC subdivisions and CA-densities in their respective target structures are found, although a tendency of correlation of neuron numbers of Ch4am, Ch4am and Ch4i appears to be present with CA-densities of, respectively, area 7 ($r=-0.51$; $p=0.090$), area 23 ($r=-0.55$; $p=0.060$) and area 8 ($r=-0.58$; $p=0.090$).

Whereas a significant correlation is present between numbers of magnocellular neurons in the SON and total neuron numbers of the LC ($r=-0.66$; $p=0.005$), such a relationship was not found for the PVN (Table 9.1).

9.4 Discussion

The results give no hard support for the "olfactory pathway hypothesis" [20], although a tendency of correlation of AON neuron numbers with magnocellular Ch3 neurons is found. Moreover, neuron numbers of several subdivisions of the NBMC appear to correlate with SP-densities. However, it should be noted that only small numbers of identical hemispheres were available.

The results confirm previous studies demonstrating a relati-

onship between cortical plaque formation and loss of magnocellular neurons in the NBMC [2, 3, 16]. This finding gives no direct evidence regarding the nature of the SP or their mode of formation. Degeneration of the NBMC occurs also in other neurologic disorders but without cortical plaque formation [review: 22]. Moreover, it does not solve the controversial issue whether the NBMC is primarily or secondarily affected in AD, but it only suggests a close linkage between plaque formation and loss of cholinergic cortical innervation. In this respect, it is noteworthy, that the trophic state of the NBMC neurons selectively depends on the availability of nerve growth factor (NGF) [10], being produced in the cholinergic target areas, the neocortex and hippocampus. These latter two regions show tremendous volume reduction and cell loss in AD [6, 7, 9], resulting in severe reduction of NGF-production [13] and consequently secondary degeneration of the NBMC [28]. This selective vulnerability of the hippocampus and neocortex is not clear yet. Although this study does not confirm the "olfactory pathway hypothesis", it is still a likely candidate for the explanation of this selective vulnerability.

The tendency of a correlation of NBMC magnocellular neurons with cortical CA-densities suggests a close linkage between the degeneration of the NBMC and cortical CA, the latter known to be closely associated to SP-formation [20]. The finding that magnocellular NBMC neurons correlate not significantly with NFT-densities in the neocortex, but significantly with SP-densities supports the common view among neuropathologists that the SP has to be considered as the main neuropathological finding in AD [14].

The finding of neuronal hypertrophy in the SON and to a lesser extent in the PVN in AD [29], is further supported by the significant negative correlation between magnocellular neuron numbers in the SON and total neuron numbers in the noradrenergic locus coeruleus (LC). Therefore, increased activity of the SON and PVN in AD may be related to a reduction of noradrenergic innervation of these hypothalamic nuclei.

9.5 References

1. Appel SH. A unifying hypothesis for the cause of amyotrophic lateral sclerosis parkinsonism, and Alzheimer's disease. *Ann Neurol* 1981;10:499-505.
2. Arendt T, Bigl V, Tennstedt A and Arendt A. Correlation between cortical plaque count and neuronal loss in the nucleus basalis in Alzheimer's disease. *Neurosci Lett* 1984;48:81-5.
3. Arendt T, Bigl V, Tennstedt A and Arendt A. Neuronal loss in different parts of the nucleus basalis is related to neuritic plaque formation in cortical target areas in Alzheimer's disease. *Neurosci* 1985;14:1-14.
4. Ball MJ. Limbic predilection in Alzheimer's dementia: is reactivated herpes simplex virus involved? *Can J Neurol Sci* 1982;9:303-6.
5. Brodmann K. Vergleichende Lokalisationslehre der Grosshirnrinde. Barth, Leipzig 1909.
6. Broere CAJ. The neocortex in normal aging and Alzheimer's disease. Thesis, Nijmegen 1990.
7. Broere CAJ, Vogels OJM, Renkawek K, Keyser A. Macroscopical neocortical atrophy in Alzheimer's disease is selectively due to loss of neocortical surface. Submitted.
8. Brun A. An overview of light and electron microscope changes. In: Reisberg B, ed. Alzheimer's disease: the standard reference. The Free Press, New York 1983:pp:37-47.
9. De Vries H. The hippocampal formation in normal aging and Alzheimer's disease. Thesis, Nijmegen 1990.
10. Hefti F and Weiner WJ. Nerve growth factor and Alzheimer's disease. *Ann Neurol* 1986;20:275-81.
11. Etienne P, Robitaille Y, Gauthier S and Nair NPV. Nucleus basalis neuronal loss and neuritic plaques in advanced Alzheimer's disease. *Can J Physiol Pharmacol* 1986;64:318-24.
12. Etienne P, Robitaille Y, Wood P, Gauthier S, Nair NPV and Quirion R. Nucleus basalis neuronal loss, neuritic plaques and choline acetyltransferase activity in advanced Alzheimer's disease. *Neurosci* 1986;19:1279-91.
13. Higgins GA and Mufson EJ. NGF receptor gene expression is decreased in the nucleus basalis in Alzheimer's disease. *Exp Neurol* 1990: in press.
14. Khachaturian ZS. Diagnosis of Alzheimer's Disease. *Arch Neurol* 1985;42:1097-105.
15. Loughlin SE. Locus coeruleus projections to cortex - topography, morphology and collateralization. *Brain Res Bull* 1982;9:287-94.
16. Mann DMA, Yates PO and Marcyniuk B. Correlation between senile plaque and neurofibrillary tangle counts in cerebral cortex and neuronal counts in cortex and subcortical structures in Alzheimer's disease. *Neurosci Lett* 1985;56:51-5.
17. Mann DMA, Tucker CM and Yates PO. Alzheimer's disease: an olfactory connection? *Mech Ageing Devel* 1988;42:1-15.
18. Mesulam M-M, Mufson EJ, Levey AI and Wainer BH. Cholinergic innervation of cortex by the basal forebrain: cytochemistry and cortical connections of the septal area, diagonal band nuclei, nucleus basalis (substantia innominata) and hypothalamus in the rhesus monkey. *J Comp Neurol* 1983;214:170-97.
19. Mesulam M-M and Mufson EJ. Neural inputs into the nucleus basalis of the substantia innominata (Ch4) in the rhesus monkey. *Brain* 1984;107:253-74.
20. Miyakawa T, Shimoji A, Kuramoto R and Higuchi Y. The relationship

- between senile plaques and cerebral blood vessels in Alzheimer's disease and senile dementia. *Virchows Arch B* 1982;40:121-9.
21. Pearson RCA, Esiri MM, Hiorns RW, Wilcock GK and Powell TPS. Anatomical correlates of the distribution of the pathological changes in the neocortex in Alzheimer's disease. *Proc Natl Acad Sci USA* 1985;82:4531-4.
 22. Perry EK. The cholinergic hypothesis - 10 years on. *Br Med Bull* 1986;42:63-9.
 23. Puchtler H, Sweat F. Congo red as a stain for fluorescence microscopy of amyloid. *J Histochem Cytochem* 1965;13:693-4.
 24. Rogers J and Morrison JH. Quantitative morphology and regional and laminar distributions of senile plaques in Alzheimer's disease. *J Neurosci* 1985;5:2801-8.
 25. Saper CB, Wainer BH and German DC. Axonal and transneuronal transport in the transmission of neurological disease: potential role in system degenerations, including Alzheimer's disease. *Neurosci* 1987;23:389-98.
 26. Ter Laak HJ. The bulbous olfactorius in normal aging and Alzheimer's disease. In preparation.
 27. Van Domburg P. Some brainstem nuclei in normal aging and Alzheimer's disease. Thesis, Nijmegen 1990.
 28. Vogels OJM, Broere CAJ, Ter Laak HJ, Ten Donkelaar HJ, Nieuwenhuys R and Schulte BPM. Cell loss and shrinkage in the nucleus basalis Meynert complex in Alzheimer's disease. *Neurobiol Aging* 1990;11(1): in press.
 29. Vogels OJM, Broere CAJ, Nieuwenhuys R. Neuronal hypertrophy in the human supraoptic and paraventricular nucleus in aging and Alzheimer's disease. *Neurosci Lett* 1990: in press.
 30. Zatta P, Giordano R, Corain B and Bombi GG. Alzheimer dementia and the aluminum hypothesis. *Medical Hypotheses* 1988;26:139-42.

SUMMARY AND CONCLUSIONS

With respect to the pathogenesis of Alzheimer's disease the cholinergic hypothesis (Chapter 1) is a central issue. The reported loss of large cholinergic neurons in the nucleus basalis of Meynert complex (NBMC, i.e., the nucleus basalis of Meynert, the diagonal band of Broca, and the medial septal nucleus) correlates significantly with the degree of dementia, the number of senile plaques and neurofibrillary tangles in the neocortex and hippocampus, and the decreasing amounts of choline acetyltransferase in these structures. However, a closer look at the pertinent neuropathological and morphometric studies reveals several methodological errors especially in the neuroanatomical definition of the NBMC and of its ill-defined subdivisions as well as in the quantitative and morphometric procedures applied.

With regard to the neuroanatomical definition of the NBMC and its constituting subdivisions, a topographical map is presented (Chapter 2) in order to get a clear arrangement of the different subdivisions in rostrocaudal direction in relation to its surrounding structures. Moreover, the presented review of the chemoarchitecture and the hodology of the NBMC suggests, that the NBMC is functionally in a position to act as a cholinergic relay for transmitting predominantly limbic and paralimbic information to the neocortex. Therefore, the NBMC may influence complex behaviour (integrated motor or emotional responses, learning and memory) according to the prevailing emotional and motivational states encoded by the limbic and paralimbic regions of the brain (Chapter 2).

In order to avoid the methodological errors in quantitative and morphometric procedures made in previous studies, unbiased and efficient sampling procedures have been developed according to modern stereological principles (Chapter 3). It is shown that in unbiased quantitative morphology the nucleolus is the sampling item of first choice in histological sections with a minimal thickness of 10 μm (Chapter 4). Most morphological studies of the NBMC introduced two criteria for neurons to be counted: a minimum size criterion (magnocellular neurons, usually

larger than 30 μm) and a subjective staining criterion (hyperchromatic neurons showing abundance of Nissl substance). However, it was not known whether neuronal loss is restricted to magnocellular neurons and whether shrinkage of cells prior to death might lead to inaccurate estimations of the loss of magnocellular neurons. Moreover, the decreased functional state of the NBMC neurons in AD is reflected by dissolution of the Nissl substance in the cytoplasm. Therefore, the use of a minimum size criterion and a staining criterion make these parameters less reliable as markers for the NBMC in AD, as these parameters are subjected to the disease process itself. Consequently, in the present study neurons are sampled efficiently and in an unbiased way without neuron size or staining restrictions. This approach shows that neuron shrinkage rather than neuron death in the NBMC in AD is the main neuropathological feature. Moreover, a differential involvement of the subdivisions of the NBMC is found, showing a rostrocaudal increase in pathology with the posterior tail of the NBMC being the most affected (Chapter 5). This degeneration of the NBMC neurons may be related to reduced cortical and hippocampal amounts of nerve growth factor, a trophic factor that prevents specifically cholinergic neurons from death.

With regard to the specificity of the degeneration of the NBMC, two adjacent hypothalamic structures, i.e., the supraoptic and paraventricular nuclei, are also investigated (Chapter 6). An unexpected neuronal hypertrophy is found, whereas neuron numbers remain constant in AD. This activation of the supraoptic and paraventricular nuclei may be secondary to an age-related decline in vasopressin binding sites in the kidney and to an age-related decline in noradrenergic innervation of the hypothalamus due to severe cell loss in the locus coeruleus.

Numbers of senile plaques (SP) and neurofibrillary tangles (NFT), as well as the distribution of congophilic angiopathy (CA) and lipofuscin in the NBMC are presented in Chapter 7. It is demonstrated that a rostrocaudal increase of SP and NFT is present, whereas the CA is evenly distributed along the NBMC. No major amyloid depositions are detected in the SON and PVN. The

lipofuscin accumulation in NBMC neurons in AD does not differ from normal aging. No differences in amyloid depositions are found in the organum vasculosum of the lamina terminalis, a region devoid of a continuous blood-brain barrier, suggesting a cerebral rather than a haematogeneous origin of the amyloid in AD (Chapter 7).

Considering the presumably important role of the noncholinergic interneurons of the NBMC in modulating cholinergic function, the neuropeptide galanin is chosen for immunoreactivity studies (Chapter 8). Galanin is known to inhibit the evoked release of acetylcholine in the rat hippocampus. It is shown, that in AD galanin-like immunoreactivity is decreased in the vertical limb nucleus of the diagonal band of Broca, that has major cholinergic projections to the hippocampus. It is suggested, that this decreased galanin-like immunoreactivity reflects a negative feedback mechanism to a degenerating cholinergic system.

In Chapter 9 anatomical correlates of the distribution of pathological changes in cortical and subcortical regions in AD are presented. No conclusive evidence for "the olfactory pathway hypothesis" is found. Significant correlations of numbers of magnocellular neurons in the subdivisions of the NBMC with SP-densities in their respective cortical projection areas are shown, whereas no correlations with NFT-densities are demonstrated.

The two most important findings of the present study may be summarized as follows:

1. Neuronal shrinkage rather than death of NBMC neurons prevails in Alzheimer's disease, strongly suggesting a secondary degeneration of the NBMC due to deficits of cortical nerve growth factor.
2. Neuronal hypertrophy occurs in the SON and PVN in AD, indicating a reserve capacity and/or plasticity of functional neuronal circuits.

Both findings may implicate future therapeutic possibilities either by neurotrophic factors or by "reserve capacity stimulators" c.q. "plasticity-enhancers".

SAMENVATTING EN CONCLUSIES

Gedurende de laatste tien jaar heeft het internationale onderzoek naar dementie een enorme vlucht genomen. Reden hiervoor is de stijging van het aantal dementie-patiënten tengevolge van het toenemend aantal ouderen in de samenleving. In Nederland zijn momenteel naar schatting ongeveer 240.000 personen lijdende aan enigerlei vorm van dementie. Bij ruim 70.000 van hen is er sprake van een zo ernstige vorm van ziekte dat volledige handelingsonbekwaamheid en hulpbehoefendheid bestaat. In 50% van het dementieel syndroom betreft het de ziekte van Alzheimer (ZA). De pathogenese van ZA is tot op heden onbekend. Een van de meest gangbare hypothesen betreft de cholinerge hypothese, die beschreven wordt in Hoofdstuk 1. De cholinerge hypothese postuleert een verband tussen verminderde cholinerge activiteit en een afname van het cognitief functioneren. Deze verminderde cholinerge activiteit komt tot uiting in een afname van het aantal grootcellige, cholinerge neuronen in het nucleus basalis van Meynert complex (NBMC). Dit celverlies correleert significant met de mate van dementie, de hoeveelheid seniele plaques en neurofibrillaire degeneratie (dit zijn de neuropathologische kenmerken van ZA) in de hersenschors en de hippocampus, en met de verminderde hoeveelheid van het acetylcholine synthetiserende enzym choline acetyltransferase in deze hersenstructuren. Echter, een nauwkeurige analyse van de literatuur aangaande de cholinerge hypothese laat meerdere methodologische fouten zien, met name met betrekking tot zowel de neuroanatomische afgrenzing en indeling van het NBMC, als ook tot de kwantitatieve en morfometrische methoden ter bepaling van het celaantal.

In Hoofdstuk 2 wordt een nauwkeurige neuroanatomische beschrijving gegeven van het NBMC en de subdivisies van het NBMC. De atlas laat de verscheidene subdivisies van het NBMC in rostrocaudale richting zien in relatie met omgevende hersenstructuren. Tevens wordt een literatuuroverzicht van de chemo-architectuur en de zenuwverbindingen van het NBMC gegeven. Hieruit mag men afleiden, dat het NBMC functioneel in staat is om

voornamelijk limbische en paralimbische informatie (emotie en motivatie) door te schakelen naar de hersenschors en hippocampus. Daardoor kan het NBMC complexe gedragingen beïnvloeden (geïntegreerde emotionele en motorische reacties, het leervermogen en geheugen) afhankelijk van de bestaande emotionele en motivationele uitgangssituatie die gestuurd wordt door de limbische en paralimbische hersenstructuren.

Om fouten in kwantitatieve en morfometrische methoden ter bepaling van het celaantal van het NBMC te voorkomen, wordt in **Hoofdstuk 3** een aanname-vrije en efficiënte bemonsteringsmethode beschreven die in overeenstemming is met de huidige stereologische inzichten.

In **Hoofdstuk 4** blijkt, dat wanneer het kernlichaampje in de celkern van neuronen (zenuwcellen) gekozen wordt om te bemonsteren, er in principe voldaan is aan de stereologische eisen van een aanname-vrije, kwantificatie methode, mits de dikte van de histologische coupe niet minder wordt dan 10 micron.

In de introductie van **Hoofdstuk 5** wordt beschreven, dat eerdere kwantificatie-onderzoeken van het celaantal van het NBMC twee aannames gebruikten: alleen grootcellige neuronen werden geteld, én deze grootcellige neuronen dienden veel Nissl-korrels te bevatten. Het was echter niet bekend of celverlies zich beperkte tot de grootcellige neuronen of dat celkrimpings voorafging aan het beschreven celverlies. Bovendien werd voorbijgegaan aan het feit dat door het ziekteproces zelf de Nissl-korrels verdwenen. Door de toepassing van dit celgrootte- en korrel-criterium zijn deze celtellingen van het NBMC in feite onbetrouwbaar, omdat beide criteria door het ziekteproces zelf beïnvloed kunnen worden. Daarom worden in het huidige onderzoek (**Hoofdstuk 5**) alle neuronen, welke een kernlichaampje bevatten, bemonsterd. Deze aanname-vrije benadering laat zien dat celkrimpings van NBMC neuronen het belangrijkste neuropathologische kenmerk is en waarschijnlijk voorafgaat aan celdood, die eveneens maar in veel geringere mate dan tot nu toe werd aangenomen, optreedt. Tevens blijkt, dat de subdivisies van het NBMC in verschillende mate aangedaan zijn: er bestaat een rostrocaudale toename van de pathologie. Er wordt gesuggereerd

dat de krimpings van de NBMC neuronen veroorzaakt wordt door een tekort aan het "nerve growth factor", een zenuwgroei-factor, die geproduceerd wordt in de hersenschors en de hippocampus. Dierexperimenteel werk heeft namelijk laten zien, dat het "nerve growth factor" de dood van specifiek de cholinerge NBMC neuronen kan voorkomen.

Om zeker te zijn van de specificiteit van de pathologie in het NBMC in ZA, worden in Hoofdstuk 6 de resultaten van cellellingen van twee andere naburige zenuwcelgebieden beschreven, te weten de nucleus supraopticus (SON) en de nucleus paraventricularis (PVN). In ZA blijft het cellaantal constant, en worden de neuronen niet kleiner (zoals de NBMC neuronen) maar juist groter. Deze aktivatie van de SON en PVN neuronen kan verklaard worden door een aan de leeftijd gerelateerd tekort aan nier-receptoren voor het hormoon vasopressine dat deze neuronen aanmaken. Tevens wordt gesuggereerd, dat ernstig celverlies in de locus coeruleus (een zenuwcelgebied in de hersenstam, dat in verbinding staat met de SON en de PVN) eveneens deze aktivatie van de SON en PVN neuronen kan veroorzaken.

In Hoofdstuk 7 worden gegevens gepresenteerd over de neuropathologische afwijkingen, die naast celkrimpings en -verlies in het NBMC optreden bij ZA: de seniele plaques, de neurofibrillaire degeneratie en de congofiele angiopathie (deze drie afwijkingen bestaan alle uit amyloid). Opnieuw wordt er een rostrocaudale toename van seniele plaques en neurofibrillaire degeneratie vastgesteld, terwijl de congofiele angiopathie gelijkelijk verdeeld is over de diverse subdivisies van het NBMC. In de SON en PVN worden behoudens de celzwellings geen neuropathologische afwijkingen vastgesteld. Er wordt geen verschil in hoeveelheid lipofuscine, een afvalprodukt van de stofwisseling, tussen normale veroudering en ZA waargenomen in het NBMC, de SON en PVN. In het organum vasculosum van de lamina terminalis, een klein gebiedje dat geen intacte bloed-hersenen barrière bezit, is er geen verschil in congofiele angiopathie tussen normale veroudering en ZA gevonden. Deze bevinding suggereert dat het amyloid niet afkomstig is uit de bloedbaan, maar in de hersenen zelf aangemaakt wordt.

In Hoofdstuk 8 wordt de waarschijnlijk belangrijke rol van schakelneuronen in het NBMC nader belicht. Deze schakelneuronen zijn mogelijk in staat de functie van de cholinerge neuron te beïnvloeden. Een type schakelneuron produceert galanine, waarvoor de cholinerge cellen receptoren bevatten. Galanine kan in de rat de afgifte van acetylcholine in de hippocampus remmen. Het blijkt dat bij ZA de hoeveelheid galanine verlaagd is in die cholinerge neuron die juist met de hippocampus in verbinding staan.

In Hoofdstuk 9 worden significante correlaties aangetoond tussen het verlies van grootcellige, cholinerge neuron in de diverse subdivisies van het NBMC en aantallen seniele plaques in de respectievelijke hersenschorsvelden, waarmee de subdivisies van het NBMC verbindingen onderhouden. Dergelijke significante correlaties voor de neurofibrillaire degeneratie en de congofiele angiopathie worden niet gevonden.

De twee belangrijkste bevindingen van dit onderzoek laten zich als volgt samenvatten:

1. Celkrimp van NBMC neuron is de belangrijkste neuropathologische afwijking bij ZA, en gaat waarschijnlijk vooraf aan celdood. Dit proces van celkrimp suggereert een secundaire degeneratie van het NBMC tengevolge van primaire tekorten aan "nerve growth factor" in de hersenschors en hippocampus.
 2. De celzwellen van de SON en PVN neuron duidt op een plasticiteit en reserve-capaciteit van deze neuron in het bijzonder en misschien van alle neuron in het algemeen.
- Beide bevindingen impliceren toekomstige mogelijkheden voor de ontwikkeling van nieuwe farmaca, welke mogelijk werkzaam zijn kunnen blijken bij meer dan alleen de ziekte van Alzheimer.

DANKWOORD

Iedereen die op enige wijze aan de totstandkoming van dit proefschrift heeft bijgedragen wil ik bedanken. De volgende personen wil ik met name noemen: Piet van Kalmthout, Raymond Koopmans en Marie-Anne Willekens-Bogaers, artsen van het verpleeghuis St. Joachim & Anna te Nijmegen, Dr. R. Ravid van de Hersenbank van het Nederlands Instituut voor Hersenonderzoek te Amsterdam, en Dr. M. Horstink, neuroloog van het Instituut voor Neurologie te Nijmegen, leverden allen een essentiële bijdrage aan dit onderzoek door het beschikbaar stellen van hersenmateriaal. Dr. K. Renkawek verrichtte nauwgezet de neuropathologische diagnoses en leerde mij de basisprincipes van de neuropathologie kennen. Freek van Workum, Josine van Luijt, Lilian Eshuis en Helma Mentink-Vrensen verzetten een enorme hoeveelheid histologisch werk. Zij prepareerden oneindig veel coupes met de grootste zorg. Anja Rozendaal-Verburg wist de niet aflatende en jaarlijks groeiende stroom van duizenden wetenschappelijke artikelen over veroudering en dementie in een rustig vaarwater te houden: tweemaal per maand verschaftte zij mij een uitstekend literatuuroverzicht. Bovendien verzorgde zij de literatuur-aanvragen efficiënt en accuraat. De Heer N. Dijkstra en Hans Wijnen ben ik dankbaar voor de vervaardiging van de illustraties en het foto-werk. Vele "last minutes" stonden zij altijd direkt voor mij klaar. Cees Broere, Harke de Vries, Thomas Vereecken en Peter van Domburg, de mannen van de verouderingsgroep, dank ik voor de collegiale samenwerking, hun gevoel voor humor, en voor de urenlange discussies over zaken die het onderzoek, maar meer nog de zaken die het onderzoek niet betroffen. De kaft werd spontaan door Ivo Muskens ontworpen. Mijn vrienden en familie ben ik dankbaar voor hun interesse, stimulans en met name relativiseringsvermogen. Tot slot dank ik mijn ouders die mij destijds in de gelegenheid stelden de studie van mijn keuze te volgen. Last but certainly not least, dank ik Dorine voor haar enthousiasme, morele steun, en haar onmiskenbare hulp bij de uiteindelijke versie van dit proefschrift.

CURRICULUM VITAE

Oscar Vogels werd op 28 september 1957 geboren te Oss. Hij bezocht het Titus Brandsma Lyceum te Oss, alwaar in 1975 het diploma Gymnasium β werd behaald. Van augustus 1975 tot juli 1976 studeerde hij Natuurwetenschappen aan de Landbouw Hogeschool te Wageningen. In augustus 1976 ving hij aan met de studie Geneeskunde aan de Katholieke Universiteit van Nijmegen, alwaar hij in juli 1983 zijn Doctoraalexamen behaalde. Van augustus tot en met december 1983 verrichtte hij onderzoek naar de invloed van het geslacht op het gedrag van patiënten met de ziekte van Alzheimer en multi-infarct dementie in het psychogeriatrisch verpleeghuis St. Joachim & Anna te Nijmegen (o.l.v. Prof. Drs. J.J.M. Michels en Drs. P.J.C. van Kalmthout). Vanaf januari 1984 doorliep hij de co-assistentenschappen en in februari 1986 werd het artsexamen behaald. In de lente van 1986 was hij als keuringsarts verbonden aan de "Bedrijfsgezondheidsdienst Oostelijk Gelderland" in Doetinchem, en in de zomer van 1986 was hij verpleeghuisarts van het psychogeriatrisch verpleeghuis St. Joachim and Anna te Nijmegen. Van september 1986 tot augustus 1989 werkte hij aan het onderzoeksproject "Veroudering en verouderingsziekten van het centrale zenuwstelsel" in het Research Laboratorium voor Morphologische Neurologie, Instituut voor Neurologie te Nijmegen, onder leiding van Prof. Dr. R. Nieuwenhuys (Hoofd van de afdeling Anatomie en Embryologie) en Prof. Dr. B.P.M. Schulte (Hoofd van het Instituut voor Neurologie), waarvan de resultaten in dit proefschrift zijn weergegeven. Sinds september 1989 is hij arts-assistent in opleiding tot neuroloog in het Instituut voor Neurologie te Nijmegen (Opleider: Prof. Dr. B.P.M. Schulte). Hij is getrouwd met Dorine Swinkels.

STELLINGEN

behorend bij het proefschrift

**THE NUCLEUS BASALIS OF MEYNERT COMPLEX AND ADJACENT STRUCTURES
IN NORMAL AGING AND ALZHEIMER'S DISEASE**

A neuroanatomical, neuropathological and stereological study

In het openbaar te verdedigen
op vrijdag 23 februari 1990
des namiddags te 2.15 uur

door

Oscar Vogels

STELLINGEN

I

"Do more less well" is het belangrijkste stereologische principe van elk kwantitatief onderzoek.

dit proefschrift, hoofdstukken 3, 4, 5, 6 en 7
Gundersen HJG and Osterby R. J Microsc 1981;121:65-73

II

Niet het celverlies, maar de celschrompeling vormt de belangrijkste neuropathologische determinant binnen het nucleus basalis Meynert complex bij de ziekte van Alzheimer.

dit proefschrift, hoofdstuk 5
Pearson RCA, et al. Brain Res 1983;289:375-9

III

Bij normale veroudering en in versterkte mate bij de ziekte van Alzheimer treedt hypertrofie van neuronen van de nucleus supraopticus en nucleus paraventricularis op.

dit proefschrift, hoofdstuk 6
Fliers E, et al. Brain Res 1985;342:45-53

IV

De subkernen van het nucleus basalis Meynert complex zijn niet in gelijke mate aangedaan bij de ziekte van Alzheimer: er bestaat een rostrocaudale toename van de celschrompeling, het celverlies, de seniele plaques en neurofibrillaire degeneratie, en parallel hieraan een rostrocaudale afname van de gen-expressie van receptoren voor "nerve growth factor".

dit proefschrift, hoofdstuk 7
Higgins GA and Mufson EJ. Exp Neurol 1989;106:222-36

V

Er zijn aanwijzingen dat de bloed-hersen barrière niet wezenlijk aangedaan is bij de ziekte van Alzheimer.

dit proefschrift, hoofdstuk 7
Roze Muller JM, et al. Neurobiol Aging 1988;9:383-91

VI

Het nucleus basalis Meynert complex is secundair aangedaan bij de ziekte van Alzheimer.

dit proefschrift, hoofdstukken 5, 7 en 9

VII

Er ontbreekt een rationele basis voor therapieën als acetylcholine precursors en acetylcholine-esterase remmers bij de ziekte van Alzheimer.

dit proefschrift, hoofdstukken 5, 7 en 9

VIII

De ziekte van Alzheimer dient niet opgevat te worden als een versneld verouderingsproces.

IX

In het onderzoek naar het atherogeen gedrag van low-density lipoproteïns (LDL) dienen de LDL-subfracties afzonderlijk betrokken te worden.

Swinkels DW. Thesis Nijmegen 1989

X

Het dominante gen voor schizofrenie is niet gelinked met de regio q11-13 op chromosoom 5.

Sherrington R, et al. Nature 1988;336:164-7
Detera-Wadleigh SD, et al. Nature 1989;340:391-3

XI

Het gebruik van de standaard fout van het gemiddelde, is een standaard fout van de gemiddelde onderzoeker, en kan beter vervangen worden door de variatie-coëfficiënt.

XII

Door de ont-aarding van Carnaval krijgt dit oorspronkelijk katholieke feest ongemerkt weer een religieus tintje.